Intrinsic proton sensitivity of GPR4 is necessary for CO_2/H^+ activation of retrotrapezoid nucleus neurons and CO_2-stimulated breathing

Elizabeth Catherine Gonye

BS, Biochemistry and Molecular Biology, Computer Science
University of Richmond, 2016

A Dissertation Presented to the Graduate Faculty of the
University of Virginia in Candidacy for the
Degree of Doctor of Philosophy

Department of Pharmacology

University of Virginia
March, 2024

Abstract

Breathing is essential to life and as such it is a tightly regulated and protected process driven by conscious and reflexive mechanisms. One of the reflexive mechanisms that alters breathing in response to increased arterial CO_2/lowered arterial pH is the hypercapnic ventilatory response (HCVR). While work on this reflex was first published more than a century ago, the cellular and molecular mechanisms underlying it are still not fully understood. The central nucleus initiating the HCVR is thought to reside on or near the ventral surface of the medulla but there are a number of nuclei within those anatomical boundaries that have been shown to express some intrinsic CO_2/pH sensitivity. One such nucleus, first identified due to its observed anatomical projections to the central respiratory pattern generator, is the retrotrapezoid nucleus (RTN). RTN neurons are intrinsically pH sensitive (i.e., pH sensitivity persists under synaptic blockade and when neurons are dissociated ex vivo) and this sensitivity depends on expression of two distinct proton sensors, GPR4 and TASK-2. However, it is unknown whether both sensors control excitability of the RTN generally or if they are only necessary to provide background excitation at homeostatic arterial/cerebrospinal fluid pH. Additionally, there are no specific antibodies for the native form of either protein that are currently available.

This first section of this work aims to characterize the expression pattern of GPR4 using a knock-in approach to introduce a small epitope tag into the endogenous locus to leverage the highly specific antibodies that exist for those epitopes. We then examine expression of *Gpr4* mRNA and protein throughout the mouse brain. The second part of this work focuses on demonstrating that it is the specific pH-sensing capacity of GPR4 that is necessary for a normal HCVR and normal pH activation of the RTN. The individual residues necessary for pH sensing are known for both GPR4 and TASK-2. We again use a knock-in approach to generate animals expressing GPR4 containing two distinct pH-desensitizing histidine mutations. We use these animals to demonstrate that pH-sensitive

GPR4 is necessary for a normal HCVR and for normal pH sensitivity of RTN neurons without affecting baseline respiration or neuronal excitability. In an appendix, I present preliminary work using an analogous knock-in strategy to alter the pH sensitivity of TASK-2 and measure effects on the HCVR.

All together, this work describes the expression pattern of GPR4 in the brain for the first time and demonstrates the necessity of pH sensing via GPR4 for manifestation of the HCVR, possibly through its role in mediating the pH sensitivity of RTN neurons.

Acknowledgements

I don't think that anyone can complete a PhD on their own. No matter what, there is a network of people behind the scenes helping support in a multitude of different ways, not just scientifically. I want to thank some of those people here because none of this would have ever been possible without them.

First off, to my family – Mom, Dad, Anna, and Claire (and a bunch of extended family too) – thank you for always being there to answer all the questions I had about the world as a kid and to this day. You taught me to never stop being curious and to never stop learning. Thank you also for always being there to help take care of me when things got a little too hard for me to keep a handle on anything besides experiments. You made all of this possible. To Scott, you somehow put up with my chaotic energy and manage to keep me grounded even when things were getting out of hand. You remind me to take a deep breath, keep doing the things that make me happy, eat lunch when I forget, and are always there to give me a hug and tell me it's going to be okay. And to Luna (even though you can't read), thank you for always wanting to snuggle and lay your head on the space bar while I'm writing, you're the best.

Second, to my chosen family, my friends. To the Biddies, thank you for always checking in to make sure that I was doing alright and getting excited for me when I didn't always know how to be excited for myself. You provide the support that I don't always know how to provide for myself and I love you all always. To my D&D group, you are the best possible thing that could have come out of a global pandemic. I love you guys and I can't wait to go on more adventures together, in person and in the Forgotten Realms. To my Crossfit Charlottesville 6:15 pm crew, especially Mel and Joanna, you have taught me how to achieve goals that I never thought I would be capable of and you set the best example to live up to. I can't wait to keep getting stronger together, even from afar. And finally, to the people I've met through the BIMS program, thank you for sharing your cute

pet pictures, new recipes, restaurant suggestions, board games, coffee, and your own PhD experiences with me. It helped so much to know that I wasn't alone in the hard times.

To my undergraduate mentor at the University of Richmond, Dr. Krista Stenger, your advice and guidance in my first lab experience was critical in helping me realize that I wanted to complete a PhD and eventually end up teaching at a place like UR. You taught me so much about experimental design, project management, and collaboration.

To Doug and the rest of the Bayliss lab, members current and previous, you have given me a scientific training that I know will serve me well always. You challenged me to try new things, learn new strategies, and most importantly how to ask and address any research question. I used to pretend that I didn't want to do neuroscience work, but seeing how incredible the brain is during these past 6 and a half years has finally convinced me that it's what I will always love. To Adi and Rachel, my fellow graduate students, thank you for always being there to bounce ideas off of when I hit a roadblock and for commiseration when I imaged yet another bad injection. To Eva, Yingtang, Keyong, and Serapio, thank you for providing your knowledge and thoughts on everything I presented in lab meeting and for answering the endless questions I would ask when learning a new protocol. Christopher, thank you for always bringing new and exciting playlists to our desks and for being an incredible friend through all the good lab times and the bad. And finally, to Doug, the scientific training you have given me is unparalleled. You were one of the first people I talked to at UVA when I interviewed and I was immediately sure I wanted to do a rotation. You captured my attention with your rigorous approach to any experiment, no matter how big or small and taught me that sometimes, all you need to do is get back on the rig and keep recording. Thank you for everything.

To my dissertation committee – Paula Barrett, Patrice Guyenet, Steve Abbott, Iggy Provencio, and Mark Beenhakker – thank you for telling me when I was on the right track and should keep going and when to drop something that was not worth the trouble. You

gave me perspective when the going got toughest and guided my work to a state that I am so proud of.

To all the BIMS and Pharmacology administrators past and present, Tammy, Deborah, Antoinette, Jack, Cierra, Nick, and Carrie. Thank you for helping me get set up to order stuff for the lab, for making sure we were all fed at seminar and journal club, and making sure I registered for my classes on time. Very little would get done on the fifth floor without help from all of you.

I was honored to be funded on the Pharmacology T32 training grant and received a F31 predoctoral fellowship from the National Heart, Lung, and Blood Institute (NHLBI). My experiments in the Bayliss lab were also supported by other grants from the NHLBI.

Table of Contents

Abstract *ii*
Acknowledgments *iv*
Table of Contents *vii*
List of Figures *ix*

Chapter 1 – Introduction **1**
1.1 – The history of central chemoreception 1
1.2 – Anatomical definition of the retrotrapezoid nucleus 2
1.3 – RTN development 5
1.4 – Phenotypic definition of the RTN 5
1.5 – Effect of RTN activity modulation on respiration 6
1.6 – Activation of RTN neurons by CO_2/H^+ in vivo 8
1.7 – Activation of RTN neurons by CO_2/H^+ in vitro 9
1.8 – Neuromodulation of the RTN 10
1.9 – Proton sensing at the RTN by TASK-2 and GPR4 11
1.9.1 – TASK-2 11
1.9.2 – GPR4 12
1.10 – Other cellular candidates for central chemoreceptors 14
1.11 – Conclusion 15
1.12 – Overview of this dissertation 16

Chapter 2 – Methods **18**
2.1 – Animal care 18
2.2 – GloSensor cAMP assay 18
2.3 – Cell surface biotinylation and western blot 19
2.4 – Immunocytochemistry 19
2.5 – Generation of $Gpr4^{HA}$, Gpr4-H167F, and Gpr4-H81F knock-in mouse models 20
2.6 – Whole body plethysmography 20
2.7 – Immunohistochemistry 21
2.8 – RNAscope in situ hybridization 21
2.9 – Cell counts and analysis 22
2.10 – Image analysis 22
2.11 – Acute slice preparation 22
2.12 – Single cell RT-qPCR 23
2.13 – In vitro neuronal electrophysiology 23
2.14 – Lentivirus production 24
2.15 – Stereotaxic injection of adeno-associated virus (AAV) or lentivirus (LV) into the RTN 24
2.16 – Blood gas analysis 24
Chapter 3 – Expression of endogenous epitope-tagged GPR4 in the mouse brain **25**
3.1 – Abstract 25

3.2 – Introduction 26
3.3 – Results 28
3.3.1 – Generation of a $Gpr4^{HA}$ knock-in mouse via CRISPR/Cas9 genome editing 28
3.3.2 – Characterization of GPR4 mRNA and protein expression in nuclei throughout the mouse brain 28
3.3.2.1 – Retrotrapezoid Nucleus (RTN) 30
3.3.2.2 – Caudal Raphe 30
3.3.2.3 – Median and Dorsal Raphe 32
3.3.2.4 – Thalamus 32
3.3.2.5 – Lateral Septum 35
3.3.3 – Characterization of GPR4 mRNA and protein expression in the brain vasculature 35
3.3.4 – Characterization of GPR4 protein expression in projections of the RTN 35
3.4 – Discussion 36

Chapter 4 – GPR4-mediated pH sensitivity is necessary for normal respiratory CO_2 sensitivity **46**
4.1 – Abstract 46
4.2 – Introduction 47
4.3 – Results 50
4.3.1 – Histidine mutations disrupt pH sensitivity of mouse GPR4 50
4.3.2 – CO_2-stimulated breathing is blunted in GPR4(H81F) knock-in mice 50
4.3.3 – CO_2 sensitivity of RTN neurons is reduced in GPR4(H81F) knock-in mice 53
4.3.4 – The GPR4(H81F) substitution reduces pH sensitivity of RTN neurons in vitro 55
4.3.5 – CO_2 stimulated breathing and CO_2 sensitivity of RTN neurons is reduced in GPR4(H167F) mice 58
4.3.6 – Concurrent knockout of TASK-2 in addition to H81F mutation of GPR4 has no additive effect to blunt CO_2 sensitivity or activation of RTN neurons 63
4.3.7 – Blood chemistry is unaffected in GPR4(H81F) and GPR4(H167F) mice 64
4.4 – Discussion 70

Chapter 5 – Conclusions and future directions **73**

Publications arising from this work **76**

Appendix – Mutation of internal and external pH-sensitive residues in TASK-2 77

List of Figures

Figure 1.1: Known inputs and outputs, and molecular identity of RTN neurons.

Figure 3.1: Incorporating an HA epitope tag into GPR4 does not alter receptor function *in vitro* or the hypercapnic ventilatory reflex *in vivo*. 27

Figure 3.2: GPR4 transcript and protein expression in the retrotrapezoid nucleus (RTN). 29

Figure 3.3: GPR4 transcript and protein expression in the caudal raphe. 31

Figure 3.4: Location and proportion of serotonergic caudal raphe neurons that express GPR4. 33

Figure 3.5: GPR4 transcript and protein expression in the dorsal and median raphe. 34

Figure 3.6: *Gpr4* transcript expression in multiple nuclei of the thalamus. 37

Figure 3.7: GPR4 protein expression in the thalamus. 38

Figure 3.8: GPR4 transcript and protein expression in the geniculate nucleus. 39

Figure 3.9: GPR4 transcript and protein expression in the lateral septum. 40

Figure 3.10: GPR4 transcript, but not protein, is detectable in brain endothelial cells. 42

Figure 3.11: GPR4 is evident in the processes of Nmb-expressing RTN neurons but undetectable at terminals in the preBötC or lPBN. 44

Figure 4.1: His-mutated GPR4 constructs are expressed on the cell surface and show blunted pH-dependent cAMP accumulation. 49

Figure 4.2: Mutation of a pH sensing residue (His81) in GPR4 blunts CO_2-stimulated breathing in mice**.** 51

Figure 4.3: Oxygen-modulated breathing is unaltered in GPR4(H81F) mice 52

Figure 4.4: CO_2-stimulated RTN neuron activation *in vivo* is blunted in GPR4(H81F) mice. 54

Figure 4.5: The RTN is intact in GPR4(H81F) mice, with equal numbers of *Nmb*-, *Gpr4*-, or *Kcnk5*-expressing RTN neurons. 56

Figure 4.6: Fos protein expression after CO_2 challenge is decreased in Phox2b+ neurons of GPR4(H81F) mice**.** 56

Figure 4.7: A subset of RTN neurons from GPR4(H81F) mice lack pH sensitivity in acute slices. 59

Figure 4.8: H81F mutation affects distribution of pH sensitive cell number and pH_{50} without grossly affecting input resistance or excitability. 60

Figure 4.9: Expression levels of key molecular markers are not different in RTN neurons from GPR4 WT and GPR4(H81F) mice**.** 61

Figure 4.10: Mutation of a pH sensing residue (His167) in GPR4 blunts CO_2-stimulated breathing and CO_2-evoked RTN neuron activation in mice. 62

Figure 4.11: Oxygen modulated breathing is unaltered in GPR4(H167F) mice. 65

Figure 4.12: H167F animals have decreased activation of *Gpr4* expressing RTN neurons in response to CO_2 challenge without alterations in total number of *Gpr4*+, *Kcnk5*+, or *Nmb*+ cells. 66

Table 4.1: Arterial blood gas chemistry from H81F, H81F-Jx, H167F, and H81-TASK2 lines. 67

Figure 4.13: Concurrent deletion of TASK-2 in addition to GPR4(H81F) knock-in does not affect magnitude of HCVR decrease but may further attenuate RTN neuron activation compared to GPR4(H81F) knock-in. 68

Figure 4.14: Oxygen modulated breathing is unaltered in GPR4(H81F)-TASK2 mice. 69

Chapter 1 – Introduction

The following text is adapted from my published review entitled: Criteria for central respiratory chemoreceptors: experimental evidence supporting candidate cell groups.[1]

1.1 – An abbreviated history of central chemoreception

The respiratory control system is responsible for homeostatic regulation of blood gases and rapid control of tissue pH, with dedicated sensors to detect the principal regulated variables, O_2 and CO_2/H^+, and drive the appropriate ventilatory responses. It has long been known that O_2 sensing is mediated primarily by the carotid bodies, with Corneille Heymans winning the Nobel Prize in 1938 for this discovery; the molecular mechanisms by which carotid glomus cells sense hypoxia remains an area of active investigation.[2–4] It has also been long known that detection of CO_2/H^+ takes place mainly in the brainstem. However, in this case the cellular identity of the relevant chemosensors has remained elusive, and thus the cellular and molecular mechanisms for CO_2/H^+ detection have been less clear.

The hunt for central chemoreceptors has been active for more than a century, at least since the description of the hypercapnic ventilatory reflex (HCVR) by Haldane and Priestly in 1905.[5] Subsequent research pointed to the brainstem as the most likely site for the cells controlling the chemoreflex, and various inventive approaches have been used to examine CO_2/H^+ sensitivity in various brainstem regions and link the putatively chemosensitive cells in those regions to breathing regulation. Historically, these approaches have included: determining in vivo activation of cells by CO_2, often via proxy measures such as Fos expression; identifying CO_2/H^+ sensitive cells, mostly using various in vitro preparations; measuring effects of focal acidification on breathing in vivo; and examining effects of localized, but relatively non-specific, chemotoxic lesions on respiration and the HCVR.[6] Since then, there have been staggering technological advances that have allowed precise phenotypic characterization and genetic access to distinct cell

types, cell-specific manipulation of activity using novel optogenetic and chemogenetic tools, and molecular identification of putative substrates for CO_2/H^+ detectors.

1.2 – Definition of the retrotrapezoid nucleus

The retrotrapezoid nucleus (RTN) was first identified as a group of cells near the ventral surface of the rostral medulla, inferior to the facial motor nucleus and posterior to the trapezoid bodies, that project to the dorsal respiratory group (DRG) and ventral respiratory group (VRG) in the brainstem.[7–10] The anatomical location of these RTN neurons coincided well with an acid-sensitive region of the rostral ventral medullary surface first identified in 1963,[11] prompting an early and prescient speculation that RTN neurons might be the relevant anatomical substrate for these respiratory chemoreceptors.[10] It is now known that RTN neurons project to various respiratory-related regions, including the preBötzinger complex (preBötC), nucleus of the solitary tract (NTS), Kolliker Fuse (KF), and the lateral parabrachial nucleus (lPBN).[9] This region also receives diverse neurochemical inputs from the NTS, the medullary and dorsal raphe nuclei, KF, A5, and the lPBN (fig. 1A, B).[9,12] As mentioned, the RTN appellation was originally applied to cells in the parafacial region that project to the DRG and VRG. The RTN name has been used by some groups to reference the parafacial region more generally, including all the various cells located therein. We choose a more restrictive definition, to respect both the initial hodological definition of RTN neurons and to acknowledge the subsequent characterization of those cells based on developmental lineage and molecular phenotype that has allowed further refinement of their key defining features.

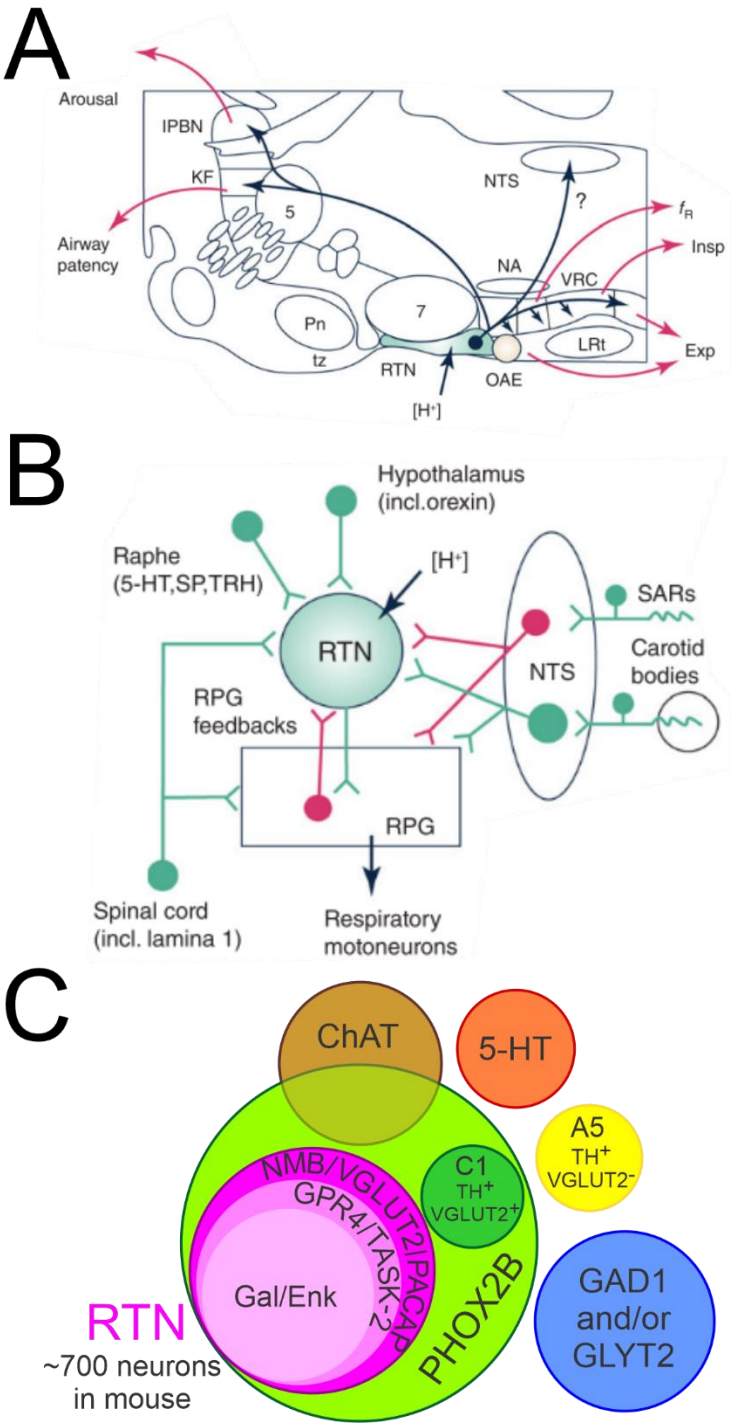
A
Arousal
IPBN
KF
Airway patency
5
NTS
?
f_R
Insp
NA
VRC
7
Pn
tz
RTN
LRt
Exp
OAE
[H+]
B
Hypothalamus (incl.orexin)
Raphe (5-HT,SP,TRH)
[H+]
SARs
RTN
NTS
Carotid bodies
RPG feedbacks
RPG
Spinal cord (incl. lamina 1)
Respiratory motoneurons
C
ChAT
5-HT
A5
TH+
VGLUT2-
C1
TH+
VGLUT2+
NMB/VGLUT2/PACAP
GPR4/TASK-2
Gal/Enk
PHOX2B
GAD1 and/or GLYT2
RTN
~700 neurons in mouse

Figure 1.1: Known inputs and outputs, and molecular identity of RTN neurons.

(A) Sagittal brainstem schematic showing location of the RTN (green) with key projections highlighted in blue; abbreviations: lateral parabrachial nuclei (lPBN), Kölliker-Fuse (KF), nucleus of the solitary tract (NTS), spinal trigeminal motor nucleus (5), nucleus ambiguus (NA), ventral respiratory column (VRC) containing from rostral to caudal the Bötzinger, preBötzinger (preBötC), and the rostral and caudal divisions of the ventral respiratory group (rVRG/cVRG), pontine nuclei (Pn), facial motor nucleus (7), trapezoid body (tz), retrotrapezoid nucleus (RTN), oscillator for active expiration (OAE), lateral reticular nucleus (LRt).

(B) Model of RTN highlighting different respiratory related inputs and output to the respiratory pattern generator (RPG, including the preBötC), abbreviations: 5-hydroxytryptophan (5-HT, serotonin), substance P (SP), thyrotrophin releasing hormone (TRH), stretch activated receptors (SARs).

(C) Current molecular definition of RTN neurons; abbreviations: choline acetyltransferase (ChAT), glutamate dehydroxylase (GAD), glycine transporter 2 (GLYT2), tyrosine hydroxylase (TH), Neuromedin B (NMB), vesicular glutamate transporter (VGLUT2), pituitary adenylate cyclase activating peptide (PACAP), G-protein coupled receptor 4 (GPR4), TWIK-related acid sensitive channel 2 (TASK-2), galanin (Gal), enkephalin (Enk). Panels A and B adapted from [13], figure 2; panel C adapted from [14], figure 12.

1.3 – RTN development

RTN neurons share a common lineage, emerging from the dB2 domain of rhombomere 5 and expressing transcription factors Egr2, Phox2b, Lbx1, and Atoh1 at various times during early development as they differentiate and migrate to their ultimate destination in the rostral ventrolateral medulla.[15] The intersectional combination of Phox2b and Atoh1 expression selectively identifies just two cell groups in the mouse brainstem: the peri-facial (periVII) neurons comprising the RTN, and a second peri-trigeminal (periV) cell population that controls lapping behavior in mice.[16–19] Of the transcription factors associated with RTN development, only Phox2b expression persists at appreciable levels in postnatal RTN neurons; however, Phox2b is also found in other neurons, including the nearby C1 adrenergic neurons and facial motoneurons.[20]

1.4 – Phenotypic definition of the RTN

Additional work using immunochemical and single cell molecular approaches has produced a more precise and limited phenotypic definition for RTN neurons (fig. 1C).[14,21] In addition to Phox2b expression, all RTN neurons express *Slc17a6* (VGlut2); they can be differentiated from other nearby Phox2b-expressing populations, like C1 neurons and motoneurons, by the absence of tyrosine hydroxylase (TH) and choline acetyltransferase (ChAT) expression.[20,22] All RTN neurons express the excitatory neuropeptide PACAP (pituitary adenylate cyclase activating peptide), and subsets also express variable levels of the inhibitory neuropeptides enkephalin and galanin, but these are not specific for the RTN.[18,19,21] Of particular note, RTN neurons can be most definitively identified in this region of the rostroventrolateral medulla by their unique and universal expression of the neuropeptide, Neuromedin B (NMB).[14,20] NMB-positive RTN neurons express a variety of receptors for other neuromodulators, including serotonin (primarily 5-HT2C), substance P (NK1R), orexin (Hcrt1/Hcrt2), and ATP (P2Y12).[22] Finally, the majority of RTN neurons (>80%) express transcripts for two putative pH sensors, the proton activated G-protein

coupled receptor GPR4, and the proton inactivated K_{2P} background K^+ channel TASK-2 (encoded by *Kcnk5*);[14] as discussed below, both GPR4 and TASK-2 have been implicated in mediating pH sensitivity of RTN neurons. Coming full circle, the NMB^+ cells project to multiple pontine and medullary respiratory regions, including to the DRG and VRG that served as the original defining hodological feature of the RTN.[23] For these reasons, we now use this constellation of specific features to define these neurons within the parafacial region as the RTN.

It is also worth noting that RTN neurons fire action potentials in a steady pacemaker-like pattern both in vitro as well as in vivo, when other respiratory-related inputs are eliminated.[24–26] The ionic basis for this tonic firing involves a background Na^+ current, carried by NALCN, and a Ca^{2+}-activated cationic current with TRPM4-like properties (fig. 2F).[27,28] These channels contribute to cell excitability, basal activity, and the firing responses to neuromodulators and H^+; however, neither is directly responsible for intrinsic CO_2/H^+ sensing by RTN neurons.[27,28] Nevertheless, the HCVR is significantly blunted in vivo after either shRNA-mediated knockdown of NALCN, or pharmacological inhibition of TRPM4 in the RTN.[27,28] These examples provide a cautionary note: they illustrate how cellular and molecular manipulations that affect general cell function and excitability can modulate the HCVR, even when the targets are not responsible for intrinsic CO_2/H^+ sensitivity (i.e., when they are not "sensors.")

1.5 – Effect of modulating RTN activity on respiration

Several different methods have been used to obtain activation and inhibition of RTN neurons, and these manipulations in turn activate or inhibit respiration in both conscious and anesthetized animals. Inhibition (acute) or ablation (chronic) of the RTN also blunts/abolishes the HCVR, both in vivo and ex vivo. The RTN region is crucial for maintaining normal respiration. Acute ablation (via local kainic acid injection or

electrolysis) decreases phrenic nerve activity, often to the point of apnea,[29,30] and this nontargeted disruption of the RTN region is also sufficient to abolish the HCVR.[30] Selective developmental elimination of the RTN has been achieved using various mouse genetic models (e.g., by Atoh1 deletion in Phox2b cells, inactivation of Phox2b in Atoh1 cells, expression of Phox2b polyalanine expansion or Lbx1 frameshift mutations); this physical deletion of the RTN in turn leads to disrupted baseline breathing in embryos and neonates, and severely blunts CO_2-evoked breathing stimulation at birth. [18,31–36] Moreover, selective intersectional deletion of VGlut2 from Phox2b-Atoh1 neurons reduces baseline ventilation and eliminates the HCVR in P0 mouse pups. Likewise, essentially complete ablation of the RTN in adults (~90-95% loss of Nmb^+ neurons), either by targeted bilateral injection of saporin-conjugated substance P in rats or viral-mediated Cre-dependent expression of caspase in Nmb-Cre mice, reduces baseline breathing (partially compensated by carotid body input) and nearly completely abolishes the HCVR.[23,37,38]

Transient activation of RTN neurons via photoactivation of channelrhodopsin 2 (ChR2) expressed in RTN neurons under the control of a Phox2b-responsive promotor (PRSx8) increases minute ventilation through effects on both tidal volume and frequency and occludes further activation by CO_2. These effects are observed in both conscious and anesthetized animals, and ChR2-mediated increases in minute ventilation (V_E) depend on glutamatergic transmission from the RTN.[39–43] Conversely, acute inhibition of Phox2b- or Nmb-expressing neurons in the RTN with the inhibitory opsin, ArchT, transiently decreases V_E in room air, and silences CO_2-stimulated RTN neuronal activity and V_E.[23,42] Similarly, inhibition of the RTN with an inhibitory GPCR (*Drosophila* allatostatin receptor) blunts phrenic nerve discharge intensity and frequency at baseline as well as during an acute hypercapnic challenge in an ex vivo brainstem-spinal cord preparation.[32]

1.6 – Activation of RTN neurons by CO_2/H^+ in vivo

Neurons in the RTN anatomical region, as well as the molecularly defined Phox2b$^+$/NMB$^+$ cells, express high levels of the neuronal activity marker Fos after acute hypercapnic challenge.[14,44–47] Direct electrophysiological assessments by extracellular recordings in anesthetized rats in vivo and in isolated brainstem-spinal cord preparations have identified neurons within the anatomical boundary of the RTN displaying "respiratory modulated" activity at baseline as well as CO_2-stimulated activity during hypercapnic challenge.[7,20,24,25,32,42,48–50] As expected for RTN neurons, the CO_2-stimulated cells are Phox2b$^+$, as demonstrated by post-hoc immunostaining of the juxtacellularly-labeled recorded neurons.[20] The CO_2-modulated RTN cell firing activity occurs in the absence of feedback from the central pattern generator, i.e., it initiates at a CO_2 threshold lower than required for phrenic nerve activity and persists after carotid body denervation, glutamate receptor blockade, or pharmacologic silencing of the respiratory central pattern generator.[24,25]

It is important to point out that these in vivo electrophysiological recordings were obtained in anesthetized animals, and because anesthetics can exert complex direct and indirect effects on RTN neurons and other respiratory nuclei,[51] this leaves open the possibility that the cells might respond differently if recorded in conscious animals. In this respect, indirect measures of RTN neuron function in freely behaving rats are also consistent with CO_2-modulated neuronal activity. That is, the ventilatory-depressant effects of ArchT-mediated inhibition of RTN neurons are enhanced under conditions of elevated CO_2 or lower arterial pH, implying that RTN neuronal activity and contribution to respiratory drive is similarly enhanced under those conditions.[42]. More recent work applying implanted miniscope imaging of neuronal GCaMP6f dynamics in the region containing the RTN demonstrates the presence of neurons in freely behaving mice that track inspired CO_2 via graded increases in Ca^{2+} signal, along with other CO_2-insensitive

cells. Whereas these experiments represent an advance in visualizing neuronal activity in a deep medullary structure, like the RTN, those specific chemosensitive cells were not directly targeted and the molecular identity of the recorded neurons was not confirmed. Thus, it remains unclear whether the mixed population that was imaged included the chemosensitive RTN neurons in the region (i.e., Phox2b$^+$/Nmb$^+$, with GPR4 and/or TASK-2 expression), and it seems certain that the sampling was diluted by recording from the multiple other neuronal subtypes present in the general parafacial region.[52] Future experiments using this technique will undoubtedly use currently available molecular targeting approaches to sample the behavior of specific phenotypically-defined cell populations. Overall, the available evidence provides strong support for the conclusion that RTN neuronal activity tracks with CO_2/H^+ in vivo, in both anesthetized and conscious animals, even if direct recordings of that activity in freely behaving animals still remain elusive.

1.7 – Activation of RTN neurons by CO_2/H^+ in vitro

RTN neurons are intrinsically sensitive to changes in CO_2/H^+ across a variety of in vitro preparations, including brainstem-spinal cord preparations, acute or cultured brainstem slices and, importantly, acutely dissociated neurons (fig. 2A).[26,47,53–60] During early development, a group of CO_2/H^+ sensitive, Phox2b-expressing neurons in the parafacial region display rhythmic pre-and post-inspiratory firing patterns in brainstem-spinal cord preparations; these have been called the embryonic parafacial oscillator (ePF) or, in the early postnatal period (P0-P2), the parafacial respiratory group (pFRG), and are most likely early precursors to the RTN.[18,61,62] In slightly older neonatal brainstem slice preparations (>P6), RTN neurons are tonically active at physiological pH levels, depolarize and increase action potential firing during bath acidification, and hyperpolarize and decrease firing during bath alkalization. This modulation is observed with changes in fixed acid in HEPES-based buffers and with changes in CO_2 in HCO_3^--based buffers (fig.

2B); these effects appear to track with changes in extracellular pH since RTN neuron firing is increased by hypercapnic acidosis and reduced by normocapnic alkalosis in CO_2/HCO_3^--based solutions.[24] The pH sensitivity of RTN neurons is retained in acute slices in the presence of tetrodotoxin (TTX, to block action potential-dependent transmitter release) and in low Ca^{2+}/high Mg^{2+} synaptic blockade solutions.[24] In addition, pH-dependent modulation of RTN neurons is preserved when slices are exposed to a variety of neurotransmitter receptor blockers, e.g., for glutamate (CNQX, APV), GABA (bicuculline), glycine (strychnine), ATP (suramin, reactive blue 2, PPADS, MRS2179), 5-HT (ketanserin, SB269970), and substance P (spantide, L-703606).[24,55,60] Finally, individual GFP-positive cells dissociated from the parafacial region of two distinct lines of Phox2b-GFP mice, which were verified as bona fide RTN neurons by single cell RT-PCR (i.e., $Phox2b^+$, $VGlut2^+$, TH-, ChAT-), were also found to retain their CO_2/H^+ sensitivity.[26,54,63] Together, these data make a compelling case that RTN neurons are intrinsically chemosensitive, and they also suggest a molecular basis for direct modulation of neuronal activity by CO_2/H^+.

However compelling, a caveat should be noted: respiration is exquisitely sensitive to changes in CO_2, and the effects of CO_2/H^+ on RTN firing in vitro appear to be quantitatively less robust than those effects in vivo, even in anesthetized animals.[25] Thus, whereas direct actions of CO_2/H^+ on RTN excitability seem certain, this does not preclude additional indirect effects by modulators that enhance baseline excitability or convey information regarding CO_2/H^+ changes that are sensed remotely.

1.8 – Neuromodulation of the RTN

Multiple neurotransmitters, including those that arise from alternative candidate chemoreceptor cells, are known to affect RTN neuronal excitability and may thereby also modulate the firing response to CO_2/H^+.[64] This includes serotonin and substance P (from raphe neurons),[60] orexin (from the lateral hypothalamus),[65] and ATP (from local astrocytes).[55,66,67] In the case of 5-HT and ATP it has been suggested that these modulators

are themselves responsible for conferring an apparent pH sensitivity onto RTN neurons that instead originates from CO_2/H^+ sensitive raphe neurons and/or astrocytes.[54,66] However, the evidence for such an obligatory role of 5-HT and ATP is inconclusive. For example, ketanserin (5-HTR_2 antagonist) or SB269970 (5-HTR_7 antagonist) can block RTN activation by exogenous 5-HT in vitro,[54,60] but these same blockers are reported in different in vitro preparations to either have no effect or abrogate the CO_2/H^+ sensitivity of RTN neurons.[54,60] In vivo, direct injection of SB269970 into the RTN of conscious mice blocked respiratory stimulation by a co-injected 5-HT_7 agonist but did not alter CO_2-stimulated breathing.[68] Similarly inconsistent results have been obtained with purinergic P2X/Y receptor antagonists (i.e., with suramin, PPADS, MRS2179, reactive blue 2), which have variably been shown to dampen[56,66] or to have no effect on [24,55,60,69] CO_2/H^+ induced RTN neuronal activity.

1.9 – Proton sensing by TASK-2 and GPR4

Under voltage clamp, in the presence of TTX and a cocktail of blockers of fast synaptic transmission, acid-evoked depolarization of the RTN is mediated by inhibition of a pH dependent background K^+ current. Activation of RTN neurons by CO_2/H^+, as well as full expression of the HCVR, requires the expression and activity of two pH sensitive molecules: TASK-2 and GPR4.[47,53,70] During initial studies identifying TASK-2 and GPR4 as the presumed pH sensors in the RTN, the genetic elimination of TASK-2 and GPR4 was global and did not disrupt the pH sensing mechanism, per se. Nonetheless, combined TASK-2/GPR4 knockout eliminates the HCVR nearly completely in conscious animals, consistent with a particularly prominent role for RTN neurons and these molecular pH sensors.

1.9.1 – TASK-2

TASK-2 is a background K^+ channel expressed in RTN neurons and in a limited number of additional brainstem cell groups.[70] It shows highest sequence similarity to

the TWIK-related alkaline-activated (TALK) subgroup of K_{2P} channels compared to the similarly named, and also pH sensitive, TASK-1 and TASK-3 channels.[71] Inhibitory gating of TASK-2 occurs through the physiological pH range and is mediated via independent intracellular and extracellular pH sensor domains, each with a pH_{50}~8.0.[71–75] Inhibition of TASK-2 by acidification leads to membrane depolarization and increased cell excitability. It has not been directly tested whether changes in internal and/or external pH changes account for TASK-2-mediated activation of RTN neurons although, as mentioned above, experimental manipulation of CO_2 and HCO_3^- levels in bath solutions suggest a primary role for extracellular pH. Whereas nearly all GFP-expressing RTN neurons with wild-type TASK-2 alleles are pH-sensitive in brain slices from Phox2b-GFP mice (~95%), only 56% of those GFP^+ RTN neurons are pH-sensitive in TASK-2 deleted mice; the pH-sensitive background K^+ current is reduced in pH-sensitive cells from these TASK-2 global knockout mice, and eliminated in ~44% of cells that emerged as pH-insensitive after TASK-2 deletion.[53] In TASK-2 global knockout mice, the stimulation of breathing by CO_2 is strongly reduced (by ~60% at 8% CO_2) while baseline respiration is unaffected.[47,53,70] Note that TASK-2 global knockout mice present with a slight metabolic acidosis (ΔpH: -0.03),[76] and it is possible that this could have influenced the HCVR. However, the HCVR is unaffected when a more severe metabolic acidosis is induced chronically in mice by NBCe1 deletion from the kidney (ΔpH: -0.2),[77] or acutely in human subjects by treatment with carbonic anhydrase inhibitors (ΔpH: -0.1).[78,79]

1.9.2 – GPR4

GPR4 is a proton sensing GPCR expressed in RTN neurons;[47,80] it senses extracellular proton concentration via protonation/deprotonation of multiple histidine residues on its outward facing surface.[81–83] Depending on the expression

system it can couple to Ga_s- and Ga_q-mediated signaling pathways with a pH_{50} of 7.2-7.6.[47,80–84] In addition to the RTN, GPR4 transcript is also detectable in a limited number of brain nuclei, including the caudal and dorsal raphe nuclei, the lateral septum, and C1, as well as in endothelial cells.[14,47,80] The localization of GPR4 protein in these regions is reported for the first time in this dissertation (Chapter 3).

In the acute slice, treatment with a GPR4 antagonist (Dalton M46)[72], or whole-body knockout of GPR4, alters the ratio of pH-sensitive to pH-insensitive RTN neurons, with the appearance of a pH-insensitive population that accounts for ~40% of the recorded cells (fig. 2D).[47] The remaining pH-responsive population of RTN neurons are presumably those that have intact TASK-2-mediated pH sensitivity. CO_2-dependent activation of RTN neurons in vivo (Fos expression) is also reduced in GPR4 global knockout mice while activation of caudal raphe neurons (pallidus, obscurus, magnus, and parapyramidal) is unaffected by GPR4 deletion.[47] Administration of the GPR4 antagonist NE 52-QQ57 to mice and rats via an intraperitoneal (i.p.) bolus injection (20 mg/kg) blunts the HCVR by a small, but significant, amount in conscious animals.[80] It is unknown what concentration NE 52-QQ57 reaches at the relevant GPR4-expressing populations after systemic administration so this inhibition may represent only a small fraction of receptor antagonism in vivo. Localized application of NE 52-QQ57 on the ventral surface of the medulla had no effect on the HCVR in anesthetized animals but it is not clear whether the compound reached efficacious levels for GPR4 inhibition at the RTN.[80] Importantly, genetic elimination of GPR4 reduced the HCVR (by ~60% at 8% CO_2) and selective re-expression of GPR4 in the RTN alone restores CO_2-induced Fos expression in RTN neurons and rescues the respiratory defects observed in GPR4 global knockout animals.[47] This indicates that expression of GPR4, specifically in RTN neurons, may be especially crucial for both RTN neuronal activation and the HCVR. Notably, simultaneous global deletion of both

GPR4 and TASK-2 in mice nearly completely abolishes the HCVR (by ~90% in 8% CO_2) (fig. 2E),[47] approximating the deficit in HCVR observed with gross ablation of RTN neurons.[23,37,38] The effect of RTN-specific deletion of either proton sensor on baseline respiration or the HCVR has not yet been reported.

1.10 – Other cellular central chemoreceptor candidates

The other chemoreceptor candidates that have accrued the most experimental support are the serotonergic raphe neurons and ventral medullary surface astrocytes. I have reviewed other neuronal candidates that have central chemoreceptor characteristics, but they remain largely uncharacterized and will not be further discussed in this dissertation.[1] For raphe neurons, elegant intersectional approaches have revealed remarkable molecular and functional diversity within the serotonergic system.[85–88] Activation of serotonergic (ePet$^+$) neurons in the raphe obscurus increases respiratory output and a subset of raphe neurons (dorsal and caudal) were found to display CO_2 modulated firing activity.[89–91] Based on work using intersectional genetics and molecular manipulation of distinct raphe populations, attention has focused specifically on the Egr2-Pet1 subset of caudal raphe neurons as potential respiratory chemoreceptors.[92,93] These particular neurons are directly CO_2/H^+ sensitive in vitro, an observation not yet verified in vivo, and inhibition of this subset of serotonergic cells blunts the HCVR.[94] It is unknown whether stimulation of this subset, specifically, can modulate respiratory activity or the central chemoreflex. To date, TASK-1/TASK-3 channels are the only molecularly identified pH sensors in serotonergic raphe neurons, but genetic deletion of those TASK channels has no effect on the HCVR in mice.[95–101] Raphe neurons across all subdivisions also express GPR4 but whole body deletion has no effect on CO_2 mediated activation of the raphe by Fos expression. Moreover, specific re-expression of GPR4 in the RTN–is sufficient to rescue the HCVR in GPR4 knockout mice.[47] The lack of molecular candidates for mediating the direct pH sensitivity of these Egr2-Pet1 neurons precludes analysis of

the molecular mechanisms of pH sensing in the presumed central chemoreceptor cells in the raphe.

There is abundant evidence from ex vivo and in vivo preparations showing that increases in CO_2/H^+ can drive calcium signaling in astrocytes and provoke release of ATP in multiple regions associated with respiratory chemosensitivity, at least in part from astrocytes.[66,67,102,103] Optogenetic activation of VMS astrocytes at the RTN evokes ATP release and stimulates local RTN neurons and respiration via a P2Y receptor mechanism;[66,67] conversely, inhibition of gliotransmitter release and ATP signaling in preBötC neurons blunts the HCVR, along with various other respiratory reflexes.[104–108] It remains to be clarified whether there is a specific site for astrocytic modulation of CO_2-dependent respiratory output or if astrocytic involvement in modulation of the HCVR is uniform throughout the brainstem. The molecular specializations proposed to support CO_2/H^+ sensing by astrocytes have not yet been clearly linked to the HCVR.[109–113]

1.11 – Conclusion

There has been a long-term quest to identify the brainstem sensory cells that detect changes in CO_2/H^+ and drive the respiratory circuits that adjust ventilation to correct deviations from normal physiological set points for $PaCO_2$ and tissue acid-base balance. As cellular candidates have emerged, there have been additional efforts to employ various technical advances to define those cell types with greater phenotypic clarity, seek molecular substrates for their CO_2/H^+ sensitivity, and validate their physiological role in respiratory chemosensitivity.

Our current working model holds that respiratory chemoreception and the HCVR is primarily subserved by a multicellular sensory apparatus. In particular, the RTN is both a direct CO_2/H^+ sensor and a principal integrative center. As such, it transduces local environmental variations in CO_2/H^+ and neuromodulatory input from the other presumptive chemosensory cell groups for onward transmission to the respiratory rhythm

and pattern generator circuits. These inputs modulate the excitability of RTN neurons, increasing their CO_2/H^+ sensitivity and input-output gain. To the extent that those other cell groups encode CO_2/H^+ in vivo, their inputs may confer a secondary CO_2/H^+ signal to RTN neurons while imparting their own chemosensitivity onto other elements of the respiratory control and output networks. The molecular mediators for CO_2/H^+ sensation at the RTN have been proposed and the necessity of TASK-2 and GPR4 expression for a normal HCVR has been robustly demonstrated. It nonetheless remains a formal possibility that TASK-2 and GPR4 are only necessary to maintain excitability of RTN neurons and that pH sensitivity is conferred to those cells through other inputs. This proposition seems unlikely as there are no deficits in baseline respiration of either GPR4 or TASK-2 knockout animals like those that occur with silencing of the RTN via chemo/optogenetic means, indicating that RTN activity remained at or above the threshold necessary to provide baseline respiratory drive in both single and double knockout animals. Importantly, the amino acid determinants of intrinsic pH sensitivity are known for both GPR4 and TASK-2, and so it should be possible to generate genetic models to test whether selective elimination of pH sensitivity, per se, is sufficient to recapitulate the observed respiratory effects of the cognate gene knockouts.

1.12 – Overview of this dissertation

In the first part of this dissertation, I determine the expression pattern of GPR4 in the mouse brain using an epitope tag knock-in strategy. I introduce a hemagglutinin (HA) epitope tag onto the C-terminal tail of GPR4 using CRISPR/Cas9 genome editing to alter the endogenous locus of *Gpr4* in the mouse genome. Using these animals, I determine that GPR4 mRNA and protein is expressed in nuclei in the fore-, mid-, and hindbrain and in neurons of multiple neurochemical identities (GABAergic, cholinergic, glutamatergic, serotonergic). These results are contained in Chapter 3 of this dissertation and are

published in a paper entitled “Expression of endogenous epitope-tagged GPR4 in the mouse brain” in eNeuro.[114]

In the second part of this dissertation, I aim to determine if the pH sensing capacity of GPR4, per se, is necessary for a normal hypercapnic ventilatory response. To this end, I generate mice expressing GPR4 with decreased pH sensitivity (His81Phe and His167Phe) and examine their CO_2/H^+ sensitivity at a whole animal and cellular level. I show that normal pH sensing capacity of GPR4 is necessary for a normal HCVR using whole body plethysmography and that histidine mutation of GPR4 leads to blunted CO_2 and pH activation of RTN neurons. These data are presented and discussed in Chapter 4 of this dissertation. Chapter 5 synthesizes these two projects to draw conclusions and discuss future directions around the role of GPR4 in mediating central chemosensitivity.

Chapter 2 (Methods)

2.1 – Animal Care

These studies were completed in accordance with the requirements of the Institutional Animal Care and Use Committee at the University of Virginia and were completed in an AALAC-accredited animal care facility. All efforts were made to minimize the number of animals used in these studies. Animals were group housed (3-5 animals per cage) on cob bedding with ad libitum access to food, water, and enrichment items. Cage bedding, food, and water were changed weekly. The animal housing facility was maintained on a 12-hour dark/light cycle at 22°C and humidity 50-60%. Animals were monitored daily by veterinary staff for distress or injury.

2.2 – GloSensor cAMP assay

HEK293T cells were plated in a poly-L-lysine coated white 96-well plate (Greiner Bio-One 655074) at a density of 5 x 10^4 cells per well in high glucose DMEM (Gibco 11965-092) with sodium pyruvate and 10% fetal bovine serum. Cells were allowed to incubate overnight at 37 C/5% CO_2. The following day, cells were transfected with the GloSensor - 22F cAMP plasmid (Promega E2301) and wildtype or histidine mutant GPR4 in pcDNA3.1 (final concentration 0.02 ng/µL). Constructs were mixed with Lipofectamine 2000 (ThermoFisher 11668027) and added to cells according to manufacturer instructions and allowed to incubate for 20 hours. The next day, transfection media was removed and replaced with HBSS (Gibco 14175-095) containing 2% v/v GloSensor Reagent (Promega E1290). Cells were equilibrated for 2 hours at 37C/5% CO_2. After equilibration, solution was replaced with HBSS or containing 10 uM forskolin (Sigma F3917) as a positive control and incubated for 20 min at room temperature. Luminescence was detected using a Synergy HTX multi-mode plate reader.

Antibodies

Antibody	Product Number	AB_RRID	Application(s)	Dilution
Mouse anti-myc	Cell Signaling 2276S	331783	WB/ICC	1:1000/ 1:4000
Mouse anti-tubulin	Sigma T9026	477593	WB	1:8000
Rabbit anti-CD46	LSBio LS-C331615	2940833	WB/ICC	1:1000/1:75
Sheep anti-mouse HRP	GE Health NA9310V	772193	WB	1:10000
Donkey anti-rabbit HRP	GE Health NA9340V	772191	WB	1:10000
Donkey anti-mouse Alexa488	Jackson Immuno 715-546-150	2340849	ICC, IHC	1:500
Donkey anti-rabbit Cy3	Jackson Immuno 711-166-152	2313568	ICC, IHC	1:500
Chicken anti-GFP	Aves Labs GFP-1010	2307313	IHC	1:1000
Goat anti-cFos	Santa Cruz sc-52-G	2629503	IHC	1:1000
Donkey anti-chicken Alexa488	Jackson Immuno 703-546-155	2340376	IHC	1:500
Donkey anti-goat Cy3	Jackson Immuno 705-166-147	2340413	IHC	1:500
Goat anti-ChAT	Millipore AB144P	2079751	IHC	1:200
Mouse anti-TPH	Sigma T0678	261587	IHC	1:250

Rat anti-PECAM	Synaptic Systems HS-351 117	2619721	IHC	1:500
Goat anti-PHOX2B	R&D Systems AF4940	2861427	IHC	1:100
Rabbit anti-HA (C29F4)	Cell Signaling Technologies #3724	1549585	IHC	1:2000
Rat anti-mCherry	ThermoFisher M11217	2536611	IHC	1:2000
Goat anti-CGRP	Abcam ab36001	725807	IHC	1:1000
Donkey anti-goat Alexa647	Jackson Immuno 705-606-147	2340438	IHC	1:500
Donkey anti-rat Cy3	Jackson Immuno 712-166-150	2340668	IHC	1:500
Donkey anti-rat Alexa647	Jackson Immuno 712-606-150	2340695	IHC	1:500

WB = western blot; ICC = immunocytochemistry; IHC = immunohistochemistry

2.3 – Cell surface biotinylation and western blot

HEK293T cells were grown until 80-90% confluent in poly-L-lysine coated 10 cm dishes. The day after plating, cells were transfected with wildtype or histidine mutant mouse GPR4 and Lipofectamine 2000 (ThermoFisher 11668027) according to manufacturer's instructions. Approximately 20 hours after transfection, cells were processed for a cell surface biotinylation and streptavidin pulldown. Briefly, cells were incubated with 1.1 mg/mL EZ-Link™ Sulfo-NHS-LC-Biotin (ThermoFisher 21335) in DPBS at 4C. Biotinylation was quenched with 100 mM glycine in DPBS. After DPBS washes, cells were lysed in RIPA/2% SDS containing protease inhibitor cocktail (Sigma–Aldrich P8340), 10 mM NaF, and 10 mM $NaVO_3$ using a probe sonicator. Protein concentration was measured using the Bradford assay. For each pulldown, *Strep*-Tactin Superflow Plus (Qiagen) beads were added to 1 mg total protein in lysis buffer and incubated with rocking at room temperature for 1 hour. Pulldowns and total protein samples were then incubated in 1X Laemmli buffer (62.5% glycerol, 12.5% SDS, 0.5% bromophenol blue, 25% fresh 2-mercaptoenthanol in 30 mM Tris-HCl, pH 6.8) for 30 min at 37C before running SDS-PAGE. After separation, protein was transferred to 0.45 um nitrocellulose membrane and blocked with 5% dry milk in TBST (10 mM Tris, 150 mM NaCl, and 0.1% Tween 20, pH 7.4). After blocking, membranes were incubated in primary antibody overnight at 4C. Amersham ECL horseradish peroxidase (HRP)-linked secondary antibodies (GE Healthcare; anti-Rabbit IgG: NA9340V or anti-Mouse IgG: NA931V; 1:10,000) and Western Lightning Plus ECL were used to visualize immunoreactive signals on Amersham Hyperfilm ECL (GE Healthcare).

2.4 – Immunocytochemistry

HEK293T cells were plated onto poly-L-lysine coated 12 mm glass coverslips in a 24 well plate. Cells were transfected with wildtype or histidine mutant mouse GPR4 and Lipofectamine 2000 (ThermoFisher) according to manufacturer's instructions. Approximately 20 hours after transfection, cell culture medium was removed and cells were washed with DPBS. Cells were then fixed with 4% paraformaldehyde. Coverslips were then permeabilized and blocked in PBS containing 10% fetal horse serum (FHS) and 0.3% TritonX100. After blocking, coverslips were incubated in primary antibody solution (PBS/0.3% TritonX100/1% FHS/1% bovine serum albumin) overnight at 4C. Coverslips were then washed with PBS/1% BSA and incubated in secondary antibody solution for 1

hour at room temperature in the dark. DAPI was added during the last minute of secondary antibody incubation to label nuclei. Coverslips were mounted using ProLong Gold antifade reagent with DAPI (Invitrogen P36935) before imaging on a Zeiss LSM 700 scanning confocal microscope.

2.5 – Generation of *Gpr4*^{HA}, *Gpr4*-H167F, and *Gpr4*-H81F knock-in mouse models

The CRISPR-assisted genome editing technology was used to generate the *Gpr4*^{HA}, *Gpr4*-H167F, and *Gpr4*-H81F knock-in mice. sgRNAs were selected based on a search via the CRISPR guide design algorithm CRISPOR (http://crispor.tefor.net/). The HA tag (YPYDVPDYA-STOP, TATCCATACGACGTTCCAGATTACGCTTAG) preceded by a Gly-Ser-Ser-Gly (GGATCCTCAGGT) linker was introduced onto the C-terminal sequence of the wild-type (WT) *Gpr4* gene to generate the *Gpr4*-HA donor (199mer ssODN, sequence below). The H167F (CAC>TTC) or H81F (CAC>TTT) point mutation was introduced into the wild-type (WT) *Gpr4* gene to generate *Gpr4*-H167F or *Gpr4*-H81F repair template (sequences below). crRNA, tracrRNA, Cas9, and ssODN were purchased from IDT (Coralville, Iowa). crRNA and tracrRNA were diluted to 200uM in RNase-free microinjection buffer (10mM of Tris-HCl, pH 7.4, 0.25mM of EDTA). 3 ul crRNA and 3 ul tracrRNA were mixed and annealed in a thermocycler by heating the mixture to 95^{o}C for 5 minutes and ramped down to 25^{o}C at 5^{o}C/min. Ribonucleic protein (RNP) complex was formed by mixing and incubating Cas9 at 0.2 ug/ul with crRNA/tracrRNA at 3uM in RNase-free microinjection buffer at 37^{o}C for 10 minutes. ssODN containing the desired amino acid substitution was added at a concentration of 0.3 ug/ul. The fertilized eggs were collected from B6SJLF1 females mated with the males (The Jackson Laboratory, Bar Harbor, Maine). The RNP/ssODN were co-delivered into the fertilized eggs by electroporation with a NEPA21 super electroporator (Nepa Gene Co., Ltd. Chiba, Japan) under the following conditions: 2 pulses at 40 V for 3 msec with 50 msec interval for poring phase; 2 pulses at 7 V for 50 msec with 50 msec interval for transferring phase. The zapped zygotes were cultured overnight in KSOM medium (EMD Millipore, Billerica, MA) at 37^{o}C in 5% CO2. The next morning, zygotes that had reached the two-cell stage were implanted into the oviducts of pseudopregnant foster mothers of ICR strain (Envigo, Indianapolis, IN). Pups born to the foster mothers were screened using tail snip DNA by PCR genotyping followed by Sanger's sequencing, with analysis of the knock-in performed using the Synthego Inference of CRISPR Edits (ICE) Analysis tool (https://ice.synthego.com). Germline transmission of the desired alleles was confirmed by breeding the founders with wildtype C57BL/6 mice (The Jackson Laboratory, Bar Harbor, Maine).

Gpr4-H81F sgRNA: GGCCGTGGATCCAGTTGTCATGG

Gpr4-H81F ssODN sequence:
GTCTACCTGATGAACTTGAGCATTGCAGACCTGCTGTACATCTGCACTTTGCCGCTGTG
GGTCGACTACTTCCTCTTTCATGACAACTGGATTCACGGCCCTGGCTCCTGCAAGCTCT
TTGGCTTCATCTTCTACAGCAACATCTATATCAGC

Gpr4-H167F sgRNA: GATCACGAAACAGCTCATCATGG

Gpr4-H167F ssODN sequence:
CAGCAGTGGCTGTGAGCTCTGTGGTCTGGGCCACGGAGCTGGGCGCCAATTCAGCACC
GCTCTTTCATGATGAGCTCTTTCGTGATCGCTACAACTTCACCTTCTGCTTTGAGAAGTT
CCCCATGGAGCGTTGGGTGGCCTGGATGAATCTGTACCGCGTCTTTGTGGGCTTC

Gpr4^{HA} sgRNA: CATGGGGCTCACTGTGCCGGGGG

Gpr4^{HA} ssODN sequence:
CGTCCGGGGCTGTCTGGGCAGTGCCTCCGACTGCCCAGGGGGACCAGGTGCCACTGAA
GGTGCTGCTGCCCCCGGCACAGGGATCCTCAGGTTATCCATACGACGTTCCAGATTACG
CTTAGGCCCCATGCCCAACTGTCATCCTGCACCCTTCCGGTTGTATGCAAATGTGTGTA
AATATGTCCATGTGAATTACAAG

2.6 – Whole body plethysmography
Ventilatory responses were measured in conscious, freely moving mice by whole body plethysmography in chambers manufactured by Data Sciences International and recorded with IOX software (EMKA Technologies, Falls Church VA). A mass flow regulator provided quiet, constant and smooth flow through the animal chamber (0.5 L/min). Mice were familiarized with the plethysmography chamber the day prior to testing (3-4 hour acclimation period), and again immediately before the testing protocol (for at least 2 hrs). The typical protocol entailed three sequential incrementing CO_2 challenges (7 min. exposures to 2%, 4%, 6%, 8% CO2, balance O2; each separated by 5 min. of 100% O2). Hypercapnic exposure was performed in hyperoxia to minimize contributions of peripheral chemoreceptors to the hypercapnic ventilatory reflex and attribute ventilatory effects to central chemoreception. CO_2 tension in the chambers was verified with a capnograph. Animals were also exposed to normoxic (21% O_2, balance N_2) and hypoxic (10% O_2, balance N_2) gas mixtures. After data collection, Poincare analysis of the breathing frequency over the final 3 minutes of each challenge period (CO_2, normoxia, or hypoxia) was performed to select periods of regular, calm breathing for analysis. Experimenter analyzing plethysmography data was blinded to mouse genotype. For cFos-based analysis of CO2-activated neurons *in vivo*, we habituated adult mice (60-100 days old) to the plethysmography chamber for 4-6 hrs on the day before the experiment, and again for 2 hrs prior to the protocol. Mice were then exposed to the CO_2 stimulus (12% CO_2/60% O_2/28% N_2) for 45 minutes. CO_2 exposure was followed by 45 minutes of hyperoxia before perfusion. Immediately following the exposure, mice were anesthetized and perfused transcardially with fixative within 10 min of anesthesia.

2.7 – Immunohistochemistry
Mice were anesthetized with ketamine/xylazine (200mg/14mg/kg, i.p.), perfusion-fixed (4%PFA/0.1M PB) tissue (30 μm sections, 1:3 serial) was prepared as previously described (Fortuna et al 2009). Sections were stored at -20 C in cryoprotectant solution consisting of the following: 0.05 M sodium phosphate buffer (PB), 30% ethylene glycol, 20% glycerol. All primary and secondary antibodies used in this study are listed in Reagents section. Upon removal from cryoprotectant solution, sections were washed in 0.1 M PB then Tris saline. Sections were blocked in TS containing 0.3% TritonX100 and 10% FHS at room temperature. Sections were then incubated in primary antibody solution (TS/0.1% TritonX100/1% FHS) overnight at 4C with gentle rocking. After primary antibody incubation, sections were washed in TS before incubation for 90 minutes at room temperature in secondary antibody solution (TS). DAPI solution was added during the last minute of secondary antibody incubation period. Sections were mounted on Superfrost Plus glass slides (Fisher Scientific 12-550-15) sealed with ProLong Gold antifade reagent with DAPI (Invitrogen P36935) before imaging on a Zeiss Axioimager Z1 widefield epifluorescence microscope or a Zeiss LSM700 scanning confocal microscope.

2.8 – RNAscope *in situ* hybridization

Gpr4, *Fos*, *Kcnk5*, and *Nmb* transcripts were detected using the RNAscope platform (Advanced Cell Diagnostics, ACD). Following tissue fixation and sectioning, tissue sections were mounted on Superfrost Plus slides and allowed to air dry overnight. Sections were washed twice in sterile water before 30 minute incubation in RNAscope Protease IV solution (ACD, 322336) at 40 C. After protease treatment, slides were washed in sterile water and then incubated with probes listed (Table 2) for 2 hours at 40C. Following probe incubation, sections were processed according to manufacturer instructions for the Fluorescent Multiplex Detection Reagent Kit v1 (ACD 320851). After processing, sections were allowed to dry before slides were sealed with ProLong Gold antifade reagent with DAPI (Invitrogen P36935) before imaging on a Zeiss Axioimager Z1 widefield epifluorescence microscope.

Probe Target	ACDBio Catalog Number
Gpr4	427941
Nmb	459931-C2
Kcnk5	427951-C3
Slc17a6	319171-C2
Fos	316921-C3
Tph2	318691-C2
Slc32a1	319191-C3
Pecam1	316721-C2

2.9 – Cell counts and analysis

Serial sections (1:3 series) through the rostrocaudal extent of the RTN were analyzed during all IHC experiments, and images were acquired using an epifluorescence microscope (Zeiss AxioImager Z1) equipped with Neurolucida software. Labeled cells were counted and aligned for averaging according to defined anatomical landmarks (Paxinos and Franklin, 2001). Tracings were exported to NeuroExplorer software (MBF Biosciences) for analysis of RTN cell number within the ventral brainstem. The text and figures present the actual number of cells counted from the 1:3 series of tissue sections, with no stereological correction factor applied (i.e., the actual number of cells would be ~3 times higher). The investigator performing cell counts and analysis was blind to mouse genotype.

2.10 – Image analysis

For both widefield and confocal images, Z-stacks were collected through the thickness of the tissue and collapsed into maximum intensity projections for image processing. Background was corrected using the MOSAIC Suite background correction tool in Fiji. Brightness and contrast were adjusted using Fiji in order to maximize signal and minimize background. Images from sections from the same brain region were adjusted by an equal amount. For certain images, adjacent frames were stitched together using the built-in stitching tool in Fiji to generate larger composites for figures.

2.11 – Acute Slice Preparation

For single neuron collection and patch clamp recordings from GPR4 wildtype and H81F mice, transverse brainstem slices were prepared as previously described (Shi et al., 2016, 2021). For neonates (P6-P12) animals were anaesthetized with ketamine and xylazine (375 mg kg−1 and 25 mg kg−1, intramuscularly); after establishing no response to firm toe pinch, the mice were rapidly decapitated, and brainstems were immediately removed and sliced in the coronal plane (300 μm) using a vibrating microslicer (DTK Zero 1; Ted Pella, Inc., Redding, CA, USA) in ice-cold, sucrose-substituted Ringer solution containing the following (in mM): 260 sucrose, 3 KCl, 5 $MgCl_2$, 1 $CaCl_2$, 1.25 NaH_2PO_4, 26 $NaHCO_3$, 10 glucose, and 1 kynurenic acid. Slices were held in normal Ringer's solution containing in mM: 130 NaCl, 3 KCl, 2 $MgCl_2$, 2 $CaCl_2$, 1.25 NaH_2PO_4, 26 $NaHCO_3$ and 10 glucose. Cutting and holding solutions were constantly bubbled with 5% CO_2/95% O_2. Adult animals (60-120 days old) were deeply anaesthetized by intraperitoneal injection of ketamine/xylazine (as above), and perfused transcardially with 25 mL of ice cold NMDG aCSF (in mM: 93 NMDG, 2.5 KCl, 1.2 NaH_2PO_4, 30 $NaHCO_3$, 20 HEPES, 25 glucose, 5 Na-ascorbate, 2 thiourea, 3 Na-pyruvate, 12 N-acetyl-L-cysteine, 10 $MgSO_4$, 0.5 $CaCl_2$, pH adjusted to 7.3-7.4 with 10N HCl). Animals were rapidly decapitated and heads were submerged in NMDG-aCSF. Brainstems were removed and sliced in the coronal plane (150 μm) with a vibrating microslicer in NMDG-aCSF. After a brief recovery period (≤ 12

minutes at 32-34C) in NMDG-aCSF, slices were held in HEPES-aCSF (in mM: 92 NaCl, 2.5 KCl, 1.2 NaH_2PO_4, 30 $NaHCO_3$, 20 HEPES, 25 glucose, 5 Na-ascorbate, 2 thiourea, 3 Na-pyruvate, 12 N-acetyl-l-cysteine, 2 $MgSO_4$, 2 $CaCl_2$, pH was adjusted to 7.3–7.4 with KOH or HCl if necessary) until use. All solutions were constantly bubbled with 5% CO_2/95% O_2.

2.12 – Single cell RT-qPCR

Individual green fluorescent protein (GFP)-labeled RTN neurons were harvested under direct vision from mouse brainstem slices (n = 176, N = 25) in a HEPES-based solution (mM): 140 NaCl, 3 KCl, 2 MgCl2, 2 CaCl2, 10 HEPES, 10 glucose, pH 7.4 at room temperature) in the recording chamber of a fluorescence microscope (Zeiss Axioimager FS, Carl Zeiss Microscopy). Neurons were targeted based on a healthy appearance (e.g. soma size and turbidity, membrane transparency, dendritic process visibility) and fluorescence intensity. A pipette loaded with a sterile HEPES-based buffer (tip diameter: ~10 μm) was advanced toward the cell, with application of gentle positive pressure to clear away nearby cellular debris and extracellular matrix (delivered by mouth, via a side port on the pipette holder with an intervening 0.22 μm sterile filter in the line). Subsequently, gentle suction was used to collect the cell, while minimizing aspiration of non-somatic cellular components. Once the cell was picked, ~1 μL of internal solution containing the cytoplasmic contents were expelled into a sterile tube containing reverse transcriptase reaction reagents (SuperScript III First-Strand, Invitrogen 18080-051). Neurons were analyzed simultaneously for expression of multiple transcripts (*Gpr4*, *Kcnt*, *Nmb*, *Slc17a6, Gapdh*) by multiplex quantitative sc-PCR (sc-qPCR) (Shi et al., 2016, 2021). We used primer sets for sc-qPCR that yielded short amplicons (Table x); the cycle threshold (Ct) levels of test transcripts were re-scaled by their average, transformed into relative quantities using the amplification efficiency, normalized to *Gapdh* (an internal reference gene; ΔCt = Ct(test) – Ct(*Gapdh*)), and expressed as $2^{-\Delta Ct}$

2.13 – In vitro neuronal electrophysiology

Cell-attached and whole cell recordings of pH sensitivity of GFP-labelled RTN neurons were performed in transverse brain slices (300 μm) prepared from neonatal GPR4 wildtype or H81F animals (P6–P12), as previously described above. Investigator performing recordings was blinded to mouse genotype throughout data collection and analysis. Slices were placed in a chamber on a fixed-stage fluorescence microscope equipped with fluorescence and infrared optics (Zeiss AxioSkop) at room temperature in HEPES-based buffer (mM): 140 NaCl, 3 KCl, 2 $MgCl_2$, 2 $CaCl_2$, 10 HEPES, 10 glucose, with pH adjusted between 7.0 and 7.8 by addition of HCl or NaOH. Patch electrodes (3–6 MΩ) for cell-attached recordings were filled with (mM): 120 KCH_3SO_3, 4 NaCl, 1 $MgCl_2$, 0.5 $CaCl_2$, 10 HEPES, 10 EGTA, 3 Mg-ATP, and 0.3 GTP-Tris (pH 7.2, adjusted with KOH). Firing activity was recorded using pCLAMP software, a Multiclamp 700A amplifier and Digidata 1440A digitizer (Molecular Devices). All recordings were made in the presence of strychnine (30 μM), bicuculline (10 μM), and 6-cyano-7 -nitroquinoxaline-2,3-dione (CNQX, 10 μM). For cell attached recordings, cells were held at -60 mV. Firing rate histograms of RTN neuronal discharge were generated by integrating action potential discharge in 10 s bins using Spike2 software (Cambridge Electronic Design) and the pH sensitivity of individual RTN neurons was assessed by linear regression analysis to obtain a pH50 value (that is, pH at which firing rate was half that obtained at pH 7.0). For whole cell current clamp recordings, cells were held at -60 mV via DC current injection before exposure to current step protocols.

2.14 – Lentivirus production

Lentiviral vectors were prepared from pWPXL targeting constructs, (Addgene plasmid 12257) containing the PRSX8 promotor (extracted from PRSx8-ChR2-mCherry (Abbott et al 2009)) to drive expression of mouse GPR4 or control constructs only in Phox2b-expressing cells (Abbott et al 2009, Hwang et al 2001). HEK293T cell expression was enabled by a CMV promoter upstream of the lentiviral cassette. To identify transduced cells, we inserted a downstream internal ribosome re-entry site (IRES) followed by mCherry (Clontech). Replication-deficient high titer lentivirus was produced by VectorBuilder. The delivered virus was resuspended in DMEM and stored at -80°C until use.

2.15 – Stereotaxic injection of adeno-associated virus (AAV) or lentivirus (LV) into the RTN

Adult (8-12 weeks) Phox2b::GFP/GPR4$^{-/-}$ mice (LV studies) or *Nmb*$^{Cre/+}$;*Gpr4*$^{HA/HA}$ mice (AAV studies) were anaesthetized with ketamine/dexmedetomidine HCl (100 mg kg–1 and 0.2 mg kg–1 , intraperitoneally), mounted in a stereotaxic apparatus and maintained at 37 °C with a servo-controlled heating pad. After craniotomy, a pipette filled with virus (VectorBuilder, diluted to around 2 × 10^9 transducing units per ml) was inserted at coordinates approximately 1.4 mm lateral to midline, 1.4 mm caudal to lambda and 5.2–5.5 mm ventral to the pial surf×ace of the cerebellum. In addition to stereotaxic coordinates, we recorded antidromic field potentials elicited by stimulating the mandibular branch of the facial nerve to locate the position of the facial motor nucleus more precisely. For bilateral injections in the RTN, the tip of the injection pipette was positioned 100 μm below the facial motor nucleus, and at 4 rostro-caudally aligned sites along the facial motor nucleus separated by 200 μm. The glass injection pipette was connected to an electronically-controlled pressure valve (Picospritzer II) and brief pressure pulses (3–6 ms) were used to inject 100–150 nl of virus at each site. After surgery, mice were treated with ketoprofen (4 mg kg–1, subcutaneously). At least 4 weeks elapsed after virus injection before mice were examined in ventilatory and histochemical assays.

2.16 – Blood gas analysis

Mice were habituated to a tail warmer and restraint apparatus (BrainTree Scientific Inc) on two occasions before blood was sampled. On the day of sampling, mice were habituated to the laboratory space for ~2 h following transportation from the vivarium and then gently restrained for at least 30 minutes before blood sampling. Arterial blood from the ventral tail artery (~100 μl) was collected from the awake mouse into a heparinized capillary tube and immediately analyzed with an iSTAT handheld analyzer (CG4+ cartridge, Heska, Fort Collins, CO).

Chapter 3: Expression of endogenous epitope-tagged GPR4 in the mouse brain

3.1 – Abstract

GPR4 is a proton-sensing G protein-coupled receptor implicated in many peripheral and central physiological processes. GPR4 expression has previously been assessed only via detection of the cognate transcript or indirectly, by use of fluorescent reporters. In this work, CRISPR/Cas9 knock-in technology was used to encode a hemagglutinin (HA) epitope tag within the endogenous locus of *Gpr4* and visualize GPR4-HA in the mouse central nervous system using a specific, well characterized HA antibody; GPR4 expression was further verified by complementary *Gpr4* mRNA detection. HA immunoreactivity was found in a limited set of brain regions, including in the retrotrapezoid nucleus (RTN), serotonergic raphe nuclei, medial habenula, lateral septum, and several thalamic nuclei. GPR4 expression was not restricted to cells of a specific neurochemical identity as it was observed in excitatory, inhibitory, and aminergic neuronal cell groups. HA immunoreactivity was not detected in brain vascular endothelium, despite clear expression of *Gpr4* mRNA in endothelial cells. In the RTN, GPR4 expression was detected at the soma and in proximal dendrites along blood vessels and the ventral surface of the brainstem; HA immunoreactivity was not detected in RTN projections to two known target regions. This localization of GPR4 protein in mouse brain neurons corroborates putative sites of expression where its function has been previously implicated (e.g., CO_2-regulated breathing by RTN), and provides a guide for where GPR4 could contribute to other CO_2/H^+ modulated brain functions. Finally, GPR4-HA animals provide a useful reagent for further study of GPR4 in other physiological processes outside of the brain. *This work was published in the paper entitled "Expression of endogenous GPR4 expression in the mouse brain."*[114]

3.2 – Introduction

GPR4 is a class A G protein-coupled receptor (GPCR) and a member of the proton-sensing subfamily of GPCRs that also includes TDAG8 (*Gpr65*), OGR1 (*Gpr68*), and G2A (*Gpr132*) [81,115,116]. GPR4 has been implicated in both peripheral and central physiological functions. It plays a role in angiogenesis[117–123], monocyte migration[124–126], chronic inflammation[123,127–131], ischemia/reperfusion injury[132], maintenance of acid-base balance by the kidney[117,133–135], and cancer cell migration/metastases[128,136–141]. In the central nervous system, GPR4 has been associated with central respiratory chemosensitivity, contributing both to an atypical CO_2/H^+-dependent vasoconstriction in brainstem regions associated with CO_2-regulated breathing and to direct modulation by CO_2/H^+ of putative respiratory chemosensory neurons in the retrotrapezoid nucleus [47,80,142].

Detection of GPR4 within the mouse, including in the brain, has proven technically challenging due to a lack of specific antibodies. Previous experiments examining GPR4 localization in the mouse have indirectly inferred sites of expression using a GPR4 promotor-driven fluorescent marker [127,128,143], Cre expression from the GPR4 locus to enable fluorescent marker lineage tracing[80], or relied on RNA detection as a proxy for protein expression [14,47,80,139,144,145]. These methods each have limitations: they either do not reflect GPR4 expression at the time of tissue harvest or do not inform subcellular localization of GPR4 itself.

To circumvent these technical limitations, we pursued an endogenous knock-in strategy to incorporate a small hemagglutinin (HA) tag into GPR4 using CRISPR/Cas9 genome editing. With this approach, we used well characterized, highly specific, and easily accessible epitope antibodies to characterize GPR4 expression in the mouse brain. We compare protein and RNA distribution and provide new quasi-quantitative information on regional and subcellular localization of GPR4 protein in different cell populations.

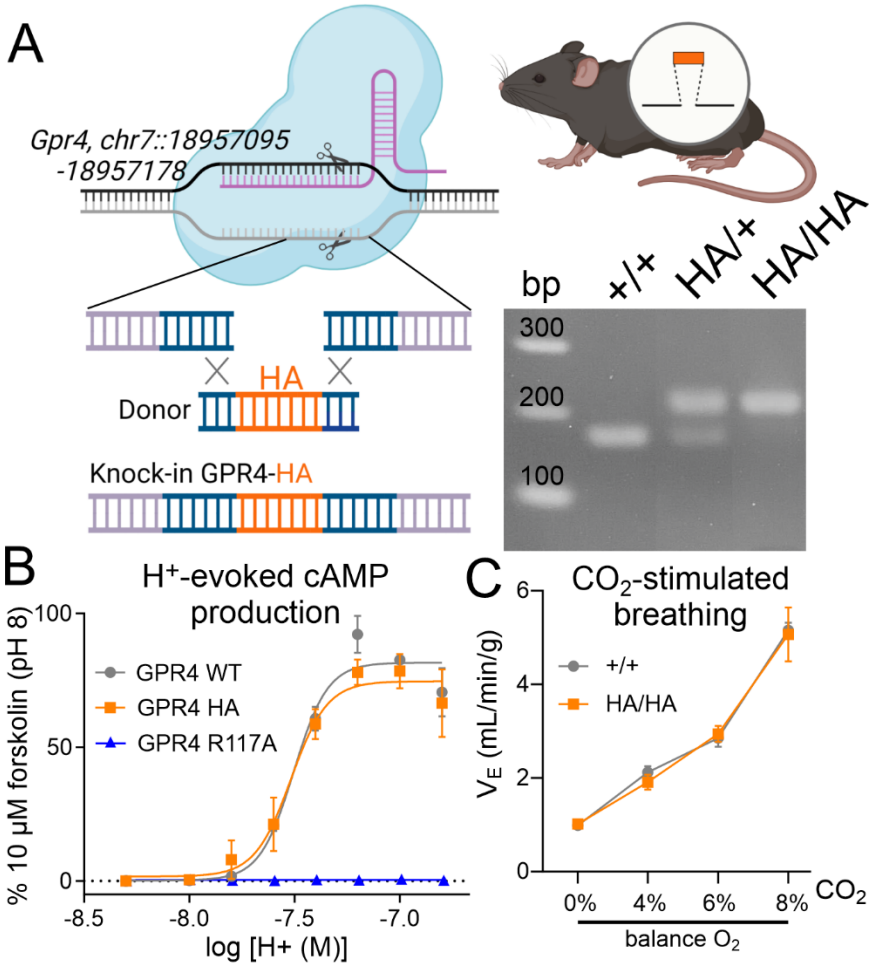

Figure 3.1: Incorporating an HA epitope tag into GPR4 does not alter receptor function *in vitro* or the hypercapnic ventilatory reflex *in vivo*. (A) Illustration of the CRISPR/Cas9 knock-in strategy, generated in BioRender, and a representative agarose gel of the diagnostic PCR used to detect the HA tag at the C-terminal end of GPR4. (B) Activation by acidification of wildtype and HA-tagged GPR4 in HEK293T cells detected using the luminescent GloSensor assay for cAMP production (normalized to pH-independent, forskolin activated cAMP production). Note that acidification does not increase cAMP in cells expressing a non-signaling GPR4(R117A). (C) Minute ventilation of *Gpr4*$^{HA/HA}$ and wildtype *Gpr4*$^{+/+}$ mice assessed by whole body plethysmography.

3.3 – Results:

3.3.1 – Generation of a *Gpr4*^{HA} knock-in mouse.

A CRISPR/Cas9 knock-in strategy was used to incorporate an HA tag sequence to the 3' end of the *Gpr4* coding region at the endogenous locus in the mouse genome (**fig. 3.1A**). The addition of this nonapeptide epitope tag (YPYDVPDYA-STOP, preceded by a 4 residue GSSG linker) to the extreme C-terminus of GPR4 has no effect on pH-dependent cAMP production by GPR4 receptors transiently transfected in HEK293T cells (**fig. 3.1B**). In addition, by whole animal plethysmography, GPR4$^{HA/HA}$ knock-in animals demonstrate a normal hypercapnic ventilatory response, by comparison to their wildtype GPR4$^{+/+}$ littermates (**fig. 3.1C**). Thus, HA-tagged GPR4 retains normal function in these two established assays, in vitro and in vivo.

3.3.2 – Characterization of GPR4 mRNA and protein expression in cell groups throughout the mouse brain

Target brain regions chosen for assessing GPR4 protein expression using the HA knock-in tag were determined based on previous studies examining *Gpr4* mRNA expression[14,47,80,139,146,147] as well as on our own *Gpr4* mRNA expression screen throughout the brain. For each region described in the following text, we present expression of both GPR4 mRNA and protein.

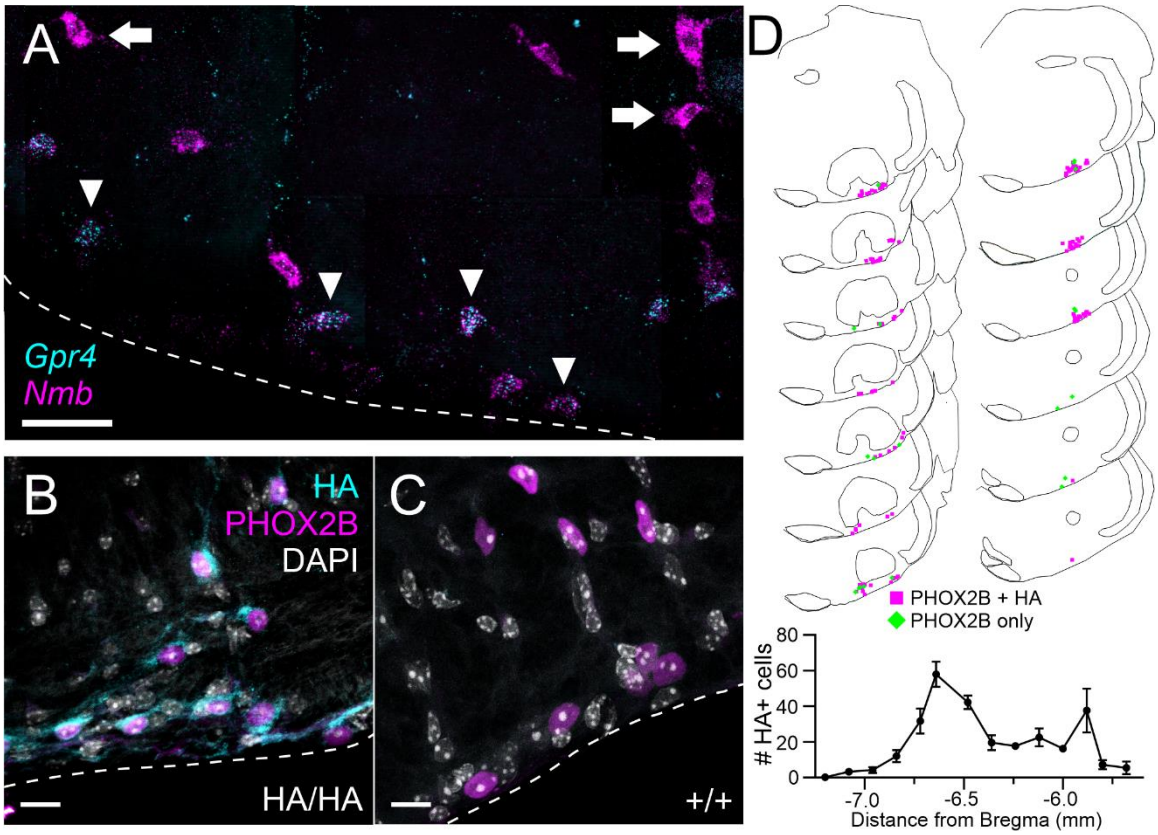

Figure 3.2: GPR4 transcript and protein expression in the retrotrapezoid nucleus (RTN). (**A**) RNAscope multiplex *in situ* hybridization (ISH) labeling for *Gpr4* and the RTN marker *Nmb* at bregma level -6.48 mm. *Arrowheads* indicate RTN neurons that co-express *Nmb* and *Gpr4*; *arrows* indicate more dorsally located neurons with high levels of *Nmb* that do not express *Gpr4* [14]. (**B-C**) HA immunostaining in the RTN of $Gpr4^{HA/HA}$ (**B**) and wildtype $Gpr4^{+/+}$ (**C**) mice; RTN neurons are identified by expression of PHOX2B (**D**) Representative maps of PHOX2B+/HA+ cells and PHOX2B-only cells through the rostrocaudal extent of the RTN (*upper*, bregma -5.8 to -7.08), and average distribution of HA+ cells through the RTN (*lower*). Data are averaged (± SEM) from 4 mice; scale bars represent 50 μm.

3.3.2.1 – Retrotrapezoid Nucleus (RTN)

RTN neurons are required for CO_2/H^+-evoked respiratory chemoreflexes [1,22,148], and they can be identified within the parafacial region of the mouse rostral ventrolateral medulla by their expression of PHOX2B, and more specifically by expression of Neuromedin B (Nmb)[14]. *Nmb*-expressing RTN neurons express high levels of *Gpr4* transcript[14,47,80]. Indeed, in wildtype C57BL6/J mice (**fig. 3.2A**), *Gpr4* expression can be clearly localized to *Nmb*$^+$ (RTN) neurons in the parafacial region of the medulla (*arrowheads*); as described earlier[14], some dorsally located neurons with especially high levels of *Nmb* do not express *Gpr4* (*arrows*). In this region, specific HA staining is observed in the cell bodies of PHOX2B$^+$ neurons and in their processes along the ventral surface of the medulla (**fig. 3.2B**). HA positive signal is only evident in GPR4$^{HA/HA}$ animals, not their GPR4$^{+/+}$ littermates (**fig. 3.2B-C**). The rostrocaudal distribution of HA$^+$ cells in this region closely mirrors that of RTN neurons (**fig. 2D**)[14,26,47], and the percentage of PHOX2B$^+$ cells that are immunoreactive for HA (74.6 ± 6.4, n = 4 animals) is comparable to that previously reported for the percentage of PHOX2B-expressing neurons that contain *GPR4* transcripts (~70%, Kumar et al., 2015).

3.3.2.2 – Caudal Raphe Nuclei

The caudal raphe nuclei (**fig. 3.3A**) have been proposed as an important cell group contributing to central respiratory chemoreception[149–151], and previous work has localized *Gpr4* transcripts to serotonergic raphe neurons[47,80]. Likewise, we find that *Gpr4* mRNA expression can be observed in serotonergic *Tph2*$^+$ cells throughout the raphe magnus (RMg), raphe pallidus (RPa), raphe obscurus (ROb) as well as the parapyramidal (PPy) raphe (**fig. 3.3B**). Using these mRNA expression results as a guide, we assessed HA staining patterns in the same raphe nuclei. Indeed, HA immunoreactivity is detected in all subdivisions of the serotonergic raphe that display

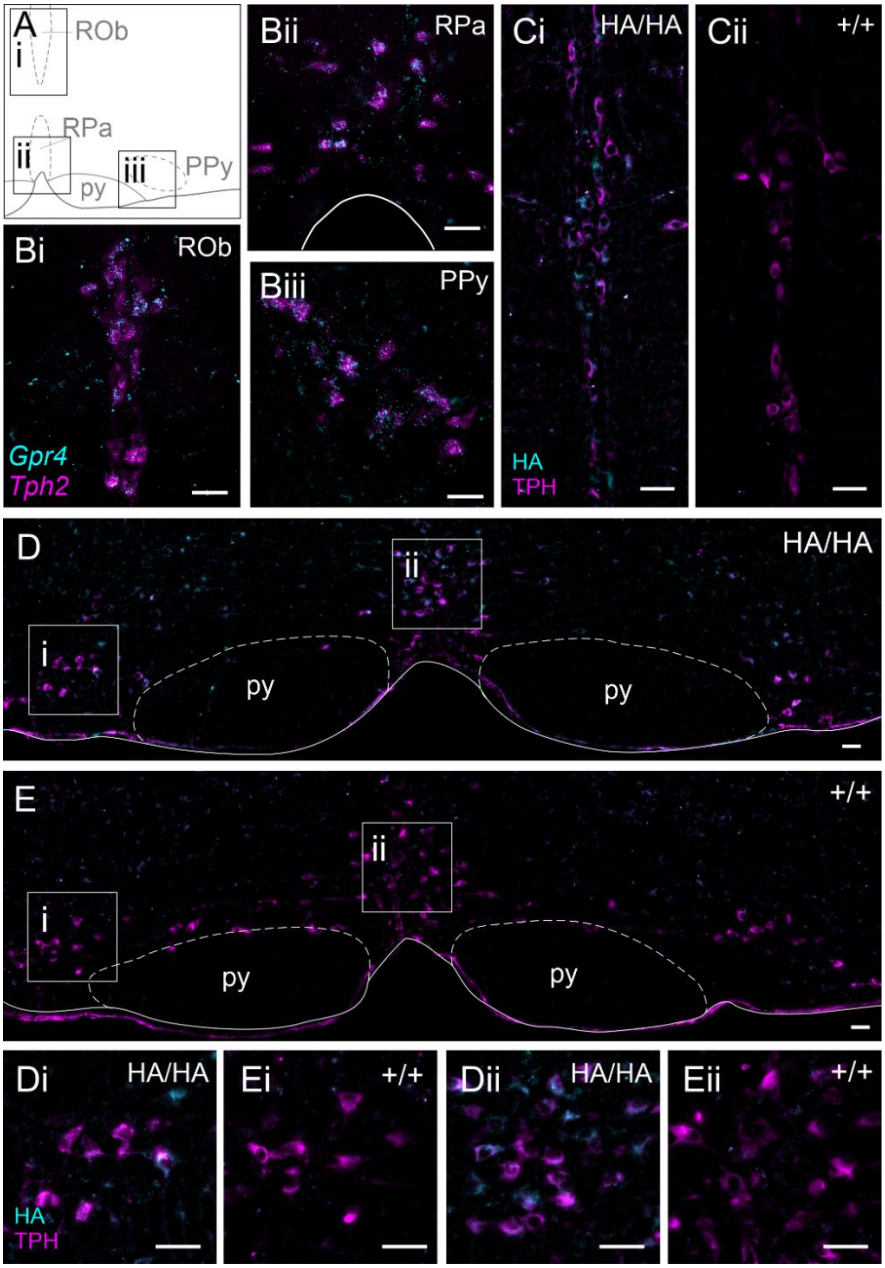

Figure 3.3: GPR4 transcript and protein expression in the caudal raphe. (**A**) Representative diagram of 3 caudal raphe nuclei and notable landmarks, based on the Paxinos and Franklin atlas, bregma -6.64 mm. Abbreviations: ROb, raphe obscurus; RPa, raphe pallidus; PPy, parapyramidal nucleus; py, pyramidal tract. (**Bi-iii**) RNAscope ISH labeling of *Gpr4* expression in serotonergic raphe neurons identified by *Tph2* expression. (**Ci-ii**) HA staining in the raphe obscurus serotonergic (TPH^+) nucleus of $Gpr4^{HA/HA}$ (**i**) and wildtype $Gpr4^{+/+}$ (**ii**) mice. (**D-E**) HA staining in the parapyramidal (**i**) and raphe pallidus (**ii**) nuclei of $Gpr4^{HA/HA}$ (**D**) and wildtype $Gpr4^{+/+}$ (**E**) mice. Scale bars represent 50 μm.

Gpr4 transcript (**fig. 3.3C-E**). Within the cell, HA staining labels the soma and large proximal neurites. The spatial distribution of HA^+/TPH^+ neurons throughout the range of the caudal raphe nuclei (**fig. 3.4A**), mirrors transcript localization. Overall, HA staining is detected in ~90% of serotonergic (TPH^+) neurons throughout these subdivisions of the caudal raphe (**fig. 3.4B**).

3.3.2.3 – Median and dorsal raphe.

Previous lineage tracing of GPR4 expression using a Cre/fluorescent reporter system described reporter expression in both the median and dorsal raphe[80]. The same work also reported *Gpr4* transcript expression in the dorsal raphe region (**fig. 3.5A**). We also observed *Gpr4* expression in *Tph2*$^+$ cells of both the median and dorsal raphe (**fig. 3.5B**). HA staining in the serotonergic subset of dorsal and median raphe neurons directly corresponds to the expression pattern of *Gpr4* transcript and is only observed in HA knock-in mice (**fig. 3.5C, D**). HA staining is observed mainly in the soma and large neurites.

3.3.2.4 – Thalamus.

Gpr4 transcript can be observed in multiple glutamatergic thalamic nuclei (**fig. 3.6**), in which neurons express the vesicular glutamate transporter 2 (VGlut2, encoded by *Slc17a6*). Similarly, GPR4-HA staining can be noted in the same locations as *Gpr4* transcript throughout the thalamus (**fig. 3.7A-E**). In addition, *Gpr4* transcripts are evident in the medial habenula (**fig. 3.6E**); in the habenula, HA staining labels the cell bodies of the cholinergic neurons (choline acetyltransferase, $ChAT^+$) cells in the ventrolateral division of the nucleus (**fig. 3.7E**). The intensity of HA staining varies between individual cells within the habenula, but $ChAT^-/HA^+$ cells were not observed in the sections examined for these studies. A small population of $ChAT^+/HA^-$ cells are also present. In addition to thalamic cell groups described in figures 6 and 7, high levels of *Gpr4* transcript are observed in the glutamatergic (*Slc17a6*$^+$) cells of the dorsal

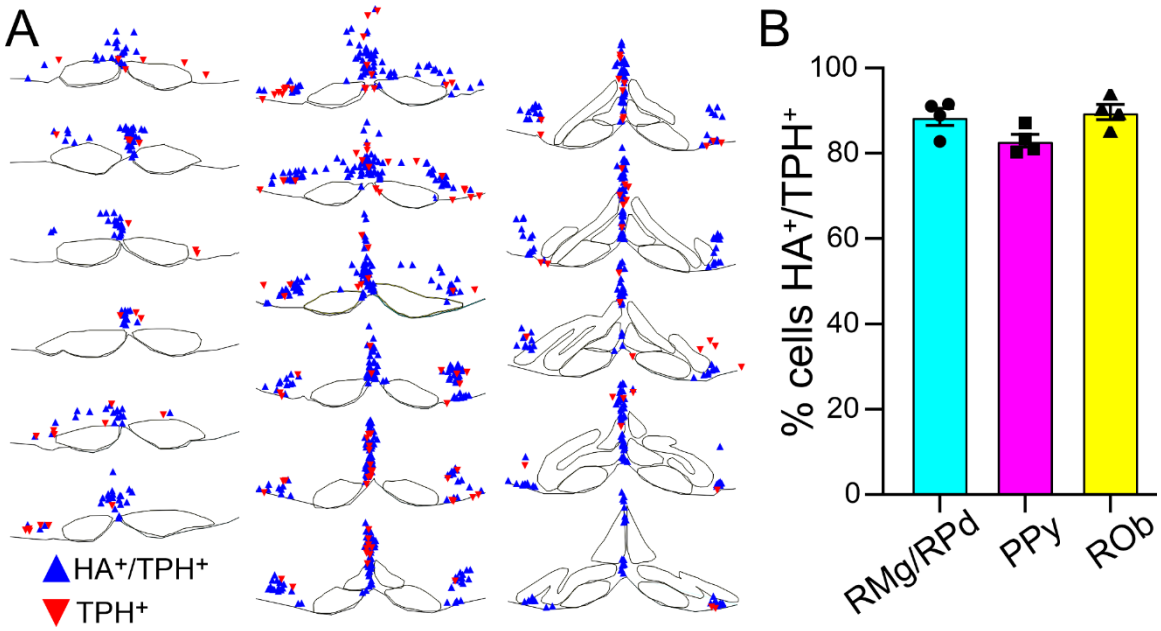

Figure 3.4: Location and proportion of serotonergic caudal raphe neurons that express GPR4. (A) Representative maps of HA+/TPH+ cells and TPH+ cell locations through the caudal raphe, bregma levels -5.80 to -7.12. (B) Average percentage of TPH+ cells that are also HA+ (% HA+/TPH+) within ROb (33±4 TPH+ cells/section), RPa/RMg (23±3 TPH+ cells/section), and PPy (26±3 TPH+ cells/section). Data are averaged (± SEM) from 4 mice.

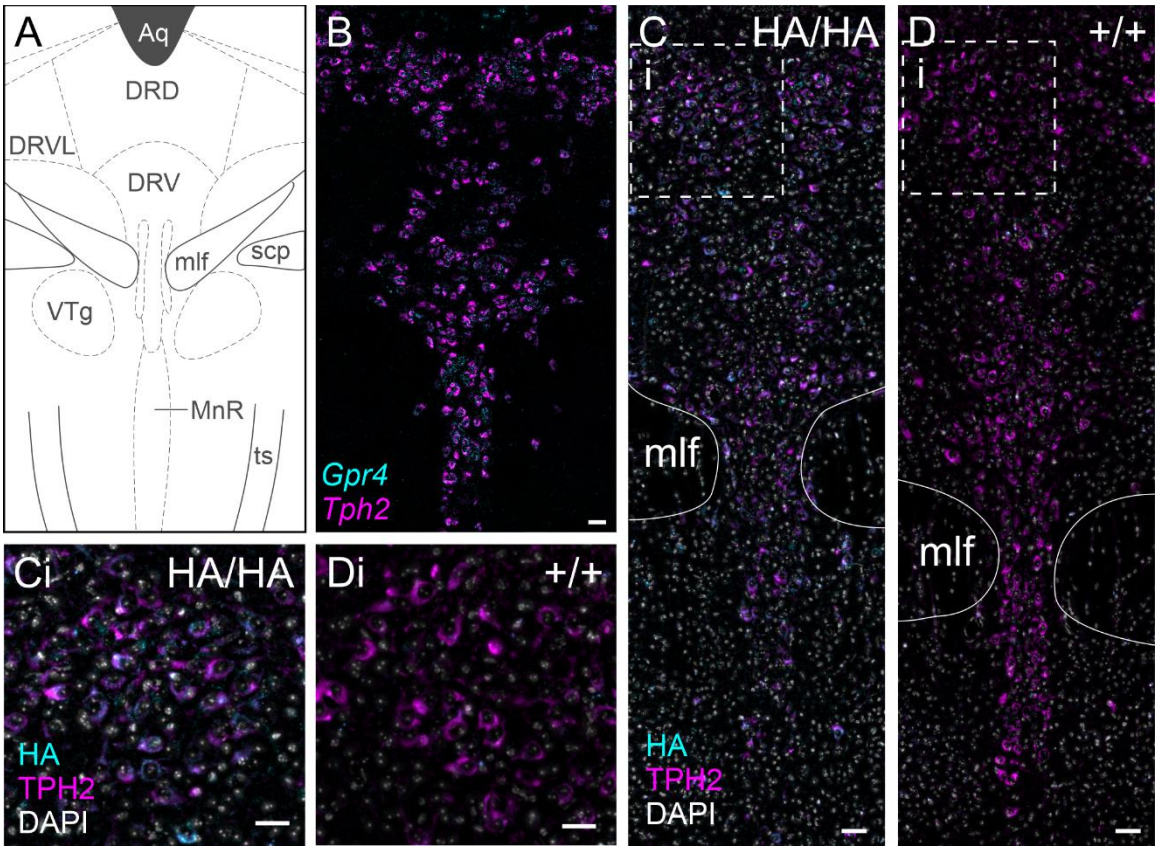

Figure 3.5: GPR4 transcript and protein expression in the dorsal and median raphe. (**A**) Representative diagram of key nuclei and landmarks at bregma -4.84 mm, including the nuclei of the dorsal and median raphe, according to the Paxinos and Franklin atlas. Abbreviations: Aq, aqueduct (Silvius); DRD, dorsal raphe nucleus, dorsal part; DRVL, dorsal raphe, ventrolateral; DRV, dorsal raphe nucleus, ventral; mlf, medial longitudinal fasciculus; scp, superior cerebellar peduncle (brachium conjunctivum); VTg, ventral tegmental nucleus; MnR, median raphe nucleus; ts, tectospinal tract. (**B**) RNAscope ISH labeling demonstrating *Gpr4* expression in *Tph2*$^{+}$ cells of the dorsal and median raphe. (**C-D**) GPR4-HA immunolabeling in the dorsal and median raphe of *Gpr4*$^{HA/HA}$ (**C**) and wildtype *Gpr4*$^{+/+}$ (**D**) mice; (**i**) represents section of the image viewed in higher magnification in Ci-Di. Scale bars represent 50 μm.

aspect of the medial geniculate nucleus (**fig. 3.8A, B**). Strong GPR4-HA staining can be also observed in calbindin-expressing cells at the same anatomical location, corresponding to the excitatory neurons identified by *Gpr4* transcript expression and corresponding to cluster of neurons previously identified in the geniculate via single nucleus RNA sequencing [152](**fig. 3.8C, D**).

3.3.2.5 – Lateral Septum.

As previously reported[80], *Gpr4* expression can be observed in the GABAergic cells of the lateral septum (marked by expression of the GABA vesicular transporter, Vgat1; *Slc32a1*). Increasing levels of *Gpr4* expression are apparent moving medially from the lateral ventricle toward the intermediate portion of the lateral septum (**fig. 3.9A-B**). HA staining in $GPR4^{HA/HA}$ mice exhibits the same spatial pattern as observed for transcript expression and is not observed in wildtype controls (**fig. 3.9C-D**). These protein expression results also match previous lineage tracing results [80]. In the lateral septum, HA staining is mainly observed in the cell bodies and large proximal neurites.

3.3.3 – Characterization of GPR4 mRNA and protein expression in the brain vasculature.

Gpr4 transcript can be detected in brain vascular endothelium, where non-neuronal *Gpr4* labeling in the brainstem overlays strikingly with labeling for the endothelial marker, *Pecam1* (**fig. 3.10A**). However, HA labeling is undetectable in $PECAM^{+}$ vascular endothelial cells in sections from $GPR4^{HA/HA}$ mice (**fig. 3.10B-D**).

3.3.4 – Characterization of GPR4 protein expression in projections of the RTN.

We further examined the subcellular organization of HA labeling in the RTN. We leveraged the cell-specific expression of neuromedin B by RTN neurons in the parafacial region of the mouse brainstem [14] to specifically label those neurons by injecting an

mCherry-expressing, Cre-dependent AAV into that region of *Gpr4*$^{HA/HA}$ animals crossed with an Nmb-Cre mouse [148]. We then examined HA expression in the mCherry^{+} (i.e., Nmb-expressing) neuronal somata and processes in the RTN itself, as well as in RTN-derived fibers at two previously described RTN projection targets, the preBötzinger complex (preBötC) and the lateral parabrachial nucleus (lPBN) (**fig. 3.11A**). At the RTN level, HA staining can be observed in mCherry-expressing cell bodies and neuronal processes within the nucleus, as well as in their projections along the ventral medullary surface (**fig. 3.11B**). In both the preBötC and lPBN regions, however, we were unable to detect HA staining in mCherry^{+} projections from the RTN (**fig. 3.11C-D**).

3.4 – Discussion

In this study, we leveraged CRISPR/Cas9 genome editing to introduce a small epitope tag sequence into the genomic locus of *Gpr4* to enable detection of GPR4 protein expressed endogenously in the brain. Introduction of the small (13 aa) linker-HA cassette onto the C-terminus of GPR4 had no apparent effect on GPR4-mediated signaling *in vitro* or on CO_2-stimulated breathing *in vivo*, two functions for which GPR4 expression is necessary. Examination of HA staining in the brain regions shown to express *Gpr4* transcript reveals detectable GPR4 protein expression in neurons from all loci displaying transcript expression. Thus, these data yield an independent validation of GPR4 protein expression in the mouse brain, confirming a relatively restricted expression of this pH-sensitive GPCR to several neuronal nuclei, and providing a new resource to examine GPR4 expression in other tissues where its function has been implicated.

GPR4 expression is not limited to only glutamatergic or GABAergic neuronal populations. GPR4 transcript and protein are present in the GABAergic (*Slc32a1*$^{+}$) neurons of the lateral septum, the glutamatergic (*Slc17a6*$^{+}$) neurons of the thalamus and

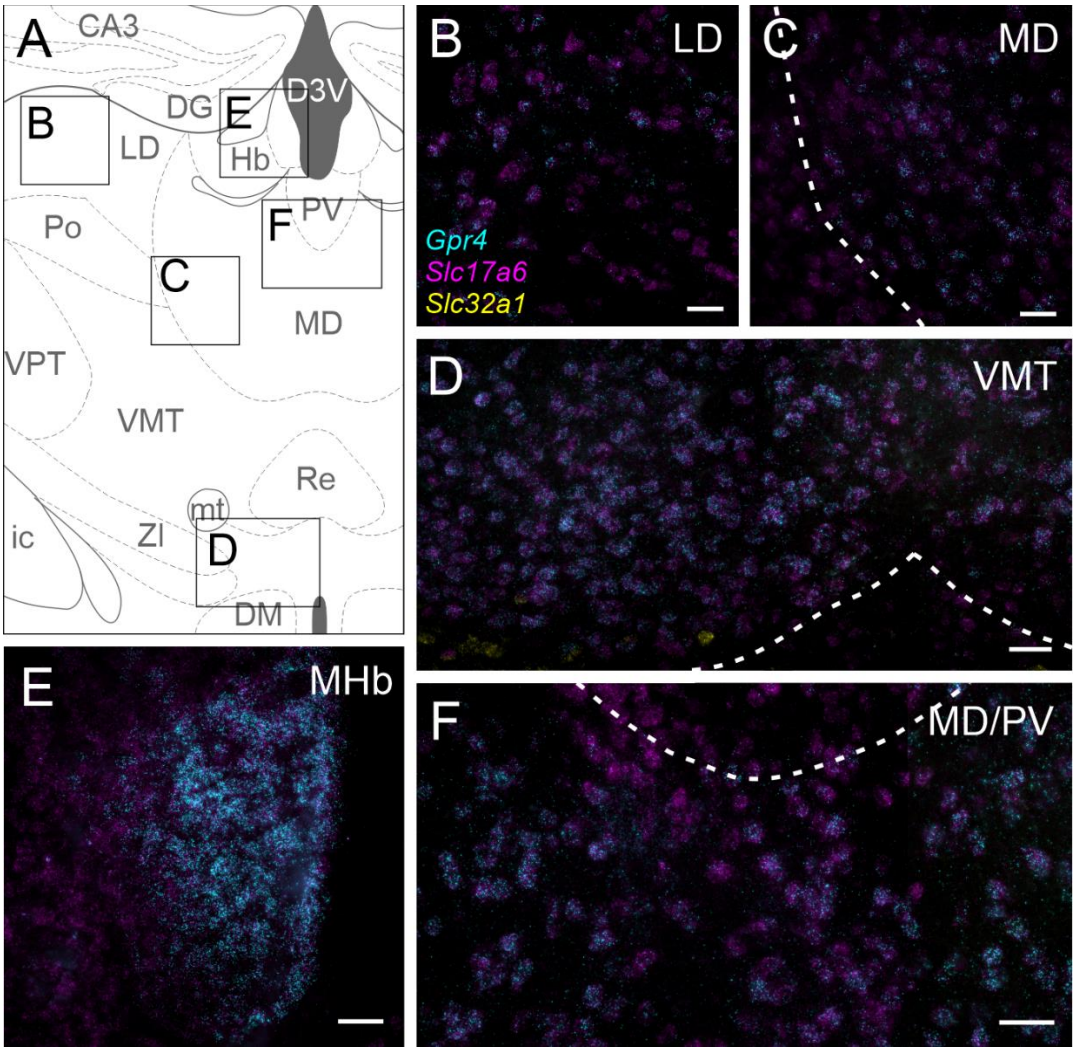

Figure 3.6: *Gpr4* transcript expression in multiple nuclei of the thalamus. (**A**) Representative diagram of key landmarks and thalamic nuclei at bregma -1.34 mm; inset rectangles represent regions presented in panels **B-F**. Abbreviations: CA3, hippocampus CA3; DG, dentate gyrus; D3V, dorsal third ventricle; LD, laterodorsal thalamus; Hb, habenula; PV, paraventricular thalamus; Po, posterior thalamic group; MD, mediodorsal thalamus; VPT, ventroposterior thalamus; VMT, ventromedial thalamus; Re, reuniens thalamic nucleus; mt, mammillary tract; ic, internal capsule; ZI, zona incerta; DM, dorsomedial hypothalamus. (**B-F**) RNAscope in situ labeling of *Gpr4* expression in glutamatergic (*Slc17a6*) cells of the laterodorsal (**B**), mediodorsal (**C, F**), medial habenula (**E**), and ventromedial (**D**) thalamic nuclei. A few GABAergic (*Slc32a1*) cells visible at the ventral border of VMT appear negative for *Gpr4*. Scale bars represent 50 μm.

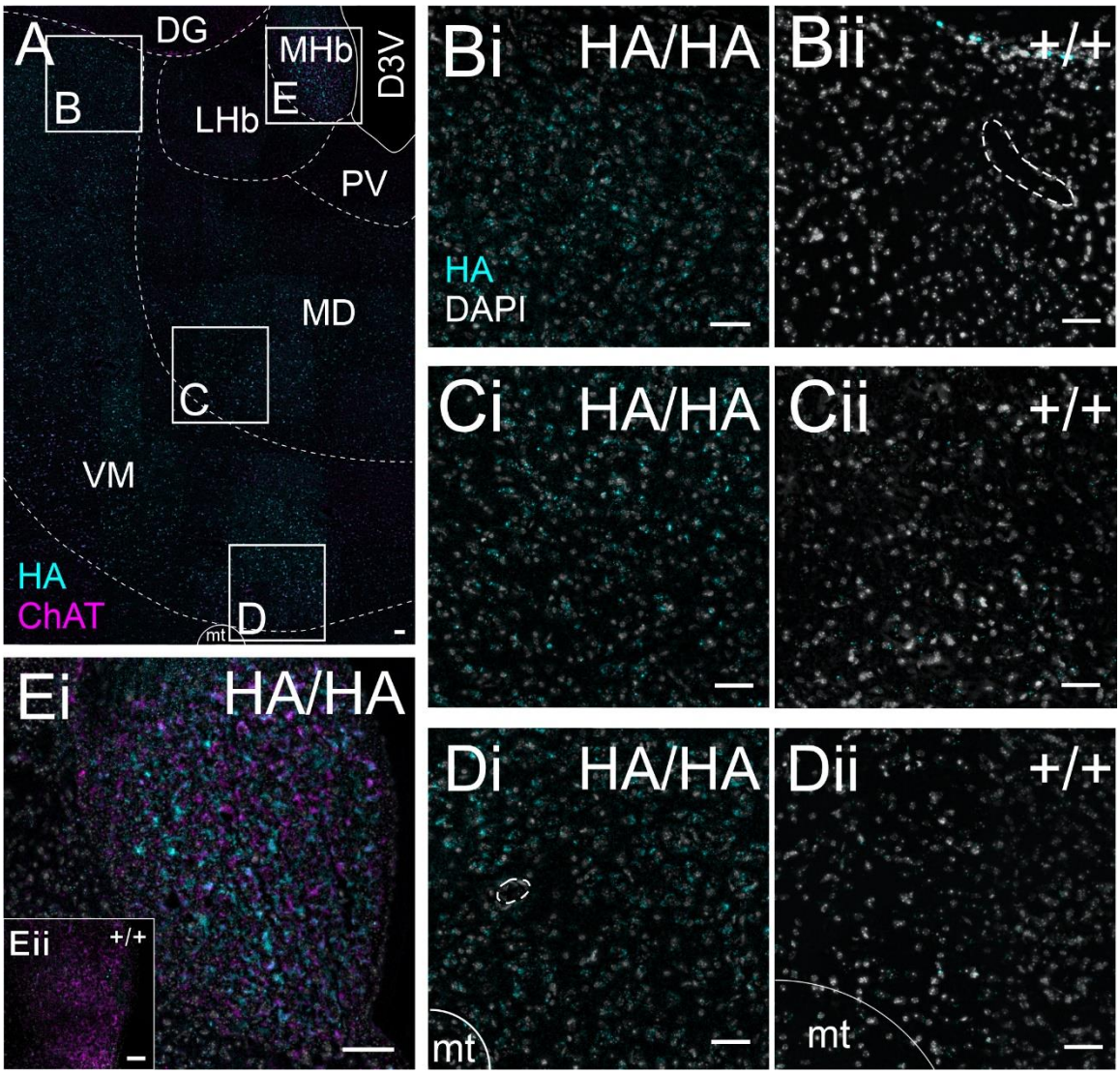

Figure 3.7: GPR4 protein expression in the thalamus. (**A**) Composite image of the thalamus of a *Gpr4*$^{HA/HA}$ mouse stained for HA and ChAT, with general landmarks delineated by dashed lines. Abbreviations: DG, dentate gyrus; D3V, dorsal third ventricle; LD, laterodorsal thalamus; LHb, lateral habenula; MHb, medial habenula; PV, paraventricular thalamus; VM, ventromedial thalamus. (**B-D**) HA staining (with DAPI labeling) in the laterodorsal (**B**), mediodorsal (**C**), and ventromedial (**D**) thalamus of *Gpr4*$^{HA/HA}$ (**i**) and wildtype *Gpr4*$^{+/+}$ (**ii**) mice. (**Ei**) HA and ChAT staining in the medial habenula of *Gpr4*$^{HA/HA}$ and wildtype *Gpr4*$^{+/+}$ mice (**Eii**, inset). Scale bars represent 50 μm; dotted lines identify blood vessels (in **Bii**, **Di**).

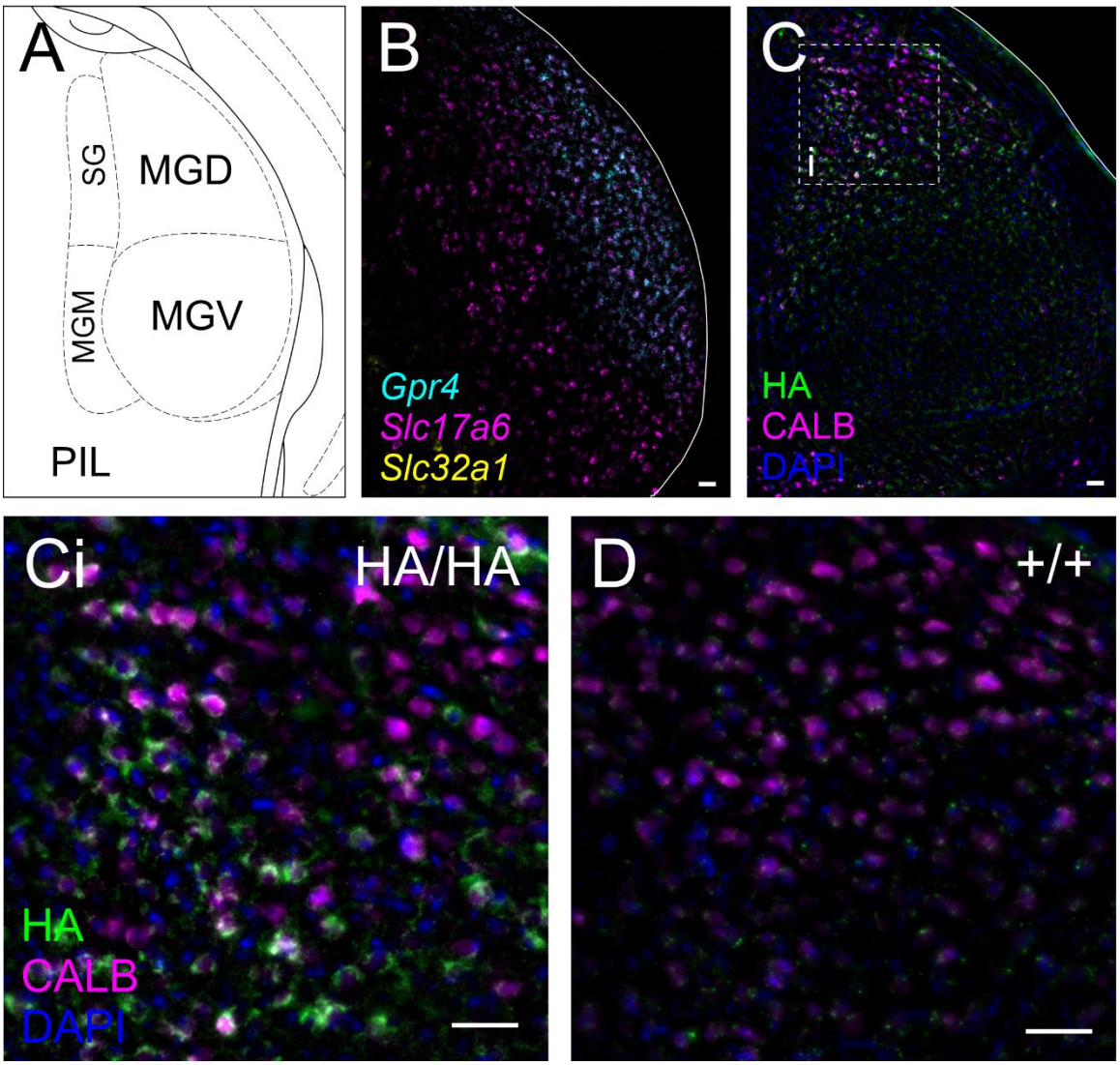

Figure 3.8: GPR4 transcript and protein expression in the geniculate nucleus. (**A**) Representative diagram of key landmarks around the medial geniculate nucleus at bregma level -3.28 mm. Abbreviations: MGD, medial geniculate nucleus, dorsal part; MGV, medial geniculate nucleus, ventral part; MGM, medial geniculate nucleus, medial part; SG, suprageniculate nucleus; PIL, posterior intralaminar thalamic nucleus. (**B**) RNAscope ISH labeling of *Gpr4* expression in the geniculate nucleus, together with markers for glutamatergic (*Slc17a6*) and GABAergic neurons (*Slc32a1*). (**C**) HA staining in the Calbindin B (CALB) expressing cells of the dorsal aspect of the geniculate nucleus of *Gpr4*$^{HA/HA}$ mice; dotted line designates region viewed at higher power in (**Ci**). (**D**) Lack of HA staining in a wildtype mouse at the region analogous to that displayed in (**Ci**).

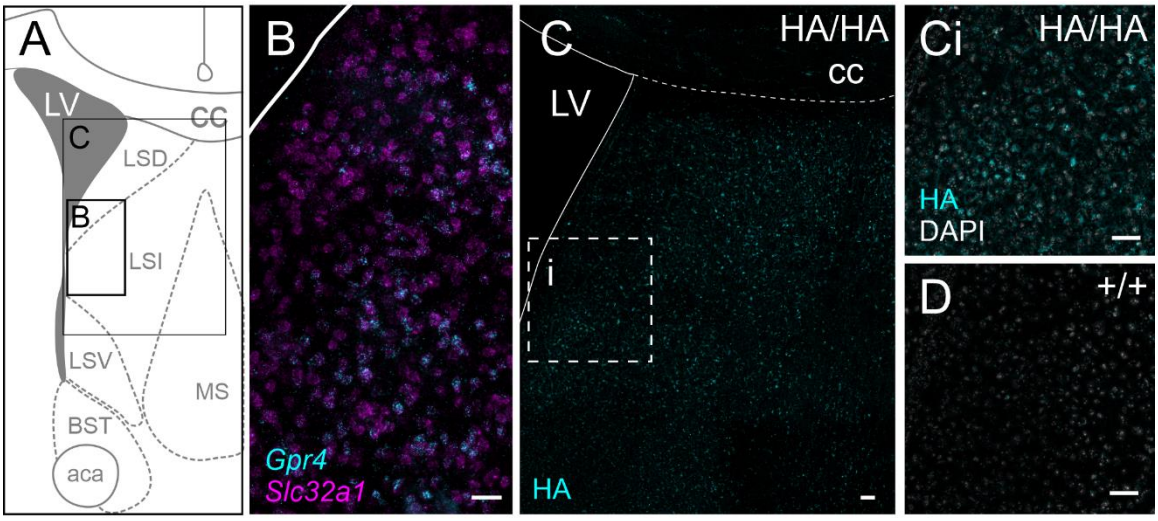

Figure 3.9: GPR4 transcript and protein expression in the lateral septum. (**A**) Representative diagram of key landmarks around the lateral septum at bregma level 0.38 mm. Abbreviations: LV, lateral ventricle; cc, corpus callosum; LSD, dorsal lateral septal nucleus; LSI, intermediate lateral septal nucleus; LSV, ventral septal nucleus; MS, medial septal nucleus; BST, bed nucleus of the stria terminalis; aca, anterior commissure anterior part. (**B**) RNAscope ISH labeling of *Gpr4* expression in GABAergic (*Slc32a1*) neurons of the lateral septum. (**C**) HA staining throughout the lateral septum of a $Gpr4^{HA/HA}$ mouse; the indicated region is displayed at higher magnification in (**Ci**). (**D**) Lack of HA staining in a wildtype mouse at a region analogous to that displayed in (**Ci**). Scale bars represent 50 µm.

RTN, and also in the cholinergic ($ChAT^+$) neurons of the habenula and the serotonergic (TPH^+) neurons of multiple raphe nuclei. The presence of GPR4 in cells representing a wide variety of molecular signatures indicates a possible role of the receptor in multiple contexts, respiratory or otherwise. In the RTN specifically, GPR4 expression is known to be necessary for a normal hypercapnic ventilatory response (HCVR); a blunted HCVR is observed in GPR4 global knockout mice and selective reintroduction of GPR4 protein expression into RTN neurons of GPR4 knockout mice is sufficient to restore the HCVR to the wildtype level [47]. Although GPR4 is also expressed in the caudal raphe nuclei, its presence is not required for the activation of serotonergic neurons by CO_2 (as assessed by Fos expression after an acute CO_2 challenge) so it may not play a role in manifesting their CO_2 sensitivity, at least under the conditions tested [47,80]. The dorsal and median raphe are critical for CO_2-induced arousal from sleep [153,154]. It is possible that GPR4 expression by these neurons may mediate, at least in part, the direct sensation of CO_2 by the DR/MR to promote arousal.

Many of the nuclei shown to express GPR4 in this study have been implicated in the manifestation and control of anxiety. CO_2 is a powerful anxiogenic stimulus in rodents and humans that causes rapid and pronounced autonomic arousal and emotional distress [155–159]. Chemo- and optogenetic activation of the GABAergic neurons in the lateral septum, in the same area as the cells found to express GPR4 in this study, induces anxiety behaviors in mice [160–162]. It is possible that the expression of GPR4 by these anxiety-initiating neurons in the lateral septum may mediate some of the anxiogenic effects of CO_2. The potential role of GPR4 in the medial habenula is more ambiguous. The MHb has been shown to be crucial for anxiety and fear responses, but the specific pathways mediating its role in mood regulation are uncharacterized [163,164]. Gross ablation of the MHb, electrolysis of MHb efferents, or inhibition of MHb neuron firing leads to increased anxiety behaviors and increased circulating corticosterone [165–169]. Ablation of the cholinergic neurons of the

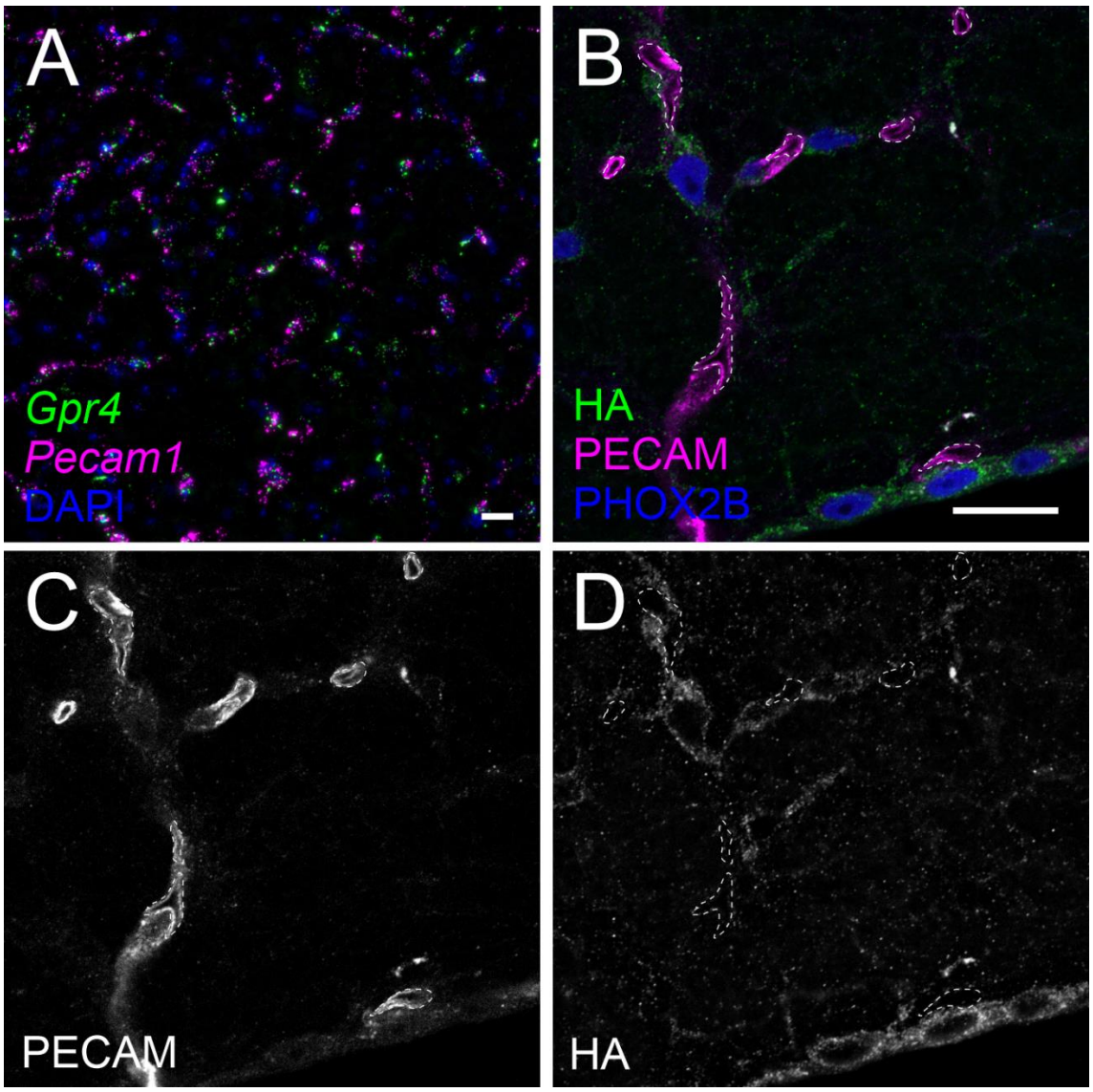

Figure 3.10: GPR4 transcript, but not protein, is detectable in brain endothelial cells. (**A**) RNAscope *in situ* labeling of *Gpr4* expression in endothelial (*Pecam1*$^{+}$) cells in the wild type mouse brainstem. (**B-C**) HA staining in RTN neurons from a *Gpr4*$^{HA/HA}$ mouse, with adjacent small vessels labeled by PECAM expression; vessel cross sections (walls and lumen) are delineated by dashed lines. (**C**) PECAM staining within vessel boundaries. (**D**) HA staining located outside of PECAM^{+} vessels. Scale bars represent 25 μm.

ventral portion of the MHb, which are the cells shown to express GPR4, leads to increased fear behavior and higher baseline anxiety [163,170]. It is unclear how activation of the MHb by GPR4 during hypercapnia would lead to the increased anxiety and freezing behavior observed, given the seemingly contradictory observations noted in ablation studies; perhaps GPR4 signaling inhibits the activity of cholinergic MHb neurons. Additionally, there is significant crossover between efferents and afferents of the GPR4-expressing forebrain nuclei, e.g. both the lateral septum and medial habenula project to the dopaminergic neurons of the ventral tegmental area (VTA), whose activation induces anxiety behaviors [160–162,171–178]. It is possible that GPR4 acts more broadly to tune the overall anxiety system during hypercapnia and not in activating distinct nuclei. Anxiety phenotypes have not yet been reported in GPR4 knockout mice.

Limitations and caveats.

We identified HA immunoreactivity in all neuronal populations where *Gpr4* mRNA was found, a correspondence suggesting faithful protein translation of the transcript and detection of the incorporated epitope tag. However, HA staining was not detected in endothelial cells of blood vessels, despite the clear presence of transcript in those same endothelial cells. From these results, it is not possible to rule out GPR4 expression in vascular endothelial cells; it is conceivable that the knock-in of a single HA tag does not provide enough sensitivity to detect GPR4 at the relatively low levels of transcript present in blood vessels. While GPR4 protein can be abundantly detected via HA labeling at the cell body and in long ventral surface dendrites of RTN neurons, it was not visible in terminals at two RTN targets. Again, this observation could be due to endogenous protein expression being too low to detect without further amplification of immunostaining signal or incorporation of multiple HA epitopes in sequence (e.g., 3xHA).

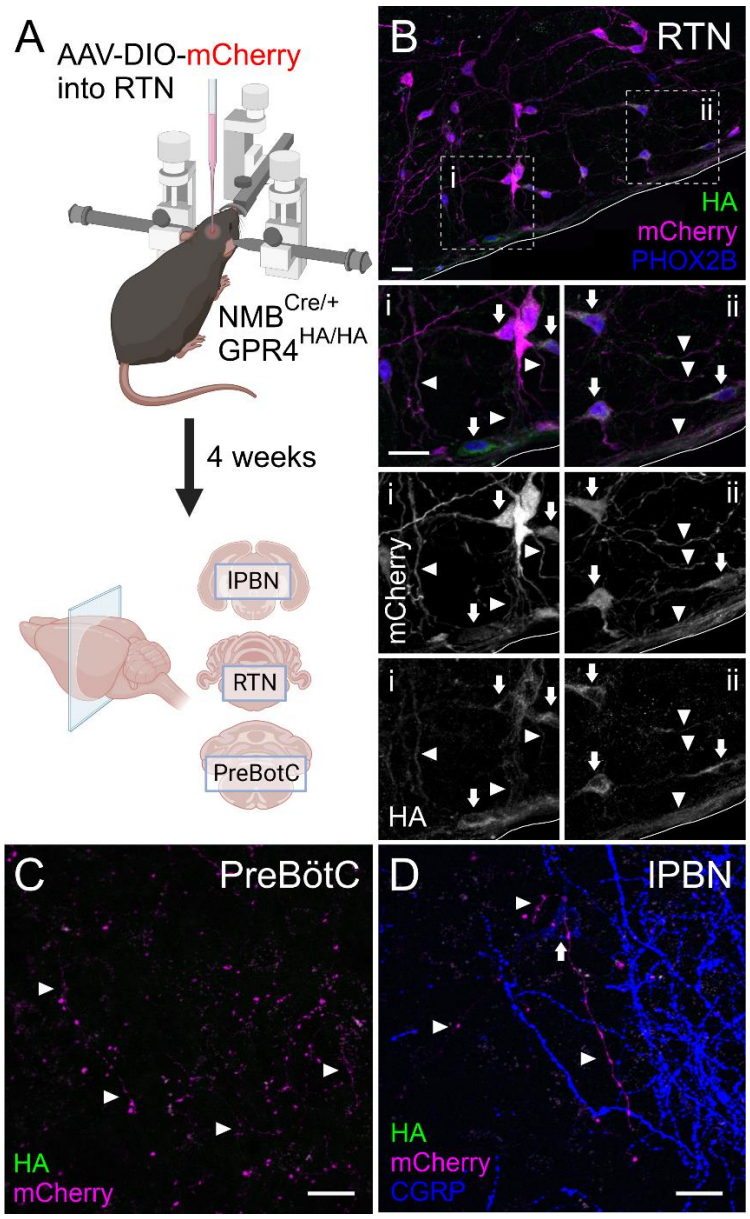

Figure 3.11: GPR4 is evident in the processes of Nmb-expressing RTN neurons but undetectable at terminals in the preBötC or lPBN. (**A**) Illustration of the viral expression and immunostaining strategy for assessing GPR4 protein expression in processes and terminals of NMB neurons in the RTN area, lPBN, or PreBötC, generated in BioRender. (**B**) HA staining in mCherry labeled neurons in the RTN area of an *Nmb*$^{Cre/+}$;*Gpr4*$^{HA/HA}$ mouse injected with AAV-DIO-mCherry with high power images of areas bounded by dotted lines (**i-ii**); arrows denote staining in RTN cell bodies, arrowheads denote staining in RTN processes. (**C**) mCherry labeled terminals in the preBötC area (bregma -7.48 mm). (**D**) mCherry labeled terminals in the lPBN (denoted by CGRP staining). Scale bars represent 25 μm.

Thus, these data do not unambiguously indicate that GPR4 protein is absent from vessels, terminals, or more long-distance projections.

Together, this work reveals a relatively restricted expression pattern of neuronal GPR4 expression in mouse brain that is nevertheless associated with a variety of cell types (i.e., glutamatergic, GABAergic, serotonergic, cholinergic). Aside from its demonstrated contribution to respiratory chemosensitivity via RTN neurons [47,80], the role of GPR4 in additional CO_2/H^+-sensitive processes (e.g., arousal, anxiety) mediated by other GPR4-expressing neurons remains to be determined. Finally, the availability of this mouse line will allow detection of GPR4 expression in other peripheral tissues where its role in (patho)physiological processes has been suggested.

Chapter 4 – GPR4-mediated pH sensitivity is necessary for normal respiratory CO_2 sensitivity

4.1 – Abstract

An interoceptive homeostatic system monitors levels of CO_2/H^+ and provides a proportionate drive to respiratory control networks that adjust lung ventilation to maintain physiologically appropriate levels of CO_2 and rapidly regulate tissue acid-base balance. The reflex by which respiration increases in response to increased levels of inspired CO_2 is known as the hypercapnic ventilatory reflex (HCVR). The cellular substrates mediating this reflex are proposed to reside in the ventral medulla. A proposed component of this sensory network is the retrotrapezoid nucleus (RTN). This group of neurons express the transcription factor Phox2b and the neuropeptide Neuromedin B (NMB) and provide a crucial excitatory drive to regulate downstream respiratory rhythm/pattern-generating circuits at baseline and in the context of increased levels of inspired CO_2. The activity of these neurons is modulated by changes in external CO_2/pH and various other sensory and arousal-state inputs. Previous work in our group has identified two H^+ sensors that are proposed to mediate direct modulation of RTN neurons by pH: the proton-activated GPCR, GPR4 and the proton-inactivated potassium channel, TASK-2. Most (90%) RTN neurons express mRNA for both sensors, but it is unclear whether the two proteins provide redundancy or underlie different cellular responses to increased H^+ concentration. Additionally, both proteins contain specific residues that are necessary for pH sensitivity within the physiological range. It is currently unknown whether the pH-sensitivity of each protein per se, and not just a basal activity contributing to general RTN neuronal excitability, is necessary for normal expression of the HCVR. The work presented here examines the necessity of direct pH sensitivity by GPR4 via crucial pH-sensitive residues for pH modulation of RTN neuron activity and the expression of the

HCVR. Using CRISPR/Cas9 genome editing, we generated animals with whole body mutation of two of the previously identified pH-sensing residues. We show that normal pH sensitivity of GPR4 through key histidine residues, His81 and His167, is necessary for a normal HCVR and for normal pH modulated activity of the RTN. These mutations have no impact on transcript expression level of GPR4, baseline respiration, or RTN neuron excitability. These results demonstrate that GPR4 expression does not merely control RTN neuronal excitability and that pH-sensitivity of the RTN mediated by GPR4 is necessary for a normal HCVR. *This work is currently being prepared to be submitted for peer review.*

4.2 – Introduction

Maintenance of breathing in mammals is a complex process that requires precise coordination of inputs from central and peripheral chemosensors, activity of central rhythm- and pattern-generating circuits, and ultimately motor output.[24,25,179,180] Dysregulation of breathing can be a cause or a symptom of a number of diseases including sleep apnea, sudden infant death syndrome, chronic obstructive pulmonary disorder, and congenital central hypoventilation syndrome (CCHS); these disorders are often accompanied by blunted responses to changes in blood gases, including CO_2. The retrotrapezoid nucleus (RTN) is one of several direct inputs to the respiratory pacemaker system.[9,12,41] RTN neurons are activated under hypercapnic conditions to enhance excitatory drive to respiratory to increase frequency and depth of breathing and balance levels of arterial CO_2.[13,26,47,53,63,179,180]

The RTN comprises ~700 neurons in mice (~1200 in rats) located on the ventral medullary surface in close proximity to the facial motor nucleus (VII).[26,40,48] The neurons of the RTN are glutamatergic (they express vGLUT2), express multiple neuropeptides (Neuromedin B (NMB), pituitary adenylate cyclase activating peptide (PACAP),

enkephalin, galanin), and express two proton-sensitive molecules that are necessary for CO_2 modulation of RTN neuronal activity and the hypercapnic ventilatory response (HCVR) the proton-activated G-protein coupled receptor GPR4 and the proton-inactivated potassium channel TASK-2.[12,14,47,53,114,148,181–183] Expression of both TASK-2 and GPR4 is necessary for a normal HCVR and re-expression of GPR4 in the RTN in the context of a global genetic knockout is sufficient to completely rescue the HCVR.[47,53]

RTN neurons also receive inputs from a number of other proposed chemosensitive cell types/nuclei, including local astrocytes (purinergic)[55,56,59,67] and the caudal raphe (5-HT).[1,54,60,184,185] It has been proposed that a majority of the CO_2/H^+ sensitivity of RTN neurons is imparted by these other chemosensory inputs and not due to any intrinsic pH sensitivity of RTN neurons themselves. In this model of the central chemoreflex, the RTN serves as a relay instead of an independent sensor, with GPR4 and TASK-2 functioning only to maintain excitability of the nucleus. By this reckoning, the decreased HCVR observed in GPR4 and/or TASK-2 knockout animals is due to reduced function of the RTN relay and not due to a defect in RTN activation by increases in CO_2/H^+.

In this study, we use CRISPR/Cas9 to generate multiple lines of knock-in mice expressing different variants of pH-desensitized GPR4 to determine if pH sensitivity of GPR4, per se, is required for a normal HCVR and normal RTN neuronal activation by increased CO_2/H^+. We find that CO_2-stimulated breathing and CO_2/H^+ activation of RTN neurons is indeed blunted in these mice, indicating that intrinsic pH sensitivity of GPR4 is critical for respiratory chemoreception.

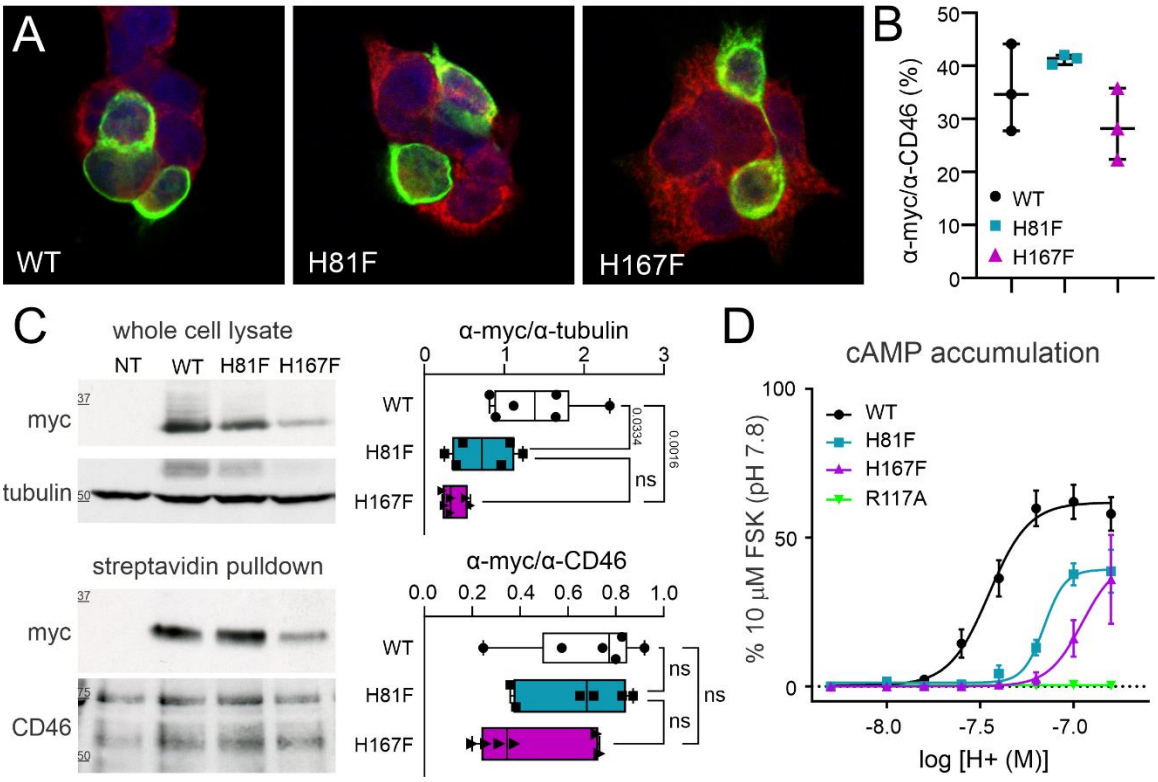

Figure 4.1: His-mutated GPR4 constructs are expressed on the cell surface and show blunted pH-dependent cAMP accumulation. (A) Left: representative images of wildtype and histidine mutant GPR4-myc constructs expressed in HEK293T cells. (B) Average transfection efficiency (% myc-positive cells) of wildtype and histidine mutant mGPR4-myc constructs. (C) Left: representative western blot showing whole cell (upper) and cell surface (lower) expression of the indicated myc-tagged GPR4 constructs expressed in HEK293T cells, Right: aggregate data from six independent experiments; *P < 0.05, **P < 0.01 by one-way ANOVA. (D) GloSensor luminescence assay of pH dependent cAMP accumulation in HEK293T cells transfected with mGPR4-myc constructs: wildtype (n = 5), H81F (n = 3), H167F (n = 3), or Gα binding-deficient (R117A, n = 3). n represents biological replicate (independent transfections).

4.3 – Results

4.3.1 – Histidine mutations disrupt pH sensitivity of mouse GPR4

GPR4 was identified as a proton-sensing adenylyl cyclase-stimulating receptor containing an extracellular shell of titratable histidine residues,[81] and subsequent mutational analyses demonstrated that three specific histidine residues in human GPR4 (corresponding to His81, His167, and His271 in the mouse receptor) are required for proton-activated GPR4 signaling without affecting receptor expression.[82] Similarly, we found that mouse GPR4 containing either of two histidine to phenylalanine substitutions -- GPR4(H81F) and GPR4(H167F) – could be expressed in HEK293T cells (**fig. 4.1**); although cytosolic expression levels of GPR4(H167F) appeared to be lower after transfection in this system, cell surface biotinylation and streptavidin pulldown assays revealed that both Phe-substituted mutants were present on the cell membrane at comparable levels to the wild-type receptor (**fig. 4.1C**). Unlike the GPR4(R117A) variant that cannot signal to downstream effectors, both GPR4(H81F) and GPR4(H167F) conferred an ability to transduce changes in extracellular acidification into elevated intracellular cAMP levels; however, they displayed a decreased sensitivity for proton activation (right shifted pH_{50}) and a lower maximum level of cAMP accumulation, by comparison to wild type GPR4 (**fig. 4.1D**).

4.3.2 – CO_2-stimulated breathing is blunted in GPR4(H81F) knock-in mice

We previously showed that genetic deletion of GPR4 in mice decreased CO_2/H^+ sensitivity of RTN respiratory chemosensory neurons, and strongly reduced CO_2-stimulated breathing.[47] To examine the role in these effects of GPR4 pH sensitivity, per se, we leveraged CRISPR/Cas9 genome editing to generate knock-in mice expressing the pH-desensitized GPR4(H81F) receptor from the endogenous *Gpr4* locus in mice (**fig. 4.2A**), and intercrossed F1 heterozygous $GPR4^{H81F/+}$ mice to produce wild type $GPR4^{+/+}$ and

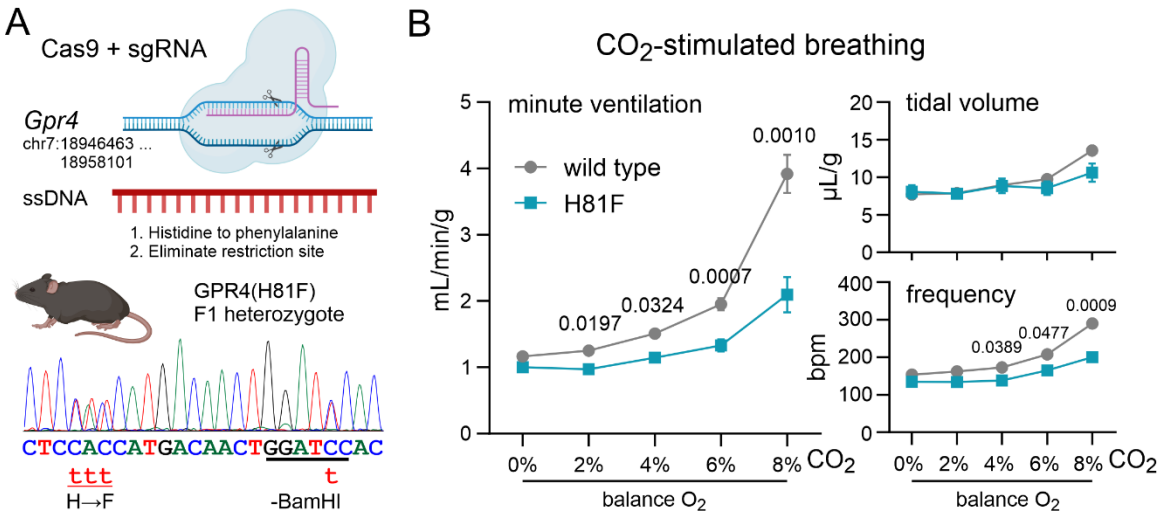

Figure 4.2: Mutation of a pH sensing residue (His81) in GPR4 blunts CO_2-stimulated breathing in mice. (A) Top: Schematic of CRISPR knock in strategy; Bottom: Sanger sequencing trace from an F1 heterozygote showing targeted alterations in *Gpr4* genomic sequence: substitution of Phe for His81, and elimination of BamHI restriction site. (B) Minute ventilation, tidal volume, and frequency of GPR4(H81F) (n = 9) and wildtype control (n = 9) mice in response to increasing levels of inspired CO_2 (balance O_2). Two-way RM-ANOVA: minute ventilation: $F_{(1, 18)} = 26.75$, $P < 0.0001$ for genotype and $F_{(4, 72)} = 15.04$, $P < 0.0001$ for CO_2 exposure × genotype; frequency: $F_{(1, 18)} = 17.65$, $P = 0.0005$ for genotype and $F_{(4, 72)} = 6.311$, $P = 0.0002$ for CO_2 exposure × genotype; tidal volume: $F_{(1, 18)} = 0.7610$, $P = 0.3945$ for genotype and $F_{(4, 72)} = 7.138$, $P < 0.0001$ for CO_2 exposure × genotype *, $P < 0.05$, **, $P < 0.01$, ***, $P < 0.001$.

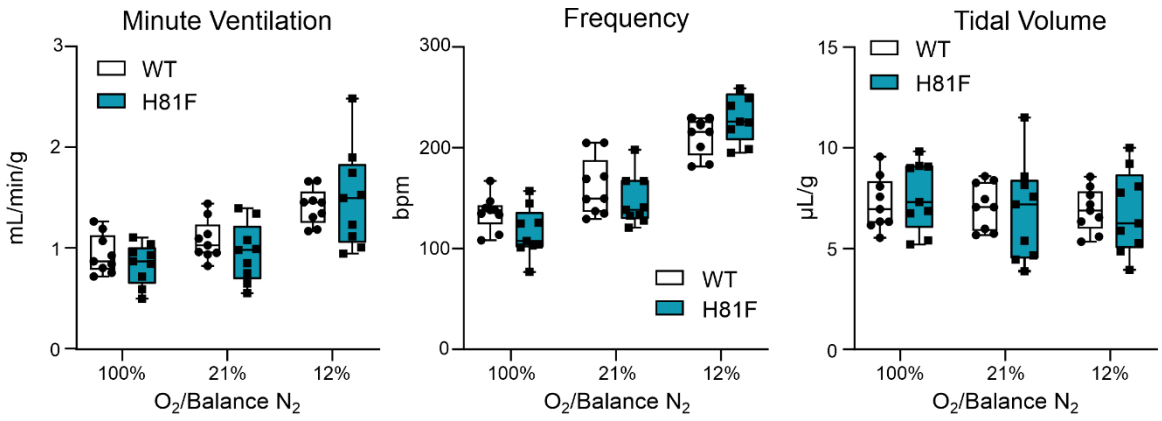

Figure 4.3: Oxygen-modulated breathing is unaltered in GPR4(H81F) mice. Minute ventilation, tidal volume, and frequency of H81F (n = 9) and wildtype control (n = 9) mice during exposure to the indicated levels of inspired O_2. Two-way RM-ANOVA for minute ventilation: $F_{(1, 16)} = 0.1569$, $P = 0.6973$ for genotype and $F_{(2, 32)} = 0.1231$, $P = 0.1231$ for O_2 exposure × genotype. Two-way RM-ANOVA for frequency: $F_{(1, 16)} = 0.2885$, $P = 0.5986$ for genotype and $F_{(2, 32)} = 8.040$, $P = 0.0015$ for O_2 exposure × genotype. Two-way RM-ANOVA for tidal volume: $F_{(1, 16)} = 0.0003705$, $P = 0.9849$ for genotype and $F_{(2, 32)} = 1.102$, $P = 0.3445$ for O_2 exposure × genotype.

GPR4$^{H81F/H81F}$ littermates on a mixed genetic background for experimental study (hereafter called WT and H81F).

We performed whole-body plethysmography to assess CO_2-stimulated breathing in WT and H81F mice, examining a range of CO_2 levels (0% to 8%) under hyperoxic conditions to minimize the influence of peripheral chemoreceptors. By comparison to WT littermates, GPR4(H81F) mice had significantly reduced ventilatory response to CO_2 (**fig. 4.2B**); the CO_2-induced increase in minute ventilation (V_E), the product of respiratory frequency (fR) and tidal volume (V_T), was significantly blunted in GPR4(H81F) mice, largely due to effects on fR (**fig. 4.2B**). These respiratory deficits were specific to CO_2 sensitivity as there was no difference in baseline respiration in room air (21% O_2) between WT and GPR4(H81F) animals, and no difference in their hypoxic ventilatory response (**fig. 4.3**).

4.3.3 – CO_2 sensitivity of RTN neurons is reduced in GPR4(H81F) knock-in mice

We used the GPR4(H81F) mice to examine the role of GPR4-mediated pH sensitivity in mediating CO_2/H^+ activation of the respiratory chemosensory neurons of the RTN in vivo. First, using RNAscope in situ hybridization, we examined *Fos* expression after 12% CO_2 exposure as a surrogate measure of CO_2-mediated activation of *Gpr4*-expressing RTN neurons in vivo; RTN neurons were definitively identified by expression of *Nmb* (**fig. 4.4**). Consistent with reduced CO_2 sensitivity, we found fewer *Fos*-labeled *Nmb*$^+$/*Gpr4*$^+$ RTN neurons (*white arrowheads*) in sections from GPR4(H81F) mice (**fig. 4.4B**). Indeed, the number of CO_2-activated RTN neurons (i.e., *Fos*$^+$/*Nmb*$^+$ cells) was lower in GPR4(H81F) mice relative to WT littermates across the rostrocaudal extent of the nucleus (**fig. 4.4C**); we found that 63 ± 1% of RTN neurons in WT mice were activated by CO_2, similar to our previous work,[47,77,183] whereas only 27 ± 2% of RTN neurons were

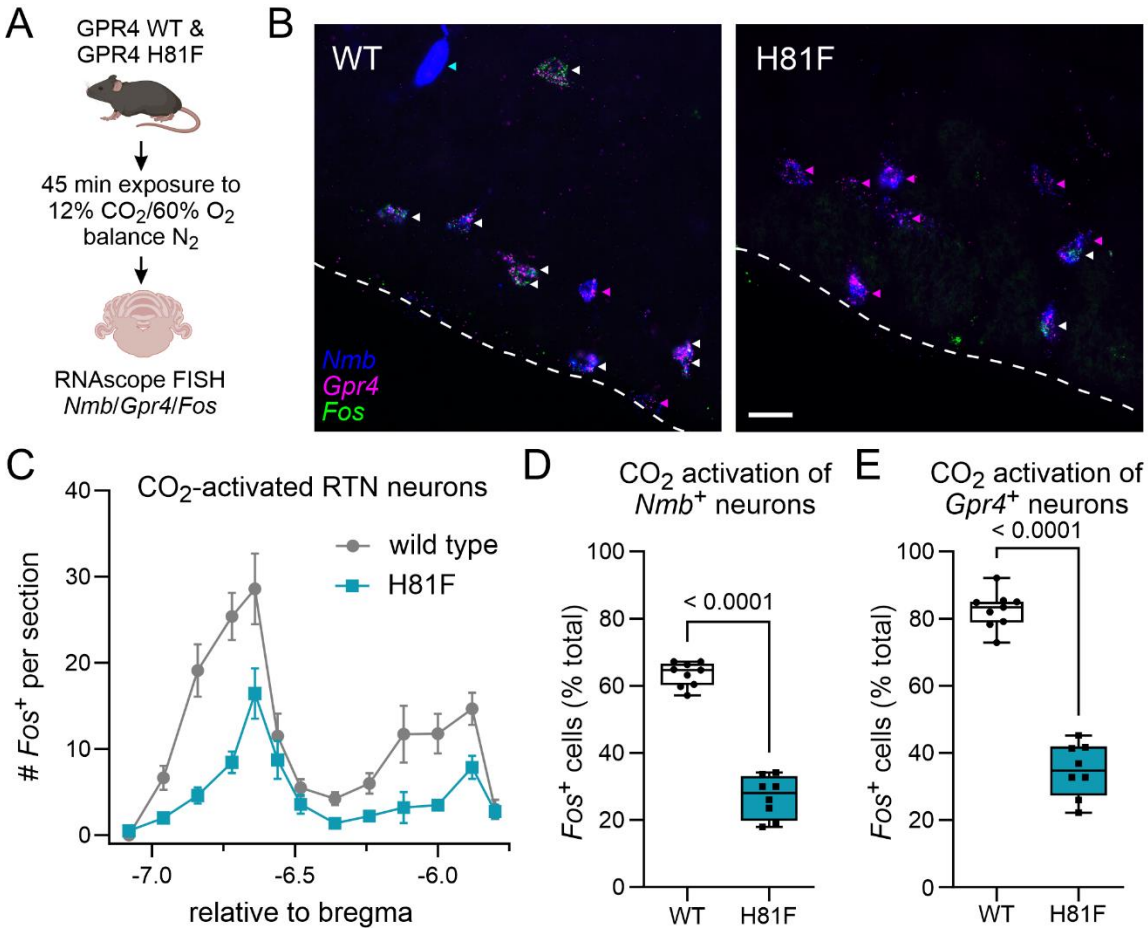

Figure 4.4: CO_2-stimulated RTN neuron activation *in vivo* is blunted in GPR4(H81F) mice. (A) Schematic of experimental design. (B) Representative RNAscope images for *Nmb*, *Gpr4*, and *Fos*. CO_2-activated RTN neurons (*Nmb*+/*Gpr4*+/*Fos*+) are denoted with white arrows; RTN neurons (*Nmb*+/*Gpr4*+) not activated by CO_2 (i.e., *Fos*-negative) are denoted with magenta arrows; blue arrow denotes *Nmb*+ cell expressing neither *Gpr4* nor *Fos*. (C) Distribution of CO_2-activated RTN neurons (*Nmb*+/*Gpr4*+/*Fos*+) throughout the rostrocaudal extent of the RTN in WT and GPR4(H81F) mice (mean ± SEM, N=9 and 8). (D) Total percent of RTN (*Nmb*+) neurons expressing *Fos*. (E) Total percent of *Gpr4*+ cells also positive for *Fos*. (WT: n = 9; GPR4(H81F): n = 8; unpaired t test, ****P < 0.0001).

activated in GPR4(H81F) mice (**fig. 4.4C**). Note that a subpopulation of RTN neurons with high levels of *Nmb* do not express *Gpr4* and those cells also tend not to express Fos after CO_2 exposure;[14] thus, when focusing only on the *Gpr4*-expressing subgroup of RTN neurons, we found an even higher percentage of *Fos*$^+$, CO_2-activated neurons in WT mice (~80%) with little difference in GPR4(H81F) mice (~30%; **fig. 4.4E**). Notably, we found no difference in the number or distribution of *Nmb*-expressing cells (i.e., RTN neurons) throughout the nucleus (**fig. 4.5A**), or in the number/distribution of RTN neurons that express *Gpr4* or *Kcnk5* (the gene encoding the other RTN proton sensor TASK-2) (**fig. 4.5B,C**). These data indicate that effects of the H81F substitution in GPR4 on CO_2-stimulated breathing are not due to differences in the number of RTN neurons, including the *Gpr4*- and *Kcnk5*-expressing populations; they also suggest that RTN neurons expressing GPR4(H81F) may be less sensitive to CO_2.

4.3.4 – The GPR4(H81F) substitution reduces pH sensitivity of RTN neurons in vitro

To provide a more direct test of the effects of CO_2/H^+ sensitivity of RTN neurons we performed in vitro electrophysiological experiments in acute brain slices from WT and GPR4(H81F) mice. In order to visualize RTN neurons for recording, we crossed the GPR4(H81F) mice with the previously described Phox2b::GFP mice (Jx99), a line in which we typically find >90% of GFP$^+$ neurons in the RTN region increase firing in response to bath acidification. We first verified that the differences observed for in vivo CO_2 sensitivity were retained in the GPR4(H81F)-Jx99 line, in which the GPR4 substitution is expressed on a different mixed genetic background. Indeed, CO_2-stimulated breathing was blunted in GPR4(H81F)-Jx99 mice, by comparison to their WT control littermates (**fig. 4.6A**), and the number of Fos immunoreactive RTN neurons observed after CO_2 exposure was reduced with no difference in the number of GFP+ neurons. (**fig. 4.6B**) Thus, the

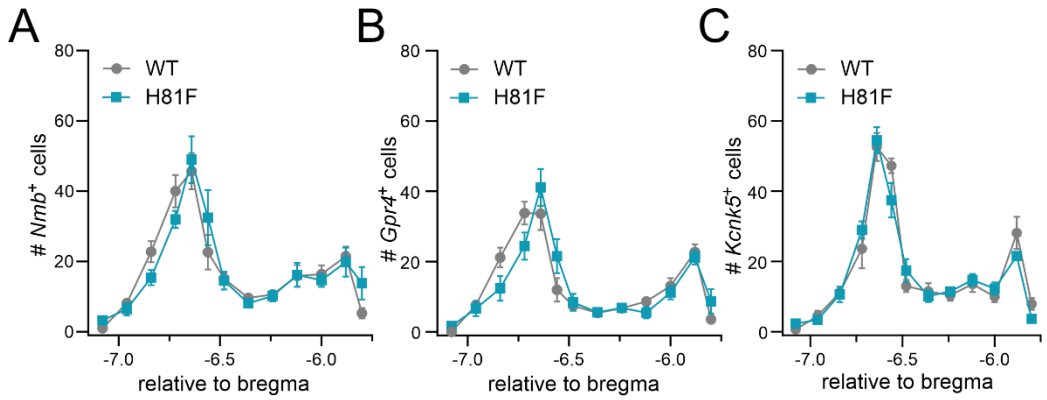

Figure 4.5: The RTN is intact in GPR4(H81F) mice, with equal numbers of *Nmb*-, *Gpr4*-, or *Kcnk5*-expressing RTN neurons. (A-C) Rostrocaudal distribution of RTN neurons (*Nmb*+, A), and of *Gpr4*+ (B) and *Kcnk5*+ (C) RTN neurons, in WT and GPR4(H81F) mice (mean ± SEM, N (A, B) = 9 and 8; N (C) = 7 and 7).

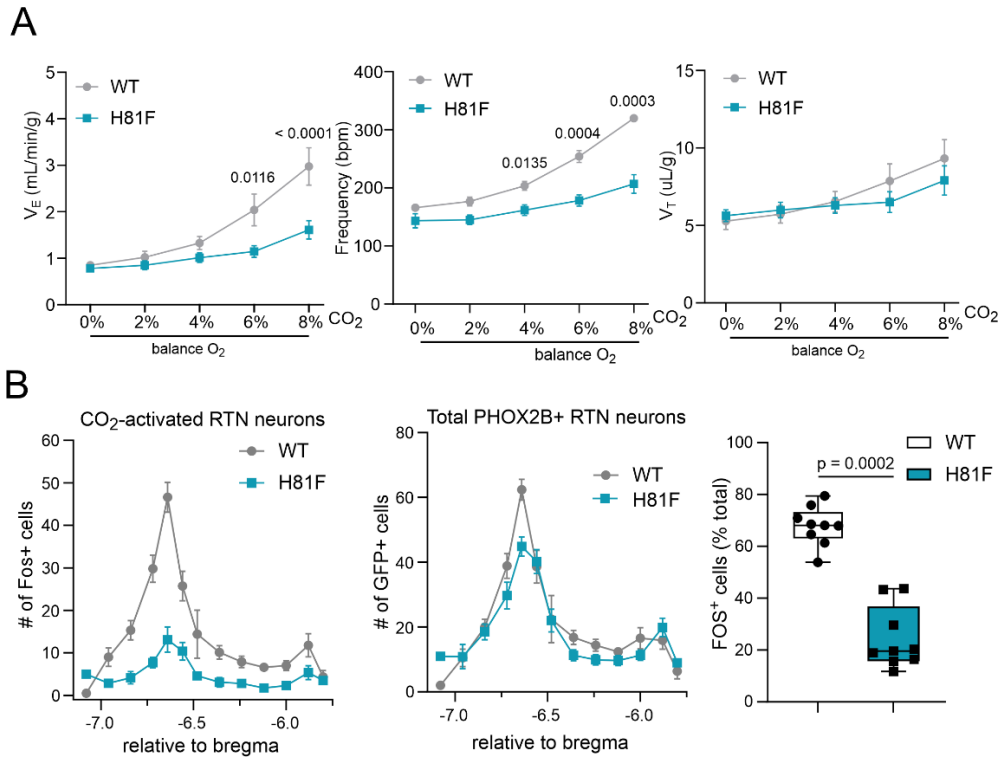

Figure 4.6: Fos protein expression after CO_2 challenge is decreased in Phox2b+ neurons of GPR4(H81F) mice**.** (A) GPR4(H81F) Phox2b::GFP mice also show blunted CO_2 sensitivity compared to wildtype Phox2b::GFP littermates (B) Distribution of Fos-immunoreactive, GFP-labeled neurons and total number of GFP-expressing neurons throughout the rostrocaudal extent of the RTN in either GPR4(H81F) or wild type Phox2b::GFP mice after exposure *in vivo* to 12% CO_2 (mean ± SEM, N = 9 and 9).

physiological effects were phenocopied in this separate line of mice that we prepared for electrophysiological studies.

We performed cell attached recordings from GFP-expressing RTN neurons to assess the effects of changing bath pH on cell firing (**fig. 4.7A**). In slices from WT Jx99 mice, RTN neurons were spontaneously active (at pH 7.3) and decreased their firing rate in response to bath alkalization (to pH 7.5 and pH 7.8) and increased their firing rate in response to bath acidification (to pH 7.0; **fig. 4.7B**); this characteristic response was observed in the majority of RTN neurons (~90%), for which a cell was considered pH-sensitive if firing rate decreased by >30% between pH 7.0 and pH 7.8 (**fig. 4.7C, fig. 4.8A**). By contrast, we observed two types of responses in recordings of RTN neurons from GPR4(H81F)-Jx99 mice. For some cells (~60%), bath alkalization and acidification led to decreased and increased firing, whereas a significant proportion (~40%) of GPR4(H81F)-expressing RTN neurons displayed no pH-modulated firing (**fig. 4.7C, D**). The pH-sensitive neurons from GPR4(H81F) mice had a significantly lower firing frequency at pH 7.0 (**fig. 4.7E**), and the pH-insensitive neurons maintained their firing across the pH range to present higher firing frequency at alkaline pH levels (**fig. 4.7E**). We subsequently obtained whole cell current clamp recordings in a subset of these neurons and found no difference among any of the groups -- wildtype and GPR4(H81F) RTN neurons, pH-sensitive or insensitive -- in intrinsic properties such as input resistance or input-output relationships (**fig. 4.8C,D**). Finally, we harvested individual GFP-labeled RTN neurons from acute slices obtained from these mice for single cell multiplexed quantitative RT-PCR. Expression of *Nmb* and Vglut2 (i.e., *Slc17a6*) was used to verify that the cells were indeed RTN neurons, and we found no difference in transcript levels for either *Gpr4* or TASK-2 (*Kcnk5*) in either neonatal or adult RTN neurons obtained from wildtype or GPR4(H81F)-Jx99 mice (**fig. 4.9**). Note that *Kcnk5* was detected in only approximately half of the RTN neurons, less than expected based on previous scRNA-Seq or RNAscope analyses (e.g., >80%);[14]

nevertheless, this was the case for both wild type and GPR4(H81F)-Jx99 mice, at both developmental stages, suggesting a higher detection threshold for *Kcnk5* with this multiplexed sc-qPCR assay. Collectively, these data indicate that introducing a GPR4(H81F) substitution in mice reduces CO2-stimulated breathing along with the sensitivity of RTN neurons to changes in CO_2/H^+, without affecting the number of RTN neurons, expression of GPR4 or TASK-2, or basic neuronal excitability.

4.3.5 – CO_2-stimulated breathing and CO_2 sensitivity of RTN neurons is reduced in GPR4(H167F) mice

We next considered the possibility that the CO_2 sensing deficits might be specific to the H81F mutation, perhaps interfering with GPR4 function in a manner independent of effects on pH sensitivity. In order to address this possibility, we introduced another pH-desensitizing mutation, His167Phe, using a CRISPR/Cas9 strategy analogous to that utilized for the H81F knock-in animals (**fig. 4.10A**); in this case, the genetic substitution was made on a C57BL/6 background. As observed in the GPR4(H81F) knock-in animals, GPR4(H167F) mice displayed a blunted hypercapnic ventilatory reflex (**fig. 4.10B, 4.11A**), again with no effect on the hypoxic ventilatory response (**fig. 4.10B, fig. 4.11B**). In addition, we again observed a decrease in the proportion of *Fos*$^+$ RTN neurons (*Nmb*$^+$ or *Nmb*$^+$/*Gpr4*$^+$) activated by an acute CO_2 challenge (**fig. 4.10C-D, fig. 4.12A**) without any effect on the overall number of *Nmb*$^+$, *Gpr4*$^+$, or *Kcnk5*$^+$ expressing cells throughout the rostrocaudal extent of the RTN (**fig. 4.12B-D**). Thus, these data from GPR4(H167F) mice essentially phenocopy results from the GPR4(H81F) mice, supporting the conclusion that the pH sensitivity of GPR4 is necessary for CO_2-stimulated breathing and CO_2 sensitivity of RTN neurons in mice.

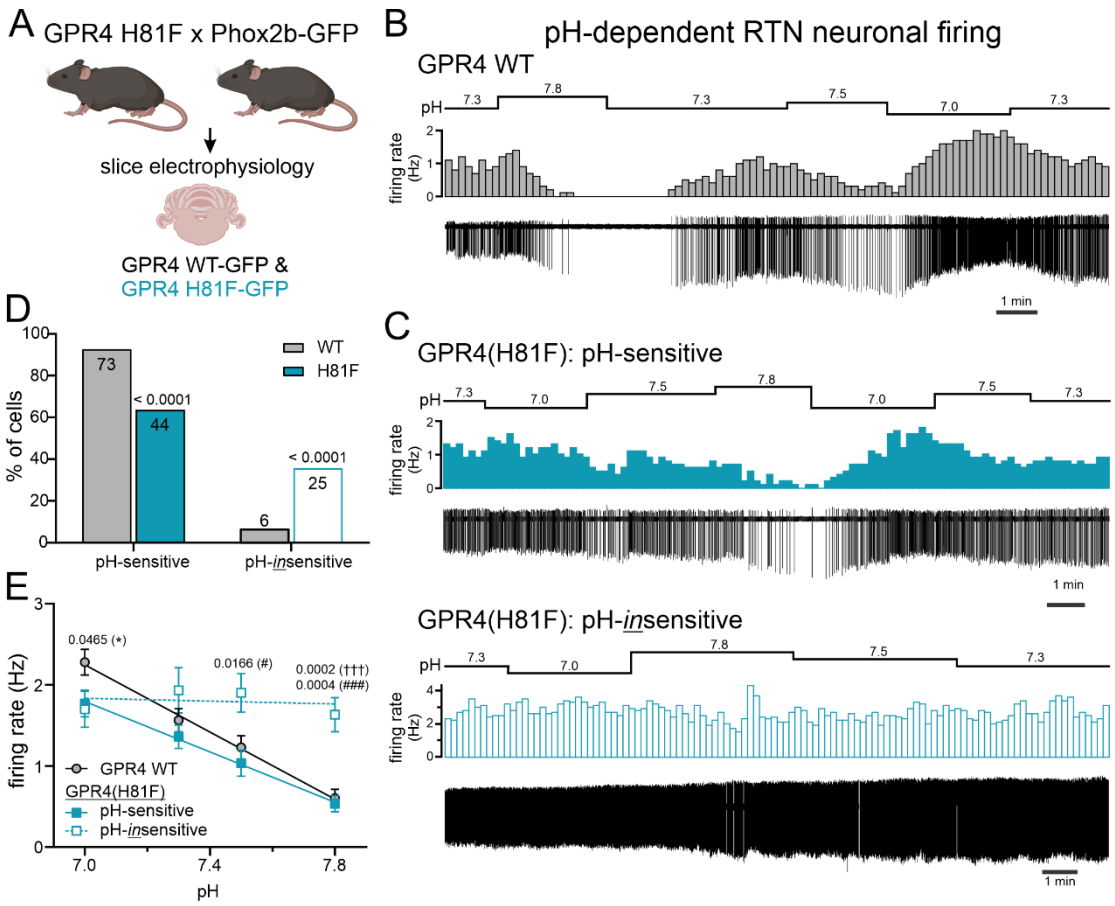

Figure 4.7: A subset of RTN neurons from GPR4(H81F) mice lack pH sensitivity in acute slices. (A) Schematic of experimental design. (B) Representative cell attached recording from a GFP-expressing RTN neuron from a wild type Phox2b::GFP mouse. (C) Representative cell attached recordings from pH-sensitive and pH-insensitive GFP+ RTN neurons from GPR4(H81F) Phox2b::GFP mice. (D) Percent of cells from each genotype that are either pH-sensitive or pH-insensitive (****P < 0.0001 by χ^2; numbers are provided within the bars for each group). (E) Averaged firing rates at different bath pH for RTN neurons from GPR4 WT mice (n = 79) and for RTN neurons from GPR4(H81F) mice that were identified as pH-sensitive (n = 44) or pH-insensitive (n = 25). *, P < 0.05 for GPR4 WT vs. GPR4(H81F):pH-sensitive; †††, P < 0.001 for GPR4 WT vs. GPR4(H81F):pH-insensitive; #P < 0.05, ###P < 0.001 GPR4(H81F):pH-sensitive vs. GPR4(H81F):pH-insensitive, by Mixed-effects model with Tukey's test (for genotype $F_{(2, 143)} = 2.553$, P = 0.0814; for pH × genotype $F_{(6, 410)} = 19.67$, P < 0.0001).

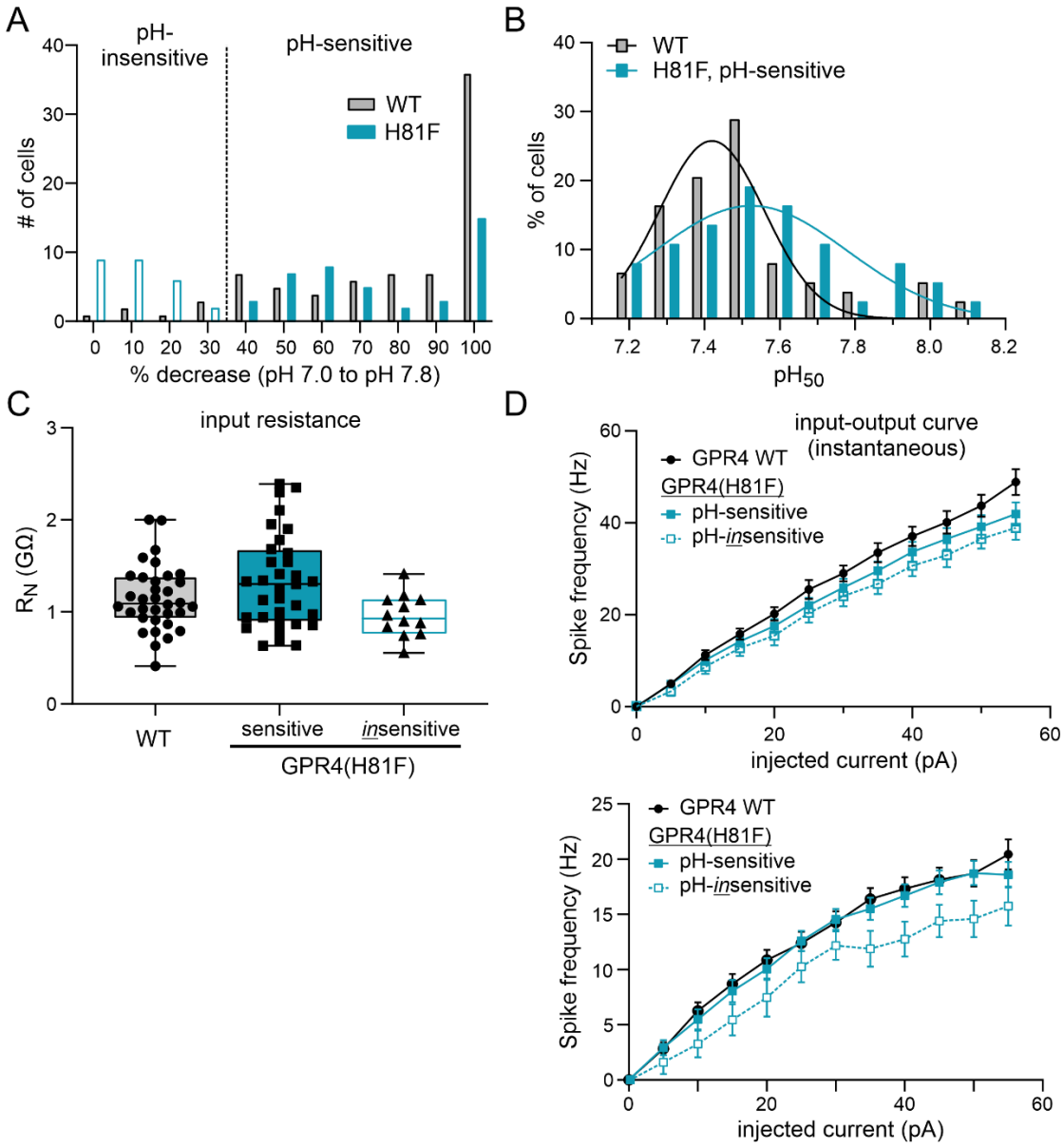

Figure 4.8: H81F mutation affects distribution of pH sensitive cell number and pH_{50} without grossly affecting input resistance or excitability. (A) Frequency distribution of pH-sensitive and pH-insensitive RTN neurons from GPR4 WT and GPR4(H81F) Phox2b::GFP mice; the cutoff for designation into these two groups is indicated. (B) Distribution of pH_{50} values (i.e., the pH at which firing rate decreased to 50% of that at pH 7.0) for pH-sensitive RTN neurons from GPR4 WT and GPR4(H81F) Phox2b::GFP mice. (C) Steady-state input resistance of RTN neurons from GPR4 WT mice, and pH-sensitive and pH-insensitive RTN neurons from GPR4(H81F) mice. (D) Instantaneous and steady state firing frequency during current injection in RTN neurons from the indicated mice.

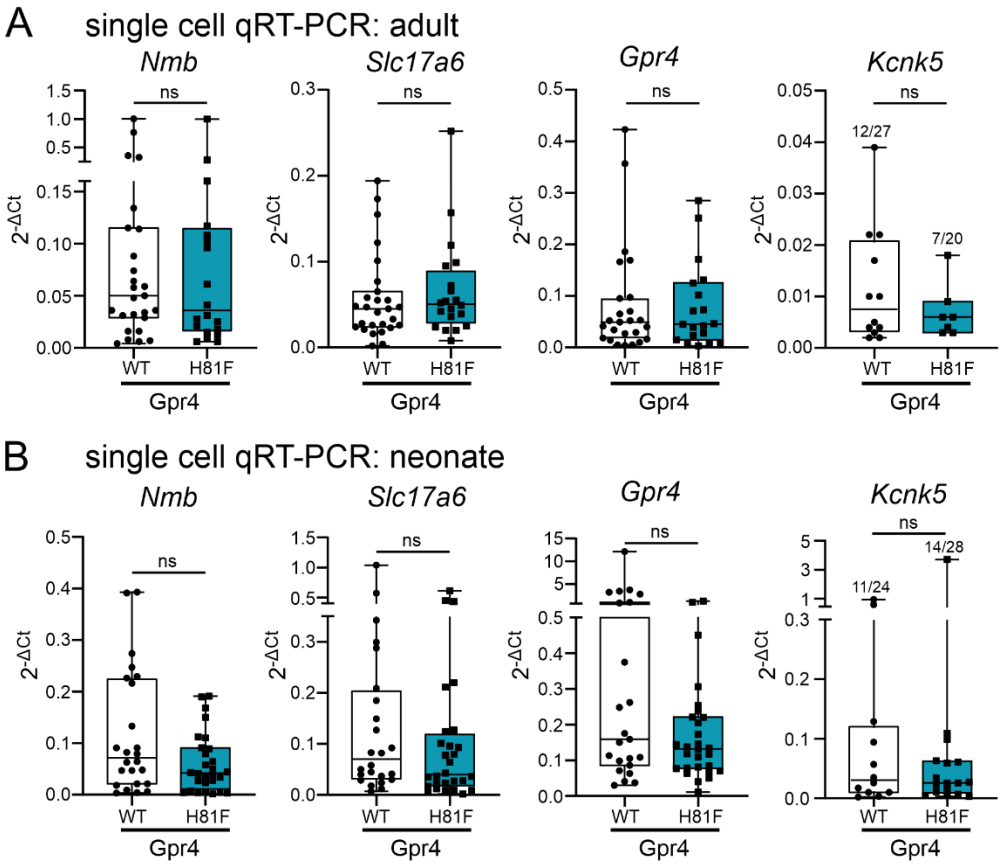

Figure 4.9: Expression levels of key molecular markers are not different in RTN neurons from GPR4 WT and GPR4(H81F) mice**.** (A,B) Single cell qRT-PCR results for RTN markers *Nmb* and *vGlut2* as well as for proton sensors *Gpr4* and *Kcnk5* from adult (A) and neonatal (B) RTN neurons (adult: WT, N = 4, n = 27; GPR4(H81F), N = 3, n = 20; neonate: WT, N = 3, n = 24; GPR4(H81F), N = 3, n = 28).

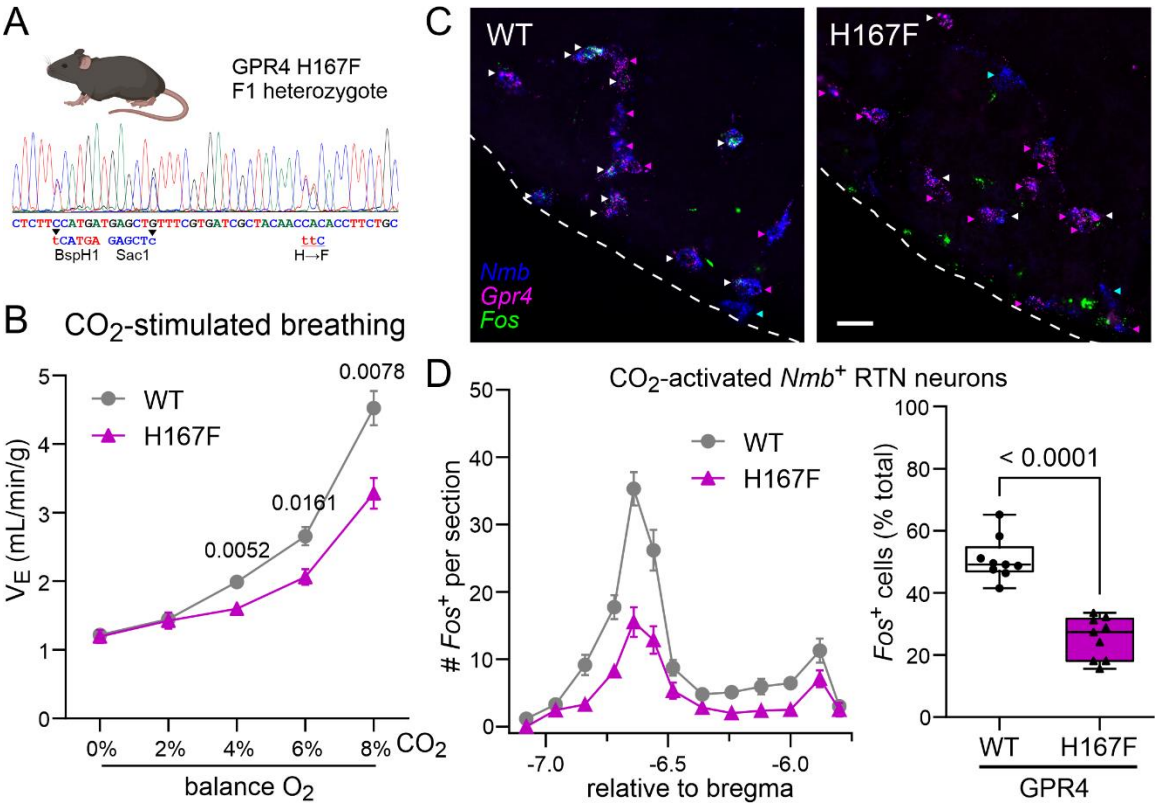

Figure 4.10: Mutation of a pH sensing residue (His167) in GPR4 blunts CO_2-stimulated breathing and CO_2-evoked RTN neuron activation in mice. (A) Sanger sequencing trace from an F1 heterozygote showing targeted alterations in *Gpr4* genomic sequence after CRISPR/Cas9 editing; substitution of Phe for His167, and introduction of silent BspHI and SacI restriction sites. (B) Minute ventilation of GPR4(H167F) (n = 10) and wildtype control (n = 11) mice in response to increasing levels of inspired CO_2 (balance O_2). Two-way RM-ANOVA: $F_{(1, 19)} = 13.03$, $P = 0.0019$ for genotype and $F_{(4, 76)} = 10.06$, $P < 0.0001$ for CO_2 exposure × genotype ; *, $P < 0.05$, **, $P < 0.01$. (C) Representative RNAscope images for *Nmb*, *Gpr4*, and *Fos*. CO_2-activated RTN neurons (*Nmb*+/*Gpr4*+/*Fos*+) are denoted with white arrows; RTN neurons (*Nmb*+/*Gpr4*+) not activated by CO_2 (i.e., *Fos*-negative) are denoted with magenta arrows; blue arrows denote *Nmb*+ cells expressing neither *Gpr4* nor *Fos*. (D) Left: Distribution of CO_2-activated RTN neurons (*Nmb*+/*Gpr4*+/*Fos*+) throughout the rostrocaudal extent of the RTN in WT and GPR4(H167F) mice (mean ± SEM). Right: Total percent of RTN (*Nmb*+) neurons expressing *Fos* (WT: n = 9, H167F: n = 9; unpaired t test, ****$P < 0.0001$).

4.3.6 – Concurrent knockout of TASK-2 in addition to H81F mutation of GPR4 has no additive effect to blunt CO_2 sensitivity or activation of RTN neurons

In previous work, we found that the hypercapnic ventilatory reflex depends on both GPR4 and TASK-2 – i.e., global deletion of either GPR4 or TASK-2 alone partially blunted the HCVR whereas loss of both genes nearly eliminated CO_2-stimulated breathing. Here, to determine if loss of TASK-2 can eliminate the residual CO_2 sensitivity observed in GPR4(H81F) animals, we generated mice homozygous for wildtype or H81F variants of GPR4 in the context of either intact or deleted TASK-2 genes (on the Jx99 background). By comparison to control littermates ($GPR4^{+/+}$;$TASK\text{-}2^{+/+}$), we found that CO_2-stimulated breathing was reduced both in mice with GPR4(H81F) mutation alone (by ~65% at 8% CO_2) and in mice with TASK-2 deletion alone (by ~60%)(**fig. 4.13A**); this is consistent with the partial reduction in the HCVR noted in previous work from GPR4 knockout and TASK-2 knockout mice. However, although CO_2-stimulated breathing was similarly reduced in doubly mutated GPR4(H81F);$TASK\text{-}2^{-/-}$ mice relative to controls (by ~72%), there was no significant difference in the magnitude of the HCVR among any of the mutated mice. These data differ from those obtained previously with global knockout mice, where combined deletion of GPR4 and TASK-2 further decreased CO_2 sensitivity compared to the loss of either gene alone. As expected, there was no effect of any of these gene mutations on the hypoxic ventilatory response (**fig. 4.14A-C**).

We then examined activation of RTN neurons by an acute CO_2 challenge in vivo, again using FOS as a proxy for neuronal activation, and with GFP immunoreactivity to label PHOX2B-expressing RTN neurons in these singly and doubly mutated Jx99 mice. The number of FOS^+ cells was reduced across the rostrocaudal extent of the RTN in all mutant mice, compared to the wildtype control littermates, with no difference in the number of GFP+ RTN neurons among any of the groups (**fig. 4.13B**). A slightly higher total number of FOS^+ cells was obtained in RTN neurons from mice deleted only for TASK-2, on a

wildtype GPR4 background, as compared to either GPR4(H81F) or GPR4(H81F);TASK-2$^{-/-}$ mice but there was no difference between the latter two groups (**fig. 4.13B-C**). Thus, RTN neuronal activation by CO_2 is disrupted by loss of function in both TASK-2 and GPR4, via the H81F mutation, with perhaps a smaller effect of TASK-2 deletion than GPR4 mutation.

4.3.7 – Blood chemistry is unaffected in GPR4(H81F) and GPR4(H167F) mice

GPR4 is expressed in relatively few neuronal populations outside the RTN,[47,80,114] but it is found in various peripheral tissues where it has been associated with several physiological processes, including acid-base regulation by the kidney.[117,133–135] We therefore performed arterial blood gas analysis on the different lines of mice to test for any chronic changes in blood gases or acid-base status (**Table 4.1**). In the GPR4(H81F) line, we found a slight metabolic alkalosis in the GPR4(H81F) mice, with elevated HCO_3^- levels in the His-substituted mice relative to their wild type littermates. However, this was not observed in either the GPR4(H81F)-Jx or the GPR4(H167F) mouse lines, and there were no differences in arterial PO_2, PCO_2 or lactate across any of the lines. Thus, we found no systematic differences in arterial blood gases or pH that can account for the effects of the GPR4 histidine substitutions on CO_2 stimulated breathing or RTN neuronal CO_2/H^+ sensitivity.

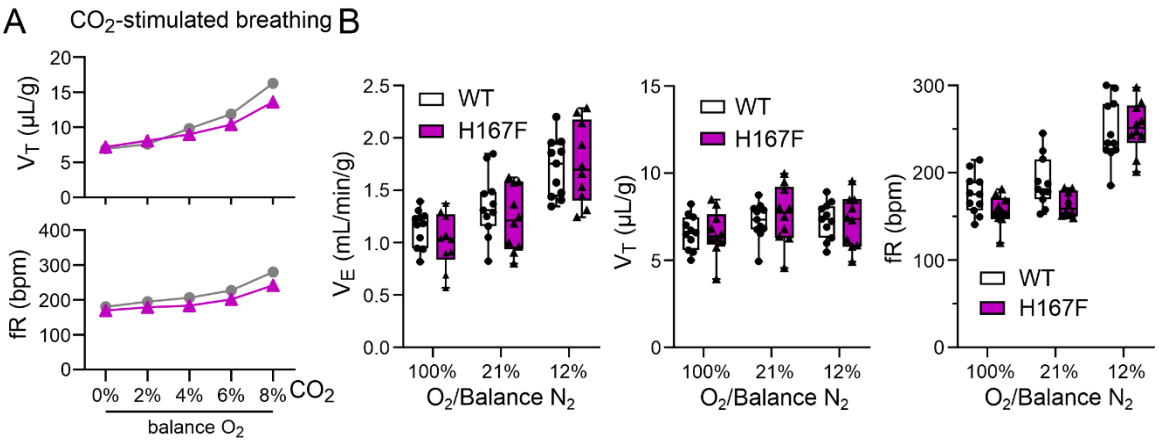

Figure 4.11: Oxygen modulated breathing is unaltered in GPR4(H167F) mice. (A) tidal volume (top) and frequency (bottom) in response to increased inspired CO_2, balance oxygen. (B) Minute ventilation, tidal volume, and frequency of H167F (n = 10) and wildtype control (n = 11) mice during exposure to the indicated levels of inspired O_2. Two-way RM-ANOVA analysis: for minute ventilation $F_{(1, 19)} = 0.4037$, P = 0.5328 for genotype and $F_{(2, 38)} = 1.823$, P = 0.1754 for O_2 exposure × genotype; for frequency $F_{(1, 19)} = 1.941$, P = 0.1796 for genotype and $F_{(2, 38)} = 5.163$, P = 0.0104 for O_2 exposure × genotype; for tidal volume $F_{(1, 19)} = 0.01746$, P = 0.8963 for genotype and $F_{(2, 38)} = 0.7348$, P = 0.4863 for O_2 exposure × genotype.

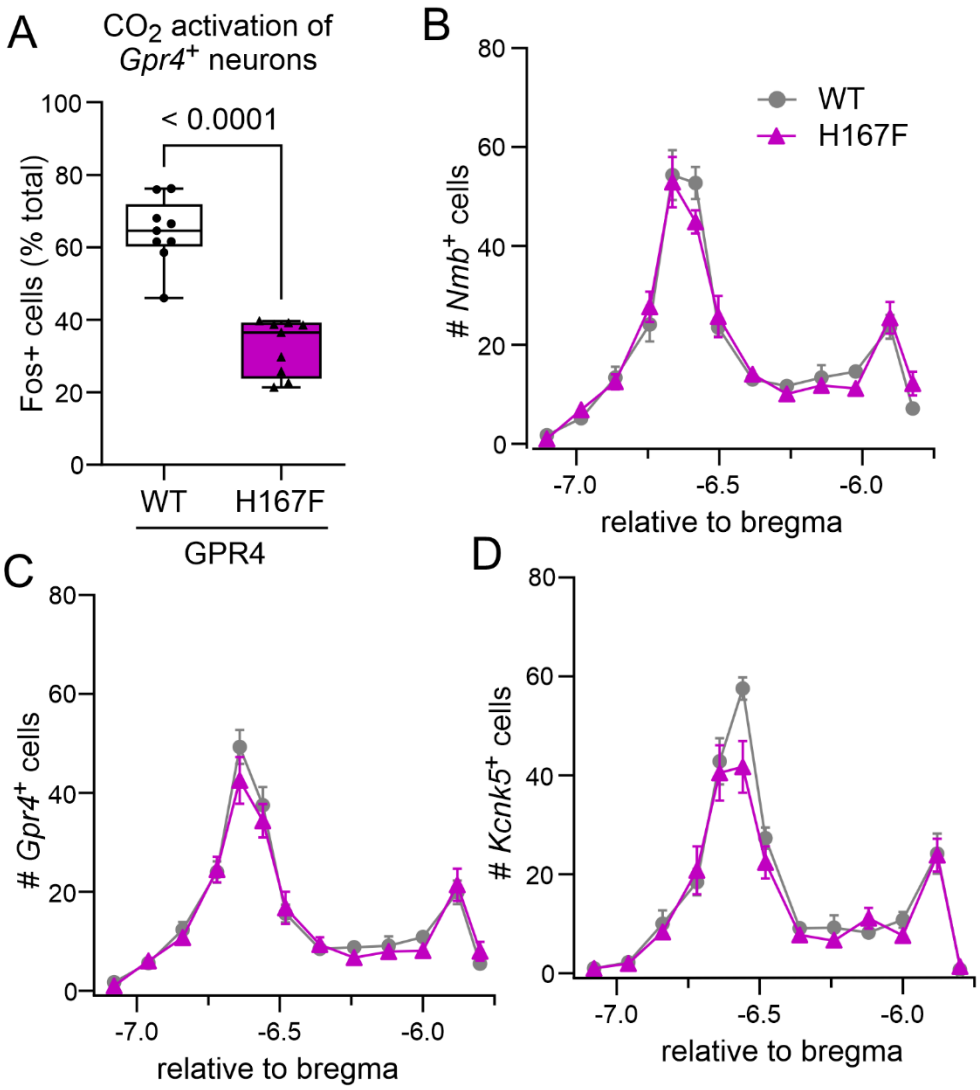

Figure 4.12: H167F animals have decreased activation of *Gpr4* expressing RTN neurons in response to CO_2 challenge without alterations in total number of *Gpr4*+, *Kcnk5*+, or *Nmb*+ cells**.** (A) Total percent of GPR4-expressing RTN (*Gpr4+ and Nmb+*) neurons expressing *Fos*. (B-D) Rostrocaudal distribution of RTN neurons (*Nmb*+, B), and of *Gpr4*+ (C) and *Kcnk5*+ (C) RTN neurons, in WT and GPR4(H167F) mice (mean ± SEM, N (B, C) = 9 and 10; N (D) = 6 and 7).

H81F-Jx	WT	H81F
pH	7.44 ± 0.01	7.44 ± 0.01
PO_2 (mmHg)	87.9 ± 2.5	89.9 ± 4.1
PCO_2 (mmHg)	30.8 ± 0.9	29.9 ± 2.2
HCO_3 (mmol/L)	21.2 ± 0.9	20.2 ± 1.5
lactate (mmol/L)	2.73 ± 0.40	3.72 ± 0.41
	n = 13	n = 13

H81F	WT	H81F
pH	7.40 ± 0.01	7.44 ± 0.01 *
PO_2 (mmHg)	84.3 ± 3.3	89.9 ± 2.3
PCO_2 (mmHg)	30.4 ± 1.2	34.3 ± 1.5
HCO_3 (mmol/L)	19.8 ± 0.9	24.3 ± 0.9 **
lactate (mmol/L)	3.71 ± 0.66	3.39 ± 0.35
	n = 12	n = 13

H167F	WT	H167F
pH	7.42 ± 0.01	7.42 ± 0.01
PO_2 (mmHg)	85.8 ± 2.2	91.2 ± 2.3
PCO_2 (mmHg)	33.5 ± 1.0	31.2 ± 1.0
HCO_3 (mmol/L)	21.7 ± 0.8	20.2 ± 0.9
lactate (mmol/L)	4.01 ± 0.51	4.05 ± 0.52
	n = 15	n = 14

H81-TASK2	WT	H81F	T2KO	mutKO
pH	7.39 ± 0.03	7.41 ± 0.02	7.35 ± 0.03	7.37 ± 0.02
PO_2 (mmHg)	94.5 ± 2.2	93.9 ± 2.7	101 ± 1.2	100 ± 2.2
PCO_2 (mmHg)	27.1 ± 1.2	29.0 ± 1.2	23.5 ± 1.3 *	20.8 ± 1.2 *
HCO_3 (mmol/L)	16.5 ± 1.0	18.2 ± 0.8	12.8 ± 0.6 *	12.3 ± 1.0 **
lactate (mmol/L)	5.22 ± 0.93	5.03 ± 0.79	5.96 ± 0.72	5.55 ± 0.72

Table 4.1: Arterial blood gas chemistry from H81F, H81F-Jx, H167F, and H81-TASK2 lines.

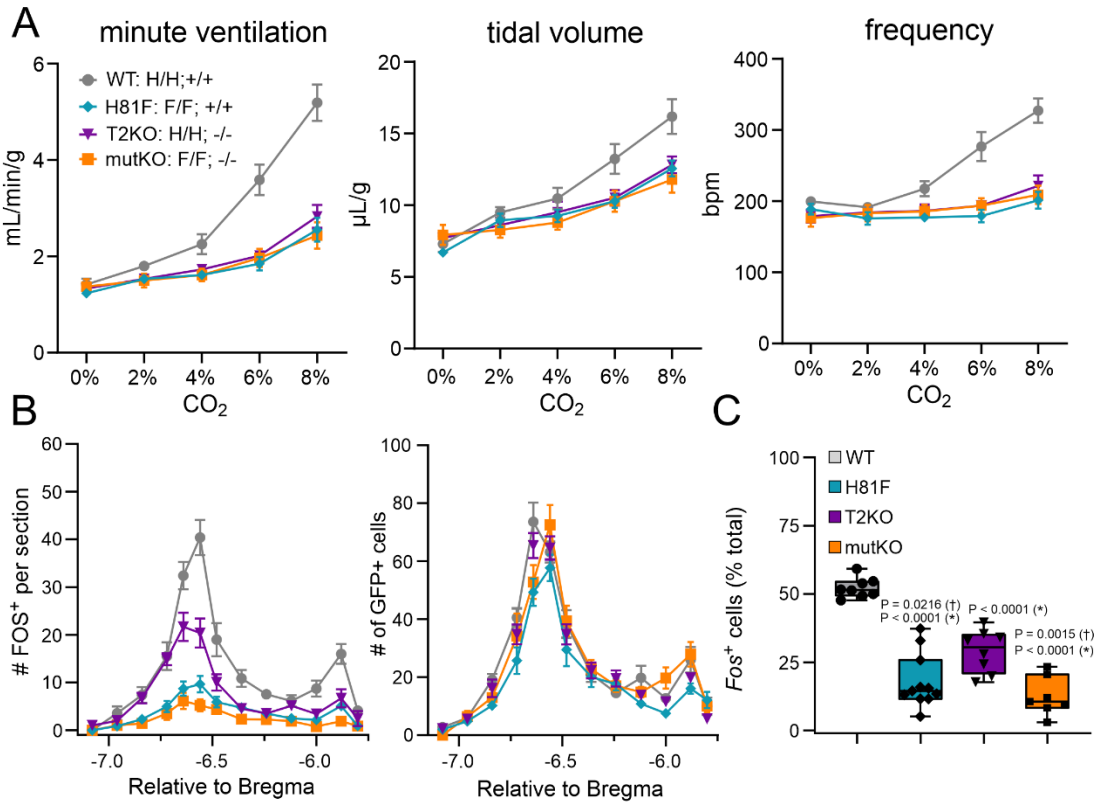

Figure 4.13: Concurrent deletion of TASK-2 in addition to GPR4(H81F) knock-in does not affect magnitude of HCVR decrease but may further attenuate RTN neuron activation compared to GPR4(H81F) knock-in**.** (A) Minute ventilation, tidal volume, and frequency of GPR4(H81F) (n = 12) TASK-2 knockout (T2KO) (n = 7), TASK-2 and GPR4(H81F) (mutKO) (n = 10), and wildtype (WT) control (n = 10) mice in response to increasing levels of inspired CO_2 (balance O_2). Two-way RM-ANOVA analysis: for minute ventilation $F_{(3, 35)} = 15.78$, $P < 0.0001$ for genotype, and $F_{(12, 140)} = 13.78$, $P < 0.0001$ for CO_2 × genotype; for frequency $F_{(3, 35)} = 10.74$, $P < 0.0001$ for genotype, and $F_{(12, 140)} = 9.016$, $P < 0.0001$ for CO_2 × genotype; for tidal volume $F_{(3, 35)} = 2.802$, $P = 0.0541$ for genotype, and $F_{(12, 140)} = 4.337$, $P < 0.0001$ for CO_2 × genotype. (B) Distribution of Fos-immunoreactive, GFP-labeled neurons and total number of GFP-expressing neurons throughout the rostrocaudal extent of the RTN in GPR4(H81F) (n = 11) TASK-2 knockout (T2KO) (n = 6), TASK-2 and GPR4(H81F) (dKO) (n = 7), and wildtype (WT) control (n = 7) mice after exposure *in vivo* to 12% CO_2. (C) Total percent of RTN (Phox2b::GFP+) neurons expressing FOS; one-way ANOVA, * = compared to WT, † = compared to T2KO).

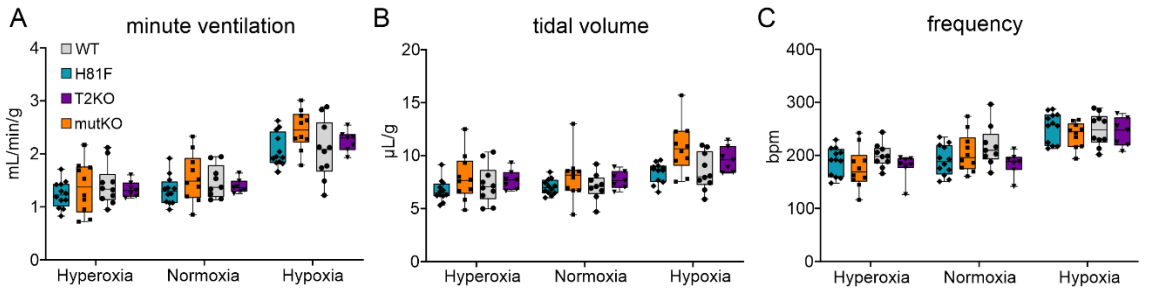

Figure 4.14: Oxygen modulated breathing is unaltered in GPR4(H81F)-TASK2 mice. Minute ventilation (A), tidal volume (B), and frequency (C) of GPR4(H81F) (n = 12) TASK-2 knockout (T2KO) (n = 7), TASK-2 knockout and GPR4(H81F) (mutKO) (n = 10), and wildtype (WT) control (n = 10) mice during exposure to the indicated levels of inspired O_2. Two-way RM-ANOVA analysis: for minute ventilation $F_{(3, 35)} = 1.029$, $P = 0.3915$ for genotype and $F_{(6, 69)} = 3.851$, $P = 0.0023$ for O_2 exposure × genotype; for tidal volume $F_{(3,35)} = 2.195$, $P = 0.1060$ for genotype and $F_{(6, 69)} = 3.812$, $P = 0.0024$ for O_2 exposure × genotype; for frequency $F_{(3, 35)} = 1.099$, $P = 0.3627$ for genotype and $F_{(6, 69)} = 2.185$, $P = 0.0547$ for O_2 exposure × genotype.

4.4 – Discussion

The data presented in this chapter support the role of GPR4-mediated pH sensitivity, per se, and not simply GPR4 protein expression in activation of the central chemoreflex by increased inspired CO_2. Animals containing two distinct pH-insensitive GPR4 mutants demonstrate a blunted HCVR. Expression of a pH-insensitive GPR4(H81F) or GPR4(H167F) receptor is sufficient to blunt CO_2 activation of RTN neurons in vivo and, in the case of GPR4(H81F) animals, pH sensitivity of RTN neuron firing frequency in vitro. The level that CO_2 and pH sensitivity is attenuated in GPR4(H81F) animals is comparable to that attained by whole body GPR4 knockout suggesting that the deficiency previously observed is likely due to loss of pH sensitivity and not just loss of basal activity provided by GPR4.[47]

It is possible that mutating the His81 or His167 in GPR4 does not disrupt activation of the receptor by decreased pH and instead disrupts its activation by an unidentified native small molecule agonist. We argue that the analogous results observed in both the H81F and H167F knock-in animals decrease, but do not eliminate, the likelihood of this explanation. Since no small molecule agonist, native or synthesized, has yet been identified it is not yet possible to demonstrate that activation of GPR4 by another agonist aside from protons is unaffected by histidine mutation.

GPR4 is expressed in multiple nuclei throughout the brain, including in a number of other cell groups that have also been proposed to be central chemoreceptors.[114] One limitation in the work presented here concerns the lack of specificity of mutant GPR4 expression. It is possible that the deficiency noted in the HCVR is due to loss of GPR4-mediated pH sensitivity in one of these other nuclei. In this alternate model, the decrease in the magnitude of RTN activation is due to reduced input from these other nuclei and not due to loss of RTN pH activation specifically. It is also possible that there is a combinatory effect where the RTN serves both as a relay and a primary sensor. However,

previous work showed that re-expression of wildtype GPR4 in the RTN is sufficient to rescue noted deficits in the HCVR and in RTN activation. An analogous experiment can be completed using a virus expressing one of the pH insensitive receptors to determine if *pH-sensitive* GPR4 expression at the RTN is sufficient to rescue the HCVR, and not just expression of GPR4 generally. Additionally, the converse (targeted knockdown) experiment could be done using siRNA to determine in which nuclei GPR4 expression is necessary for a normal HCVR or other hypercapnic behaviors.

It is interesting to note that while the results reported here with the single His mutant animals match the results observed with whole body GPR4 knockout,[47] concurrent loss of TASK-2 on the H81F mutant background has no additive blunting effect on the HCVR as was observed in the whole body GPR4 knockouts.[47] Previous work showed that double knockout of GPR4 and TASK-2 at the whole body level completely eliminated the HCVR at 8% inspired CO_2.[47] In contrast, H81F animals without TASK-2 still respond with increases in minute ventilation at the highest concentration of inspired CO_2 (8%) reported here that are nearly identical to those observed with single knockout of TASK-2 or with mutation of GPR4 alone. It is possible that this key difference is due to the residual pH sensitivity that is retained by the H81F receptor which would not be present in a whole body GPR4 knockout. At pH 7.0 cAMP accumulation of the H81F receptor matches the level of cAMP generated when the wildtype receptor is stimulated with pH 7.4 solution. It is possible that the highest concentrations of CO_2 used in this work are able to decrease pH at the GPR4-expressing chemosensors, to that pH 7.0 landmark, that the H81F receptor can still be activated and maintain the observed residual HCVR. These whole animal HCVR results slightly differ from the results examining activation of the RTN specifically. In FOS studies of RTN PHOX2B neurons, deletion of TASK-2 in addition to H81F mutation seems to have an additive effect on blunting RTN activation by an acute CO_2 challenge. These results more closely match what we would expect based on the whole

animal data observed previously with the double knockout animals. Since the RTN seems to rely on both pH sensors remaining intact and functional, it is possible that the residual HCVR observed in the mutKO animals is due to residual GPR4 function at one of the other chemosensitive nuclei that also express GPR4 (i.e. the caudal raphe).

On a related note, the work here only examines the HCVR as a model system for which we know GPR4 expression is crucial for normal function based on previous work. Since GPR4 is expressed in multiple geographically and chemically distinct brain regions, it would be interesting to determine if the histidine knock-in animals only have deficits in central chemosensitivity or if they also show dysregulation in function of some of these other nuclei regulating anxiety emotion processing, arousal, or other aspects of respiration.

Even given the shortcomings listed above, we feel that the data presented here show that introduction of a single histidine mutant GPR4 at the whole animal level is sufficient to blunt CO_2 sensitivity. We posit that this deficiency is largely due to decreased RTN neuron activation by H^+ based on the data presented here and previously but experiments definitively supporting that model have yet to be completed. It is interesting to note that the single amino acid determinants of pH-sensitivity for the other putative RTN pH sensor, TASK-2, have also been identified.[72,74,75,186–188] Thus, a similar strategy could be pursued to determine if internal, external, or a combination of activating mechanisms for TASK-2 are necessary for a normal HCVR or normal RTN activation.

Chapter 5 - Conclusions and Future Directions

This thesis work aimed to show that pH sensitivity mediated by GPR4 is necessary for a normal HCVR and for normal pH activation of the RTN. We successfully described the expression pattern of GPR4 via an epitope tag knock-in strategy. GPR4 is expressed in multiple mid and hindbrain chemosensitive nuclei where it could presumably modulate neuronal activity during an acidotic challenge, caused by increased arterial CO_2 due to altered respiration or some other pathophysiological context. In the RTN, GPR4 seems to be specifically localized to soma directly adjacent to blood vessels and to ventral surface processes, not at projections to more distant target regions. This organization may allow for minimization of time to activation of RTN by low pH contact and to maximize surface area contact with CSF bathing the ventral medullary surface. It will be interesting to determine the expression pattern of GPR4 in the other nuclei more closely mimics that of the RTN or if it is unique at each to allow for specific functions of GPR4 in each distinct nucleus. It is unclear if each of the GPR4 expressing nuclei is activated uniformly under all physiological contexts or if their respective contributions changes depending on organism state. A number of the nuclei that express GPR4 are connected to emotional regulation and might mediate some of the anxiogenic action of inhaled CO_2. It will be interesting to examine the interplay between central chemosensitivity and emotional breathing in wildtype and GPR4 mutant animals in the future. GPR4 mRNA was also detected in blood vessels where its expression has been implicated in regulation of cerebral blood flow. This regulatory role at the endothelial cell level may also point to an important role of GPR4 in emotional regulation. Additionally, the GPR4 epitope knock-in mice provide a valuable tool to study the role of GPR4 in other pathophysiological processes (vascular physiology, kidney acid base regulation, etc.).

Furthermore, we showed that phenylalanine substitutions for two distinct histidine residues that are required for receptor pH sensitivity (H81F and H167F) at the

native locus of GPR4 is sufficient to blunt the HCVR at the whole-body level and CO_2 and pH mediated activation of the RTN specifically. We used two independent histidine mutations to strengthen the claim that it is the pH-sensing capacity of GPR4, per se, and not GPR4 expression alone that is necessary for a full HCVR. While these results support this interpretation, they do not eliminate the possibility that GPR4 serves only to maintain background excitability. To more rigorously demonstrate that GPR4 activation of RTN neurons is sufficient to increase respiration in a dose-dependent manner, we would need a non-proton agonist for GPR4 which does not yet exist. This would enable us to show that histidine mutant GPR4 only interferes with proton activation and would enable manipulation of GPR4 signaling without an exogenous low pH challenge. Additionally, future experiments using spatially targeted and PHOX2B-dependent lentiviral re-expression of GPR4(H81F) in the RTN on a GPR4 whole body KO context will enable us to repeat previous experiments done with wildtype GPR4 re-expression. We will then be able to determine if re-expression of pH-insensitive GPR4 in the RTN specifically is not sufficient to rescue the HCVR, unlike expression of wildtype GPR4.

CO_2 mediates effects on RTN neurons by way of both ionotropic (TASK-2) and metabotropic (GPR4) mechanisms, but it is unclear if these two molecules provide functional redundancy in cases where one may be disrupted or if the two signaling modalities actually serve distinct purposes even at baseline. RTN neurons are glutamatergic and their stimulation of breathing when driven exogenously via channelrhodopsin activation depends on glutamate release. RTN neurons also express high levels of multiple neuropeptides, including PACAP which has been shown to directly modulate breathing via action at the preBötC. The release pattern or context of these peptides is currently unknown for the RTN. Previous work in C. elegans showed a difference in peptide release after neuron stimulation with ionotropic (ChR2) or metabotropic (light activated adenylate cyclase) modes. This work proposed that the heavy

dense core vesicles (DCVs) containing peptides need the more prolonged metabotropic signaling by something such as protein kinase A activation to provide enough stimulation to dock DCVs and initiate peptide release. GPR4 is a metabotropic receptor that can signal through Gαs/cAMP mediated signaling that could provide a peptide-specific release drive that may enable peptide release depending on level of GPR4 activation. It will be interesting to pursue more studies to specifically disentangle distinct roles for TASK-2 and GPR4, if those roles exist, in modulating respiration via tuning glutamate and peptide release balance depending on large scale physiological context.

The studies reported in this thesis strengthen the evidence that GPR4 expression and pH sensing function is critical for normal central chemosensitivity. Future work will focus on further understanding the role of GPR4 expression in other nuclei aside from the RTN, possibly in those with emotional modulatory activity. Additionally, we will use an analogous approach to that presented here with GPR4 to determine which proton sensing capacity of TASK-2, internal or external, is necessary for the HCVR and for activation of the RTN. These studies will provide crucial molecular evidence supporting the role of the RTN as an integral driver of the central chemoreflex.

Publications Arising from This Work

Published:

Gonye, E. C. and Bayliss, D. A. Criteria for central respiratory chemoreceptors: experimental evidence supporting candidate cell groups. *Front. Physiol.* **14**, (2023).

Gonye, E. C., Dagli, A. V., Kumar, N., Clements, R. T., Xu, W., and Bayliss, D. A. Expression of endogenous epitope-tagged GPR4 in the mouse brain. *eNeuro* , (2024).

Manuscript In Preparation:

Gonye, E. C., Clements, R. T., Shi, Y., Li, K., Xu, W., and Bayliss, D. A. Intrinsic proton sensitivity of GPR4 is necessary for CO2/H+ activation of retrotrapezoid nucleus neurons and CO2-stimulated breathing.

Appendix – Mutation of pH-sensitive residues in TASK-2

As a companion to the studies reported above, we used CRISPR/Cas9 editing to successfully knock-in alanine mutations at the internal (Lys245) and external (Arg224) pH gates of TASK-2 in two independent mouse lines (fig. A.1A). In preliminary studies, TASK-2(R224A) mice have a significantly blunted HCVR compared to wildtype littermates (fig. A.1B-D). Based on our results observed with the pH-insensitive GPR4 mutant animals, we expect that TASK-2(R224A) animals will exhibit decreased activation of the RTN from an acute CO_2 challenge and will display diminished pH sensing capacity in RTN neurons. We have not yet completed analogous studies with the TASK-2(K245A) animals. The activity of the RTN is driven by changes in external pH, so it is possible that only mutation of the extracellular sensor (R224) will affect the HCVR or will affect it significantly more than mutation of the internal sensor (K245). Additionally, we will be able to complete electrophysiological studies to determine if extracellular pH sensitivity of TASK-2 is necessary for normal pH/CO_2 sensitivity of RTN neurons.

Method:
The CRISPR-assisted genome editing technology was used to generate the *Kcnk5*-R224A and *Kcnk5*-K245A knock-in mice. sgRNAs were selected based on a search via the CRISPR guide design algorithm CRISPOR (http://crispor.tefor.net/). The R224A (CGA>GCA) or K245A (AAG>GCA) point mutation was introduced into the wild-type (WT) *Knck5* gene sequence to generate *Kcnk5*-R224A or *Kcnk5*-K245A repair template (200mer ssODN). Microinjection of Cas9/sgRNA complex was completed as previously described in Methods section 2.5. Homozygous mice were used for all experiments.

Kcnk5-R224A sgRNA: CCTATACCGATACTTTGTGGAGC

Kcnk5-R224A ssODN:
TCTGGCCCTTGCTGACCCTCTGGGCTTCCTGTCTTTACAGGTGTGAACCCCAGTGCCAA
CTACCACGCGCTATACGCATACTTTGTGGAGCTCTGGATCTACCTGGGGCTGGCTTGGC
TGTCCCTCTTTGTCAACTGGAAGGTGAGCATGTTT

Kcnk5-K245A sgRNA: GGCTGTCCCTCTTTGTCAACTGG

Kcnk5-K245A ssODN:
ACAGGTGTGAACCCCAGTGCCAACTACCACGCCCTATACCGATACTTTGTGGAGCTTTG
GATCTACCTGGGGCTGGCTTGGCTGTCCCTGTTCGTTAATTGGGCAGTGAGCATGTTT
GTGGAAGTACACAAAGCCATTAAAAAGAGGCGGCGGCGGCGCAAGGAATTCTTTGAGA
GCTCTCCACACTCCCGGAAGGCCCT

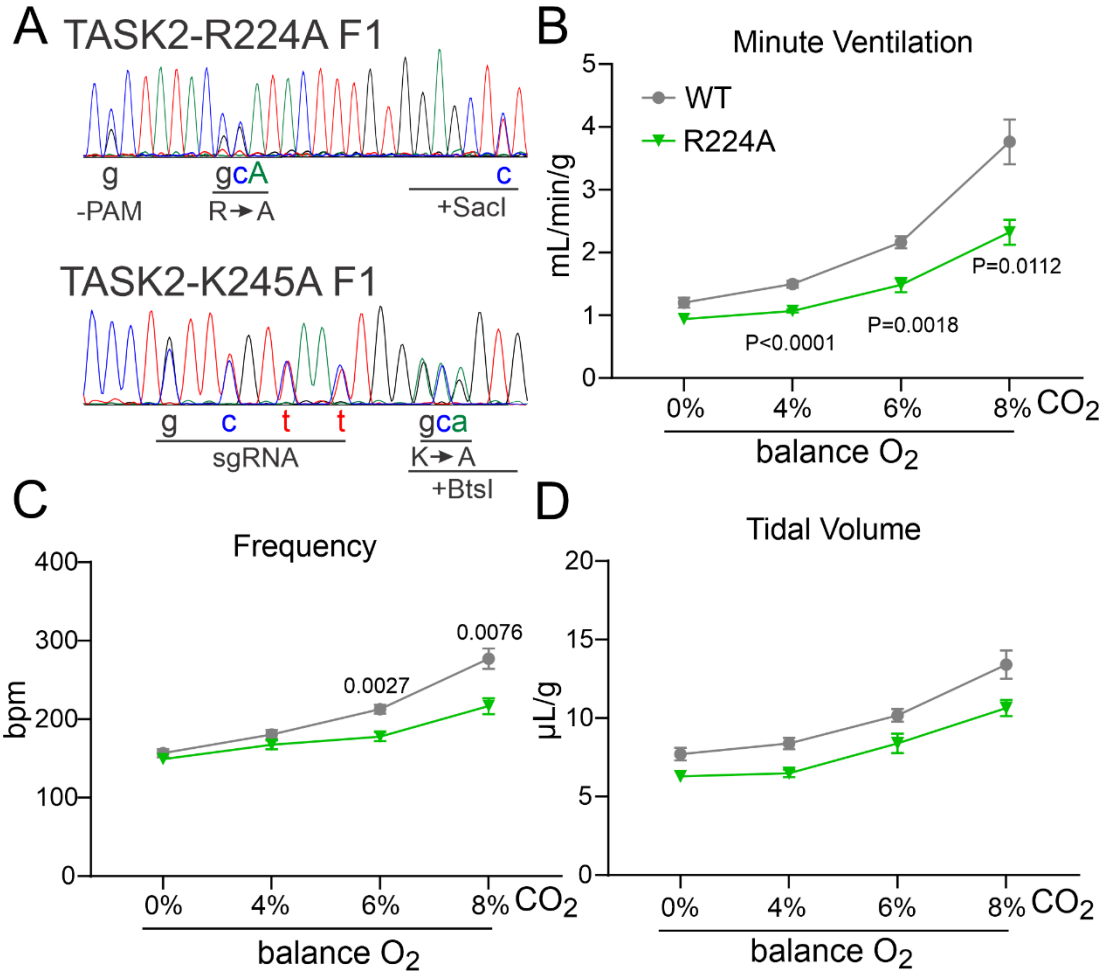

Figure A.1: Mutation of a pH sensing residue (Arg224) in TASK-2 blunts CO_2-stimulated breathing in mice. (A) Sanger sequencing traces from R224A and K245A F1 heterozygotes showing targeted alterations in *Kcnk5* genomic sequence. (B-D) Minute ventilation (B), frequency (C), and tidal volume (D) of TASK-2(R224A) (n = 7) and wildtype control (n = 12) mice in response to increasing levels of inspired CO_2 (balance O_2). Two-way RM-ANOVA: minute ventilation: $F_{(1, 17)} = 16.44$, P = 0.0008 for genotype and $F_{(3, 51)} = 4.829$, P = 0.0049 for CO_2 exposure × genotype; frequency: $F_{(1, 17)} = 10.66$, P = 0.0046 for genotype and $F_{(3, 51)} = 7.056$, P = 0.0005 for CO_2 exposure × genotype; tidal volume: $F_{(1, 17)} = 11.19$, P = 0.0038 for genotype and $F_{(3,51)} = 0.7518$, P = 0.5264 for CO_2 exposure × genotype.

References

1. Gonye, E. C. & Bayliss, D. A. Criteria for central respiratory chemoreceptors: experimental evidence supporting current candidate cell groups. *Front Physiol* **14**, (2023).
2. López-Barneo, J. Neurobiology of the carotid body. in *Handbook of Clinical Neurology* vol. 188 73–102 (2022).
3. Buckler, K. J. TASK channels in arterial chemoreceptors and their role in oxygen and acid sensing. *Pflugers Arch* **467**, 1013–1025 (2015).
4. Mokashi, A. *et al.* Role of IP3 Receptors in Shaping the Carotid Chemoreceptor Response to Hypoxia But Not to Hypercapnia in the Rat Carotid Body: An Evidence Review. in *Advances in Experimental Medicine and Biology* 1–25 (2021). doi:10.1007/5584_2020_561.
5. Haldane, J. S. & Priestley, J. G. THE REGULATION OF THE LUNG-VENTILATION. *Journal of Physiology* **32**, 225–266 (1905).
6. Feldman, J. L., Mitchell, G. S. & Nattie, E. E. Breathing: Rhythmicity, plasticity, chemosensitivity. *Annu Rev Neurosci* **26**, 239–266 (2003).
7. Connelly, C. A., Ellenberger, H. H. & Feldman, J. L. Respiratory activity in retrotrapezoid nucleus in cat. *Am J Physiol Lung Cell Mol Physiol* **258**, 33–44 (1990).
8. Ellenberger, H. H. & Feldman, J. L. Brainstem connections of the rostral ventral respiratory group of the rat. *Brain Res* **513**, 35–42 (1990).
9. Rosin, D. L., Chang, D. A. & Guyenet, P. G. Afferent and efferent connections of the rat retrotrapezoid nucleus. *Journal of Comparative Neurology* **499**, 64–69 (2006).
10. Smith, J. C., Morrison, D. E., Ellenberger, H. H., Otto, M. R. & Feldman, J. L. Brainstem projections to the major respiratory neuron populations in the medulla of the cat. *Journal of Comparative Neurology* **281**, 69–96 (1989).
11. Mitchell, R. A., Loeschcke, H. H., Severinghaus, J. W., Richardson, B. W. & Massion, W. H. Regions of Respiratory Chemosensitivity on the Surface of the Medulla. *Ann N Y Acad Sci* **109**, 661–681 (1963).
12. Bochorishvili, G., Stornetta, R. L., Coates, M. B. & Guyenet, P. G. Pre-Bötzinger complex receives glutamatergic innervation from galaninergic and other retrotrapezoid nucleus neurons. *J Comp Neurol* **520**, 1047–61 (2012).
13. Guyenet, P. G. *et al.* Proton detection and breathing regulation by the retrotrapezoid nucleus. *Journal of Physiology* **594**, 1529–1551 (2016).
14. Shi, Y. *et al.* Neuromedin B Expression Defines the Mouse Retrotrapezoid Nucleus. *J Neurosci* **37**, 11744–11757 (2017).
15. van der Heijden, M. E. & Zoghbi, H. Y. Development of the brainstem respiratory circuit. *Wiley Interdiscip Rev Dev Biol* **9**, 1–15 (2020).
16. Dempsey, B. *et al.* A medullary centre for lapping in mice. *Nat Commun* **12**, (2021).
17. Hirsch, M. R., d'Autréaux, F., Dymecki, S. M., Brunet, J. F. & Goridis, C. A Phox2b :: FLPo transgenic mouse line suitable for intersectional genetics. *Genesis* **51**, 506–514 (2013).
18. Ruffault, P.-L. *et al.* The retrotrapezoid nucleus neurons expressing Atoh1 and Phox2b are essential for the respiratory response to CO2. *Elife* **4**, (2015).
19. Huang, W. H. *et al.* Atoh1 Governs the Migration of Postmitotic Neurons that Shape Respiratory Effectiveness at Birth and Chemoresponsiveness in Adulthood. *Neuron* **75**, 799–809 (2012).

20. Stornetta, R. L. *et al.* Expression of Phox2b by Brainstem Neurons Involved in Chemosensory Integration in the Adult Rat. *Journal of Neuroscience* **26**, 10305–10314 (2006).
21. Cleary, C. M. *et al.* Somatostatin-expressing parafacial neurons are CO2/H+ sensitive and regulate baseline breathing. *Elife* **10**, (2021).
22. Guyenet, P. G. *et al.* The Retrotrapezoid Nucleus: Central Chemoreceptor and Regulator of Breathing Automaticity. *Trends Neurosci* **42**, 807–824 (2019).
23. Souza, G. M. P. R. *et al.* Neuromedin B-expressing neurons in the retrotrapezoid nucleus regulate respiratory homeostasis and promote stable breathing in adult mice. *The Journal of Neuroscience* JN-RM-0386-23 (2023) doi:10.1523/JNEUROSCI.0386-23.2023.
24. Mulkey, D. K. *et al.* Respiratory control by ventral surface chemoreceptor neurons in rats. *Nat Neurosci* **7**, 1360–1369 (2004).
25. Guyenet, P. G., Mulkey, D. K., Stornetta, R. L. & Bayliss, D. A. Regulation of ventral surface chemoreceptors by the central respiratory pattern generator. *Journal of Neuroscience* **25**, 8938–8947 (2005).
26. Lazarenko, R. M. *et al.* Acid-Sensitivity and Ultrastructure of the Retrotrapezoid Nucleus in Phox2B-Egfp Transgenic Mice. **517**, 69–86 (2010).
27. Shi, Y. *et al.* Nalcn is a "leak" sodium channel that regulates excitability of brainstem chemosensory neurons and breathing. *Journal of Neuroscience* **36**, 8174–8187 (2016).
28. Li, K. *et al.* TRPM4 mediates a subthreshold membrane potential oscillation in respiratory chemoreceptor neurons that drives pacemaker firing and breathing. *Cell Rep* **34**, 108714 (2021).
29. Nattie, E. E. & Li, A. Fluorescence location of RVLM kainate microinjections that alter the control of breathing. *J Appl Physiol* **68**, 1157–1166 (1990).
30. Nattie, E. E., Mills, J. W., Ou, L. C. & St. John, W. M. Kainic acid on the rostral ventrolateral medulla inhibits phrenic output and CO2 sensitivity. *J Appl Physiol* **65**, 1525–1534 (1988).
31. Pagliardini, S. *et al.* Central respiratory rhythmogenesis is abnormal in Lbx1-deficient mice. *Journal of Neuroscience* **28**, 11030–11041 (2008).
32. Marina, N. *et al.* Essential role of Phox2b-expressing ventrolateral brainstem neurons in the chemosensory control of inspiration and expiration. *Journal of Neuroscience* **30**, 12466–12473 (2010).
33. Ramanantsoa, N. *et al.* Breathing without CO2 Chemosensitivity in Conditional Phox2b Mutants. *Journal of Neuroscience* **31**, 12880–12888 (2011).
34. Patwari, P. P. *et al.* Congenital central hypoventilation syndrome and the PHOX2B gene: a model of respiratory and autonomic dysregulation. *Respir Physiol Neurobiol* **173**, 322–35 (2010).
35. Dubreuil, V. *et al.* A human mutation in Phox2b causes lack of CO2 chemosensitivity, fatal central apnea, and specific loss of parafacial neurons. *Proc Natl Acad Sci U S A* **105**, 1067–1072 (2008).
36. Hernandez-Miranda, L. R. *et al.* Mutation in LBX1/Lbx1 precludes transcription factor cooperativity and causes congenital hypoventilation in humans and mice. *Proceedings of the National Academy of Sciences* **115**, 13021–13026 (2018).
37. Souza, G. M. P. R. *et al.* Breathing regulation and blood gas homeostasis after near complete lesions of the retrotrapezoid nucleus in adult rats. *Journal of Physiology* **596**, 2521–2545 (2018).
38. Souza, G. M. P. R., Stornetta, R. L., Stornetta, D. S., Abbott, S. B. G. & Guyenet, P. G. Contribution of the retrotrapezoid nucleus and carotid bodies to hypercapnia-

And hypoxia-induced arousal from sleep. *Journal of Neuroscience* **39**, 9725–9737 (2019).
39. Abbott, S. B. G. *et al.* Photostimulation of Retrotrapezoid Nucleus Phox2b-Expressing Neurons In Vivo Produces Long-Lasting Activation of Breathing in Rats. (2009) doi:10.1523/JNEUROSCI.1106-09.2009.
40. Abbott, S. B. G., Stornetta, R. L., Coates, M. B. & Guyenet, P. G. Phox2b-expressing neurons of the parafacial region regulate breathing rate, inspiration, and expiration in conscious rats. *Journal of Neuroscience* **31**, 16410–16422 (2011).
41. Holloway, B. B., Viar, K. E., Stornetta, R. L. & Guyenet, P. G. The retrotrapezoid nucleus stimulates breathing by releasing glutamate in adult conscious mice. *Eur J Neurosci* **42**, 2271–82 (2015).
42. Basting, T. M. *et al.* Hypoxia silences retrotrapezoid nucleus respiratory chemoreceptors via alkalosis. *Journal of Neuroscience* **35**, 527–543 (2015).
43. Souza, G. M. P. R., Stornetta, R. L., Stornetta, D. S., Abbott, S. B. G. & Guyenet, P. G. Differential contribution of the retrotrapezoid nucleus and c1 neurons to active expiration and arousal in rats. *Journal of Neuroscience* **40**, 8683–8697 (2020).
44. Sato, M., Severinghaus, J. W. & Basbaum, A. I. Medullary CO , chemoreceptor by c-fos immunocytochemistry. *J Appl Physiol* **73**, 96–100 (1992).
45. Teppema, L. J., Berkenbosch, A., Veening, J. G. & Olievier, C. N. Hypercapnia induces c-fos expression in neurons of retrotrapezoid nucleus in cats. *Brain Res* **635**, 353–356 (1994).
46. Okada, Y., Chen, Z., Jiang, W., Kuwana, S. I. & Eldridge, F. L. Anatomical arrangement of hypercapnia-activated cells in the superficial ventral medulla of rats. *J Appl Physiol* **93**, 427–439 (2002).
47. Kumar, N. N. *et al.* Regulation of breathing by CO_2 requires the proton-activated receptor GPR4 in retrotrapezoid nucleus neurons. *Science (1979)* **348**, 1255–1260 (2015).
48. Pearce, R. A., Stornetta, R. L. & Guyenet, P. G. Retrotrapezoid nucleus in the rat. *Neurosci Lett* **101**, 138–142 (1989).
49. Nattie, E. E., Fung, M. L., Li, A. & St. John, W. M. Responses of respiratory modulated and tonic units in the retrotrapezoid nucleus to CO2. *Respir Physiol* **94**, 35–50 (1993).
50. Kawai, A., Ballantyne, D., Mückenhoff, K. & Scheid, P. Chemosensitive medullary neurones in the brainstem-spinal cord preparation of the neonatal rat. *Journal of Physiology* **492**, 277–292 (1996).
51. Lazarenko, R. M. *et al.* Anesthetic activation of central respiratory chemoreceptor neurons involves inhibition of a THIK-1-like background K+ current. *Journal of Neuroscience* **30**, 9324–9334 (2010).
52. Bhandare, A. *et al.* Analyzing the brainstem circuits for respiratory chemosensitivity in freely moving mice. *Elife* **11**, (2022).
53. Wang, S. *et al.* TASK-2 channels contribute to pH sensitivity of retrotrapezoid nucleus chemoreceptor neurons. *Journal of Neuroscience* **33**, 16033–16044 (2013).
54. Wu, Y. *et al.* Chemosensitivity of Phox2b-expressing retrotrapezoid neurons is mediated in part by input from 5-HT neurons. *Journal of Physiology* **597**, 2741–2766 (2019).
55. Mulkey, D. K., Mistry, A. M., Guyenet, P. G. & Bayliss, D. A. Purinergic P2 receptors modulate excitability but do not mediate pH sensitivity of RTN respiratory chemoreceptors. *The Journal of Neuroscience* (2006) doi:10.1523/JNEUROSCI.1696-06.2006.

56. Wenker, I. C., Sobrinho, C. R., Takakura, A. C., Moreira, T. S. & Mulkey, D. K. Regulation of ventral surface CO 2/H +-sensitive neurons by purinergic signalling. *Journal of Physiology* **590**, 2137–2150 (2012).
57. Hawryluk, J. M. *et al.* KCNQ channels determine serotonergic modulation of ventral surface chemoreceptors and respiratory drive. *Journal of Neuroscience* **32**, 16943–16952 (2012).
58. Hawkins, V. E. *et al.* HCN channels contribute to serotonergic modulation of ventral surface chemosensitive neurons and respiratory activity. *J Neurophysiol* **113**, 1195–1205 (2015).
59. Sobrinho, C. R. *et al.* Purinergic signalling contributes to chemoreception in the retrotrapezoid nucleus but not the nucleus of the solitary tract or medullary raphe. *Journal of Physiology* **592**, 1309–1323 (2014).
60. Mulkey, D. K. *et al.* Serotonergic neurons activate chemosensitive retrotrapezoid nucleus neurons by a pH-independent mechanism. *Journal of Neuroscience* **27**, 14128–14138 (2007).
61. Onimaru, H., Ikeda, K. & Kawakami, K. CO2-sensitive preinspiratory neurons of the parafacial respiratory group express Phox2b in the neonatal rat. *Journal of Neuroscience* **28**, 12845–12850 (2008).
62. Thoby-Brisson, M. *et al.* Genetic identification of an embryonic parafacial oscillator coupling to the preBötzinger complex. *Nat Neurosci* **12**, 1028–1035 (2009).
63. Wang, S., Shi, Y., Shu, S., Guyenet, P. G. & Bayliss, D. A. Phox2b-expressing retrotrapezoid neurons are intrinsically responsive to H+ and CO2. *Journal of Neuroscience* **33**, 7756–7761 (2013).
64. Moreira, T. S. *et al.* The retrotrapezoid nucleus and the neuromodulation of breathing. *J Neurophysiol* **125**, 699–719 (2021).
65. Lazarenko, R. M., Stornetta, R. L., Bayliss, D. A. & Guyenet, P. G. Orexin A activates retrotrapezoid neurons in mice. *Respir Physiol Neurobiol* **175**, 283–287 (2011).
66. Gourine, A. V. *et al.* Astrocytes Control Breathing Through pH-Dependent Release of ATP. *Science (1979)* **329**, 571–576 (2010).
67. Wenker, I. C., Kréneisz, O., Nishiyama, A., Mulkey, D. K. & Mulkey, D. K. Astrocytes in the Retrotrapezoid Nucleus Sense H+ by Inhibition of a Kir4.1–Kir5.1-Like Current and May Contribute to Chemoreception by a Purinergic Mechanism. *J Neurophysiol* **104**, 3042–3052 (2010).
68. Shi, Y. *et al.* 5-HT7 receptors expressed in the mouse parafacial region are not required for respiratory chemosensitivity. *J Physiol* **600**, 2789–2811 (2022).
69. Onimaru, H., Ikeda, K. & Kawakami, K. Postsynaptic mechanisms of CO 2 responses in parafacial respiratory neurons of newborn rats. *Journal of Physiology* **590**, 1615–1624 (2012).
70. Gestreau, C. *et al.* Task2 potassium channels set central respiratory CO2 and O 2 sensitivity. *Proc Natl Acad Sci U S A* **107**, 2325–2330 (2010).
71. Lesage, F. & Barhanin, J. Molecular physiology of ph-sensitive background k2P channels. *Physiology* vol. 26 424–437 Preprint at https://doi.org/10.1152/physiol.00029.2011 (2011).
72. Niemeyer, M. I., Cid, L. P., Pen ̃a-Münzenmayer, G. & Sepúlveda, F. V. Separate gating mechanisms mediate the regulation of K2P potassium channel TASK-2 by intra- and extracellular pH. *Journal of Biological Chemistry* **285**, 16467–16475 (2010).
73. Li, B., Rietmeijer, R. A. & Brohawn, S. G. Structural basis for pH gating of the two-pore domain K+ channel TASK2. *Nature* (2020) doi:10.1038/s41586-020-2770-2.

74. Niemeyer, M. I. *et al.* Gating of two-pore domain K+ channels by extracellular pH. *Biochem Soc Trans* **34**, 899–902 (2006).
75. Niemeyer, M. I. *et al.* Neutralization of a single arginine residue gates open a two-pore domain, alkali-activated K+ channel. *Proc Natl Acad Sci U S A* **104**, 666–671 (2007).
76. Warth, R. *et al.* Proximal renal tubular acidosis in TASK2 K+ channel-deficient mice reveals a mechanism for stabilizing bicarbonate transport. *Proc Natl Acad Sci U S A* **101**, 8215–8220 (2004).
77. Li, K. *et al.* The astrocytic Na+-HCO3- cotransporter, NBCe1, is dispensable for respiratory chemosensitivity. *J Physiol* (2023).
78. Teppema, L. J. *et al.* Influence of methazolamide on the human control of breathing: A comparison to acetazolamide. *Exp Physiol* **105**, 293–301 (2020).
79. Teppema, L. J. & Dahan, A. Acetazolamide and breathing: Does a clinical dose alter peripheral and central CO2 sensitivity? *Am J Respir Crit Care Med* **160**, 1592–1597 (1999).
80. Hosford, P. S. *et al.* CNS distribution, signalling properties and central effects of G-protein coupled receptor 4. *Neuropharmacology* **138**, 381–392 (2018).
81. Ludwig, M.-G. *et al.* Proton-sensing G-protein-coupled receptors. *Nature* **425**, 93–98 (2003).
82. Liu, J. P. *et al.* Each one of certain histidine residues in G-protein-coupled receptor GPR4 is critical for extracellular proton-induced stimulation of multiple G-protein-signaling pathways. *Pharmacol Res* **61**, 499–505 (2010).
83. Tobo, A. *et al.* Characterization of imidazopyridine compounds as negative allosteric modulators of proton-sensing GPR4 in extracellular acidification-induced responses. *PLoS One* **10**, 1–16 (2015).
84. Tobo, M. *et al.* Previously postulated "ligand-independent" signaling of GPR4 is mediated through proton-sensing mechanisms. *Cell Signal* **19**, 1745–1753 (2007).
85. Okaty, B. W., Commons, K. G. & Dymecki, S. M. Embracing diversity in the 5-HT neuronal system. *Nature Reviews Neuroscience* vol. 20 397–424 Preprint at https://doi.org/10.1038/s41583-019-0151-3 (2019).
86. Okaty, B. W. *et al.* Multi-Scale Molecular Deconstruction of the Serotonin Neuron System. *Neuron* **88**, 774–791 (2015).
87. Senft, R. A., Freret, M. E., Sturrock, N. & Dymecki, S. M. Neurochemically and hodologically distinct ascending VGLUT3 versus serotonin subsystems comprise the r2-pet1 median raphe. *Journal of Neuroscience* **41**, 2581–2600 (2021).
88. Johnson, P. L., Hollis, J. H., Moratalla, R., Lightman, S. L. & Lowry, C. A. Acute hypercarbic gas exposure reveals functionally distinct subpopulations of serotonergic neurons in rats. *Journal of Psychopharmacology* **19**, 327–341 (2005).
89. Veasey, S. C., Fornal, C. A., Metzler, C. W. & Jacobs, B. L. Single-unit responses of serotonergic dorsal raphe neurons to specific motor challenges in freely moving cats. *Neuroscience* **79**, 161–169 (1997).
90. Veasey, S. C., Fornal, C. A., Metzler, C. W. & Jacobs, B. L. Response of serotonergic caudal raphe neurons in relation to specific motor activities in freely moving cats. *Journal of Neuroscience* **15**, 5346–5359 (1995).
91. DePuy, S. D., Kanbar, R., Coates, M. B., Stornetta, R. L. & Guyenet, P. G. Control of breathing by raphe obscurus serotonergic neurons in mice. *Journal of Neuroscience* **31**, 1981–1990 (2011).
92. Hennessy, M. L. *et al.* Activity of Tachykinin1-expressing Pet1 raphe neurons modulates the respiratory chemoreflex. *Journal of Neuroscience* **37**, 1807–1819 (2017).

93. Brust, R. D., Corcoran, A. E., Richerson, G. B., Nattie, E. & Dymecki, S. M. Functional and Developmental Identification of a Molecular Subtype of Brain Serotonergic Neuron Specialized to Regulate Breathing Dynamics. *Cell Rep* **9**, 2152–2165 (2014).
94. Ray, R. S. *et al.* Impaired Respiratory and Body Temperature Control Upon Acute Serotonergic Neuron Inhibition Russell. **44**, 735–745 (2011).
95. Talley, E. M., Solórzano, G., Lei, Q., Kim, D. & Bayliss, D. A. CNS distribution of members of the two-pore-domain (KCNK) potassium channel family. *Journal of Neuroscience* **21**, 7491–7505 (2001).
96. Massey, C. A. *et al.* Isoflurane abolishes spontaneous firing of serotonin neurons and masks their pH / CO 2 chemosensitivity. *J Neurophysiol* **113**, 2879–2888 (2015).
97. Washburn, C. P., Sirois, J. E., Talley, E. M., Guyenet, P. G. & Bayliss, D. A. Serotonergic Raphe Neurons Express TASK Channel Transcripts and a TASK-Like pH- and Halothane-Sensitive K+ Conductance. *Journal of Neuroscience* **22**, 1256–1265 (2002).
98. Sirois, J. E., Lei, Q., Talley, E. M., Lynch, C. & Bayliss, D. A. The TASK-1 two-pore domain K+ channel is a molecular substrate for neuronal effects of inhalation anesthetics. *Journal of Neuroscience* **20**, 6347–6354 (2000).
99. Patel, A. J. *et al.* Inhalational anesthetics activate two-pore-domain background K+ channels. *Nat Neurosci* **2**, 422–426 (1999).
100. Mulkey, D. K. *et al.* TASK channels determine pH sensitivity in select respiratory neurons but do not contribute to central respiratory chemosensitivity. *Journal of Neuroscience* **27**, 14049–14058 (2007).
101. Trapp, S., Aller, M. I., Wisden, W. & Gourine, A. V. A role for TASK-1 (KCNK3) channels in the chemosensory control of breathing. *Journal of Neuroscience* **28**, 8844–8850 (2008).
102. Gourine, A. V., Llaudet, E., Dale, N. & Spyer, K. M. Release of ATP in the ventral medulla during hypoxia in rats: Role in hypoxic ventilatory response. *Journal of Neuroscience* **25**, 1211–1218 (2005).
103. Gourine, A. V., Llaudet, E., Dale, N. & Spyer, K. M. ATP is a mediator of chemosensory transduction in the central nervous system. *Nature* **436**, 108–111 (2005).
104. Sheikhbahaei, S. *et al.* Astrocytes modulate brainstem respiratory rhythm-generating circuits and determine exercise capacity. *Nat Commun* **9**, 1–10 (2018).
105. Erlichman, J. S., Li, A. & Nattie, E. E. *Ventilatory Effects of Glial Dysfunction in a Rat Brain Stem Chemoreceptor Region*. (1998).
106. Holleran, J., Babbie, M. & Erlichman, J. S. Ventilatory effects of impaired glial function in a brain stem chemoreceptor region in the conscious rat. *J Appl Physiol* **90**, 1539–1547 (2001).
107. Erlichman, J. S., Putnam, R. W. & Leiter, J. C. Glial Modulation of CO2 Chemosensory Excitability in the Retrotrapezoid Nucleus of Rodents. in *Advances in Experimental Medicine and Biology: Integration in Respiratory Control: From Genes to Systems* (eds. Poulin, M. J. & Wilson, J. A.) 317–321 (2008).
108. Erlichman, J. S., Leiter, J. C. & Gourine, A. V. ATP, GLIA and CENTRAL RESPIRATORY CONTROL. *Respir Physiol Neurobiol* **173**, 305–311 (2010).
109. van de Wiel, J. *et al.* Connexin26 mediates CO2-dependent regulation of breathing via glial cells of the medulla oblongata. *Commun Biol* **3**, 1–12 (2020).
110. Huckstepp, R. T. R. *et al.* Connexin hemichannel-mediated CO2-dependent release of ATP in the medulla oblongata contributes to central respiratory chemosensitivity. *Journal of Physiology* **588**, 3901–3920 (2010).

111. Meigh, L. *et al.* CO2 directly modulates connexin 26 by formation of carbamate bridges between subunits. *Elife* **2013**, 1–13 (2013).
112. Dospinescu, V. M. *et al.* Structural determinants of CO2-sensitivity in the β connexin family suggested by evolutionary analysis. *Communications Biology* vol. 2 Preprint at https://doi.org/10.1038/s42003-019-0576-2 (2019).
113. Turovsky, E. *et al.* Mechanisms of CO2/H+ sensitivity of astrocytes. *Journal of Neuroscience* **36**, 10750–10758 (2016).
114. Gonye, E. C. *et al.* Expression of Endogenous Epitope-Tagged GPR4 in the Mouse Brain. *eNeuro* **11**, ENEURO.0002-24.2024 (2024).
115. Rowe, J. B., Kapolka, N. J., Taghon, G. J., Morgan, W. M. & Isom, D. G. The evolution and mechanism of GPCR proton sensing. *Journal of Biological Chemistry* **296**, 1–24 (2021).
116. Sisignano, M., Fischer, M. J. M. & Geisslinger, G. Proton-Sensing GPCRs in Health and Disease. *Cells* **10**, 2050 (2021).
117. Yang, L. V *et al.* Vascular abnormalities in mice deficient for the G protein-coupled receptor GPR4 that functions as a pH sensor. *Mol Cell Biol* **27**, 1334–47 (2007).
118. Kim, K. *et al.* GPR4 plays a critical role in endothelial cell function and mediates the effects of sphingosylphosphorylcholine. *The FASEB Journal* **19**, 1–27 (2005).
119. Qiao, J. *et al.* Lysophosphatidylcholine impairs endothelial barrier function through the G protein-coupled receptor GPR4. *American Journal of Physiology-Lung Cellular and Molecular Physiology* **291**, L91–L101 (2006).
120. Li, R. *et al.* GPRASP1 loss-of-function links to arteriovenous malformations by endothelial activating GPR4 signals. *Brain* (2023) doi:10.1093/brain/awad335.
121. Ouyang, S. *et al.* GPR4 signaling is essential for the promotion of acid-mediated angiogenic capacity of endothelial progenitor cells by activating STAT3/VEGFA pathway in patients with coronary artery disease. *Stem Cell Res Ther* **12**, 149 (2021).
122. Ren, J. *et al.* Human GPR4 and the Notch signaling pathway in endothelial cell tube formation. *Mol Med Rep* **14**, 1235–1240 (2016).
123. Miltz, W. *et al.* Design and synthesis of potent and orally active GPR4 antagonists with modulatory effects on nociception, inflammation, and angiogenesis. *Bioorg Med Chem* **25**, 4512–4525 (2017).
124. Dong, L. *et al.* Acidosis Activation of the Proton-Sensing GPR4 Receptor Stimulates Vascular Endothelial Cell Inflammatory Responses Revealed by Transcriptome Analysis. *PLoS One* **8**, e61991 (2013).
125. Huang, F., Mehta, D., Predescu, S., Kim, K. S. & Lum, H. A Novel Lysophospholipid- and pH-Sensitive Receptor, GPR4, in Brain Endothelial Cells Regulates Monocyte Transmigration. *Endothelium* **14**, 25–34 (2007).
126. Chen, A. *et al.* Activation of GPR4 by Acidosis Increases Endothelial Cell Adhesion through the cAMP/Epac Pathway. *PLoS One* **6**, e27586 (2011).
127. Sanderlin, E. J. *et al.* GPR4 deficiency alleviates intestinal inflammation in a mouse model of acute experimental colitis. *Biochimica et Biophysica Acta (BBA) - Molecular Basis of Disease* **1863**, 569–584 (2017).
128. Marie, M. A. *et al.* GPR4 Knockout Attenuates Intestinal Inflammation and Forestalls the Development of Colitis-Associated Colorectal Cancer in Murine Models. *Cancers (Basel)* **15**, 4974 (2023).
129. Sanderlin, E. J., Marie, M., Velcicky, J., Loetscher, P. & Yang, L. V. Pharmacological inhibition of GPR4 remediates intestinal inflammation in a mouse colitis model. *Eur J Pharmacol* **852**, 218–230 (2019).

130. Krewson, E. A. *et al.* The Proton-Sensing GPR4 Receptor Regulates Paracellular Gap Formation and Permeability of Vascular Endothelial Cells. *iScience* **23**, 100848 (2020).
131. Liu, H., Liu, Y. & Chen, B. Antagonism of GPR4 with NE 52-QQ57 and the Suppression of AGE-Induced Degradation of Type II Collagen in Human Chondrocytes. *Chem Res Toxicol* **33**, 1915–1921 (2020).
132. Dong, B., Zhang, X., Fan, Y., Cao, S. & Zhang, X. GPR4 knockout improves renal ischemia–reperfusion injury and inhibits apoptosis via suppressing the expression of CHOP. *Biochemical Journal* **474**, 4065–4074 (2017).
133. Sun, X. *et al.* Deletion of the pH Sensor GPR4 Decreases Renal Acid Excretion. *Journal of the American Society of Nephrology* **21**, 1745–1755 (2010).
134. Cheval, L. *et al.* Acidosis-induced activation of distal nephron principal cells triggers Gdf15 secretion and adaptive proliferation of intercalated cells. *Acta Physiologica* **232**, (2021).
135. Sun, X., Stephens, L., DuBose, T. D. & Petrovic, S. Adaptation by the collecting duct to an exogenous acid load is blunted by deletion of the proton-sensing receptor GPR4. *American Journal of Physiology-Renal Physiology* **309**, F120–F136 (2015).
136. Castellone, R. D., Leffler, N. R., Dong, L. & Yang, L. V. Inhibition of tumor cell migration and metastasis by the proton-sensing GPR4 receptor. *Cancer Lett* **312**, 197–208 (2011).
137. Jing, Z. *et al.* The Proton-Sensing G-Protein Coupled Receptor GPR4 Promotes Angiogenesis in Head and Neck Cancer. *PLoS One* **11**, e0152789 (2016).
138. Sin, W. C. *et al.* G protein-coupled receptors GPR4 and TDAG8 are oncogenic and overexpressed in human cancers. *Oncogene* **23**, 6299–6303 (2004).
139. Wyder, L. *et al.* Reduced pathological angiogenesis and tumor growth in mice lacking GPR4, a proton sensing receptor. *Angiogenesis* **14**, 533–544 (2011).
140. Xue, C. *et al.* Association between G-protein coupled receptor 4 expression and microvessel density, clinicopathological characteristics and survival in hepatocellular carcinoma. *Oncol Lett* (2020) doi:10.3892/ol.2020.11366.
141. Yu, M. *et al.* Increased proton-sensing receptor GPR4 signalling promotes colorectal cancer progression by activating the hippo pathway. *EBioMedicine* **48**, 264–276 (2019).
142. Wenzel, J. *et al.* Impaired endothelium-mediated cerebrovascular reactivity promotes anxiety and respiration disorders in mice. *Proc Natl Acad Sci U S A* **117**, 1753–1761 (2020).
143. Sun, X. *et al.* Deletion of proton-sensing receptor GPR4 associates with lower blood pressure and lower binding of angiotensin II receptor in SFO. *Am J Physiol Renal Physiol* **311**, F1260–F1266 (2016).
144. An, S., Tsai, C. & Goetzl, E. J. Cloning, sequencing and tissue distribution of two related G protein-coupled receptor candidates expressed prominently in human lung tissue. *FEBS Lett* **375**, 121–124 (1995).
145. Mahadevan, M. S. *et al.* Isolation of a Novel G Protein-Coupled Receptor (GPR4) Localized to Chromosome 19q13.3. *Genomics* **30**, 84–88 (1995).
146. Lein, E. S. *et al.* Genome-wide atlas of gene expression in the adult mouse brain. *Nature* **445**, 168–176 (2007).
147. Magdaleno, S. *et al.* BGEM: An In Situ Hybridization Database of Gene Expression in the Embryonic and Adult Mouse Nervous System. *PLoS Biol* **4**, e86 (2006).

148. Souza, G. M. P. R. *et al.* Neuromedin B-expressing neurons in the retrotrapezoid nucleus regulate respiratory homeostasis and promote stable breathing in adult mice. *Journal of Neuroscience* (2023).
149. Hodges, M. R. & Richerson, G. B. Contributions of 5-HT neurons to respiratory control: Neuromodulatory and trophic effects. *Respir Physiol Neurobiol* **164**, 222–232 (2008).
150. Hodges, M. R. & Richerson, G. B. Respiratory Physiology & Neurobiology Medullary serotonin neurons and their roles in central respiratory. *Respir Physiol Neurobiol* **173**, 256–263 (2010).
151. Corcoran, A. E. *et al.* Medullary serotonin neurons and central CO2 chemoreception. *Respir Physiol Neurobiol* **168**, 49–58 (2009).
152. Bakken, T. E. *et al.* Single-cell and single-nucleus RNA-seq uncovers shared and distinct axes of variation in dorsal LGN neurons in mice, non-human primates, and humans. *Elife* **10**, (2021).
153. Smith, H. R. *et al.* Dorsal raphe serotonin neurons mediate Co 2 -induced arousal from sleep. *Journal of Neuroscience* **38**, 1915–1925 (2018).
154. Buchanan, G. F. & Richerson, G. B. Central serotonin neurons are required for arousal to CO2. *Proc Natl Acad Sci U S A* **107**, 16354–16359 (2010).
155. Bailey, J. E., Dawson, G. R., Dourish, C. T. & Nutt, D. J. Validating the inhalation of 7.5% CO_2 in healthy volunteers as a human experimental medicine: a model of generalized anxiety disorder (GAD). *Journal of Psychopharmacology* **25**, 1192–1198 (2011).
156. Poma, S. Z. *et al.* Characterization of a 7% carbon dioxide (CO2) inhalation paradigm to evoke anxiety symptoms in healthy subjects. *Journal of Psychopharmacology* **19**, 494–503 (2005).
157. Bailey, J. E., Argyropoulos, S. V., Kendrick, A. H. & Nutt, D. J. Behavioral and cardiovascular effects of 7.5% CO2 in human volunteers. *Depress Anxiety* **21**, 18–25 (2005).
158. Vickers, K., Jafarpour, S., Mofidi, A., Rafat, B. & Woznica, A. The 35% carbon dioxide test in stress and panic research: Overview of effects and integration of findings. *Clin Psychol Rev* **32**, 153–164 (2012).
159. Ziemann, A. E. *et al.* The Amygdala Is a Chemosensor that Detects Carbon Dioxide and Acidosis to Elicit Fear Behavior. *Cell* **139**, 1012–1021 (2009).
160. Wang, D. *et al.* Lateral septum-lateral hypothalamus circuit dysfunction in comorbid pain and anxiety. *Mol Psychiatry* **28**, 1090–1100 (2023).
161. Anthony, T. E. *et al.* Control of Stress-Induced Persistent Anxiety by an Extra-Amygdala Septohypothalamic Circuit. *Cell* **156**, 522–536 (2014).
162. Rizzi-Wise, C. A. & Wang, D. V. Putting Together Pieces of the Lateral Septum: Multifaceted Functions and Its Neural Pathways. *eNeuro* **8**, ENEURO.0315-21.2021 (2021).
163. Lee, H. W., Yang, S. H., Kim, J. Y. & Kim, H. The role of the medial habenula cholinergic system in addiction and emotion-associated behaviors. *Front Psychiatry* **10**, (2019).
164. Roy, N. & Parhar, I. Habenula orphan G-protein coupled receptors in the pathophysiology of fear and anxiety. *Neuroscience and Biobehavioral Reviews* vol. 132 870–883 Preprint at https://doi.org/10.1016/j.neubiorev.2021.11.008 (2022).
165. Murphy, C. A., DiCamillo, A. M., Haun, F. & Murray, M. Lesion of the habenular efferent pathway produces anxiety and locomotor hyperactivity in rats: a comparison of the effects of neonatal and adult lesions. *Behavioural Brain Research* **81**, 43–52 (1996).

166. Jacinto, L. R., Mata, R., Novais, A., Marques, F. & Sousa, N. The habenula as a critical node in chronic stress-related anxiety. *Exp Neurol* **289**, 46–54 (2017).
167. Cho, C. *et al.* TMEM16A expression in cholinergic neurons of the medial habenula mediates anxiety-related behaviors. *EMBO Rep* **21**, (2020).
168. Kobayashi, Y. *et al.* Genetic dissection of medial habenula–interpeduncular nucleus pathway function in mice. *Front Behav Neurosci* **7**, (2013).
169. Mathuru, A. S. & Jesuthasan, S. The medial habenula as a regulator of anxiety in adult zebrafish. *Front Neural Circuits* **7**, (2013).
170. Zhang, J. *et al.* Presynaptic Excitation via GABAB Receptors in Habenula Cholinergic Neurons Regulates Fear Memory Expression. *Cell* **166**, 716–728 (2016).
171. Yamaguchi, T., Danjo, T., Pastan, I., Hikida, T. & Nakanishi, S. Distinct Roles of Segregated Transmission of the Septo-Habenular Pathway in Anxiety and Fear. *Neuron* **78**, 537–544 (2013).
172. Herkenham, M. & Nauta, W. J. H. Afferent connections of the habenular nuclei in the rat. A horseradish peroxidase study, with a note on the fiber-of-passage problem. *Journal of Comparative Neurology* **173**, 123–145 (1977).
173. Qin, C. & Luo, M. Neurochemical phenotypes of the afferent and efferent projections of the mouse medial habenula. *Neuroscience* **161**, 827–837 (2009).
174. McLaughlin, I., Dani, J. A. & De Biasi, M. The medial habenula and interpeduncular nucleus circuitry is critical in addiction, anxiety, and mood regulation. *J Neurochem* **142**, 130–143 (2017).
175. Namboodiri, V. M. K., Rodriguez-Romaguera, J. & Stuber, G. D. The habenula. *Current Biology* **26**, R873–R877 (2016).
176. Gouveia, F. V. & Ibrahim, G. M. Habenula as a Neural Substrate for Aggressive Behavior. *Front Psychiatry* **13**, (2022).
177. Besnard, A. & Leroy, F. Top-down regulation of motivated behaviors via lateral septum sub-circuits. *Mol Psychiatry* **27**, 3119–3128 (2022).
178. Qi, G. *et al.* NAc-VTA circuit underlies emotional stress-induced anxiety-like behavior in the three-chamber vicarious social defeat stress mouse model. *Nat Commun* **13**, 577 (2022).
179. Guyenet, P. G. & Bayliss, D. A. Central respiratory chemoreception. in *Handbook of Clinical Neurology* (eds. Chen, R. & Guyenet, P. G.) vol. 188 37–72 (2022).
180. Guyenet, P. G. & Bayliss, D. A. Neural Control of Breathing and CO2 Homeostasis. *Neuron* vol. 87 946–961 Preprint at https://doi.org/10.1016/j.neuron.2015.08.001 (2015).
181. Stornetta, R. L. *et al.* Galanin is a selective marker of the retrotrapezoid nucleus in rats. *J Comp Neurol* **512**, 373–383 (2009).
182. Bautista, T. G. *et al.* The Expression of Galanin in the Parafacial Respiratory Group and its Effects on Respiration in Neonatal Rats. *Neuroscience* **384**, 1–13 (2018).
183. Shi, Y. *et al.* A brainstem peptide system activated at birth protects postnatal breathing. *Nature* 1–5 (2020) doi:10.1038/s41586-020-2991-4.
184. Ptak, K. *et al.* Raphe Neurons Stimulate Respiratory Circuit Activity by Multiple Mechanisms via Endogenously Released Serotonin and Substance P. *Journal of Neuroscience* **29**, 3720–3737 (2009).
185. Hodges, M. R. & Richerson, G. B. The role of medullary serotonin (5-HT) neurons in respiratory control : contributions to eupneic ventilation , CO 2 chemoreception , and thermoregulation. *J Appl Physiol* **108**, 1425–1432 (2010).

186. Morton, M. J., Abohamed, A., Sivaprasadarao, A. & Hunter, M. pH sensing in the two-pore domain K+ channel, TASK2. *Proc Natl Acad Sci U S A* **102**, 16102–16106 (2005).
187. Morton, M. J., O'Connell, A. D., Sivaprasadarao, A. & Hunter, M. Determinants of pH sensing in the two-pore domain K+ channels TASK-1 and -2. *Pflugers Arch* **445**, 577–583 (2003).
188. Zúñiga, L. *et al.* Gating of a pH-sensitive K2P potassium channel by an electrostatic effect of basic sensor residues on the selectivity filter. *PLoS One* **6**, (2011).